IBRACON

REVISTA IBRACON DE ESTRUTURAS E MATERIAIS

IBRACON STRUCTURES AND MATERIALS JOURNAL

Volume 7, Number 6

December, 2014

ISSN 1983-4195

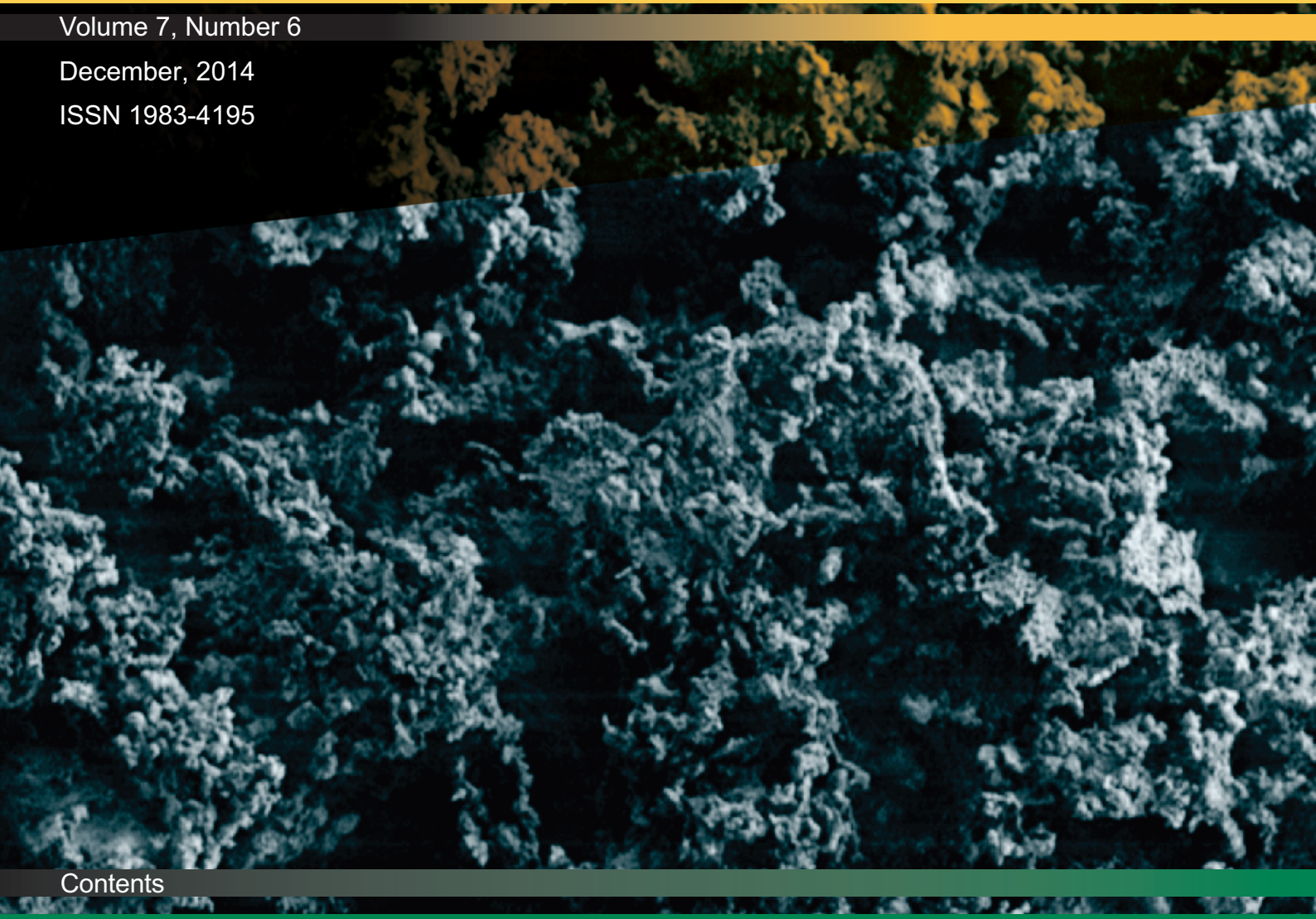

Contents

Editorial

Editorial Board

- Américo Campos Filho
  (Editor, UFRGS, Porto Alegre, RS, Brazil)
- José Luiz Antunes de Oliveira e Sousa
  (Editor, UNICAMP, Campinas, SP, Brazil)
- Roberto Caldas de Andrade Pinto
  (Editor, UFSC, Florianópolis, SC, Brazil)
- Romilde Almeida de Oliveira
  (Editor, Universidade Católica de Pernambuco, Recife, PE, Brazil)
- Antonio Carlos R. Laranjeiras
  (ACR Laranjeiras, Salvador, BA, Brazil)
- Bernardo Horowitz
  (UFPE, Recife, PE, Brazil)
- Denise C. C. Dal Molin
  (Former Editor, UFRGS, Porto Alegre, RS, Brazil)
- Emil de Souza Sánchez Filho
  (UFF, Rio de Janeiro, RJ, Brazil)
- Geraldo Cechella Isaia
  (UFSM, Santa Maria, RS, Brazil)
- Gonzalo Ruiz
  (UCLM, Ciudade Real, Spain)
- Guilherme Sales Melo
  (Former Editor, UnB, Brasilia, DF, Brazil)
- Ivo José Padaratz
  (UFSC, Florianópolis, SC, Brazil)
- Joaquim Figueiras
  (FEUP, Porto, Portugal)
- José Marcio Fonseca Calixto
  (UFMG, Belo Horizonte, MG, Brazil)
- Luiz Carlos Pinto da Silva Filho
  (Former Editor, UFRGS, Porto Alegre, RS, Brazil)
- Mounir Khalil El Debs
  (USP, São Carlos, SP, Brazil)
- Nicole Pagan Hasparyk
  (Former Editor, FURNAS, Aparecida de Goiânia, GO, Brazil)
- Osvaldo Luís Manzoli
  (UNESP, Bauru, SP, Brazil)
- Paulo Helene
  (Former Editor, USP, São Paulo, SP, Brazil)
- Paulo Monteiro
  (Berkeley, University of California, Berkeley, CA, USA)
- P.K. Mehta
  (Berkeley, University of California, Berkeley, CA, USA)
- Pedro Castro Borges
  (CINVESTAV, México, D.F , México)
- Rafael Giuliano Pileggi
  (USP, São Paulo, SP, Brazil)
- Romildo Dias Toledo Filho
  (Former Editor, UFRJ, Rio de Janeiro, RJ, Brazil)
- Ronaldo Barros Gomes
  (UFG, Goiânia, GO, Brazil)
- Rubens Machado Bittencourt
  (Former Editor, FURNAS, Aparecida de Goiânia, GO, Brazil)
- Túlio Nogueira Bittencourt
  (Former Editor, USP, São Paulo, SP, Brazil)
- Vladimir Antonio Paulon
  (UNICAMP, Campinas, SP, Brazil)

Reviewers

Reviewers are selected by the Editors among the IBRACON members with recognized competence in the specific field of each contribution. They are acknowledged at the end of each volume.

IBRACON Structures and Materials Journal is now releasing the sixth and last issue of the 2014 volume. This issue brings five articles on relevant topics on concrete structures and materials. The first article describes a study on the properties of peanut husk ashes aiming at its use in cement mortars as partial substitute of Portland cement. The next article presents a case study on challenges and solutions devised to execute an anti-flotation reinforced concrete slab for the new Sound and Image Museum, in Copacabana, Rio de Janeiro. A third article draws on the rheological properties of pumped concrete. The goal is an investigation on the effects of important Portland concrete design variables in the rheological characteristics of pumped concrete cement pastes. The fourth article describes a model to predict the flexural behavior of reinforced concrete slabs, combining Mazars damage model for simulating concrete cracking, the perfect elastoplastic model for yielding and rupture of the reinforcing steel, and the classical theory of laminates. The issue closes with an article on the development and behavior analysis of high performance fiber reinforced cement composites applied as a transition layer of reinforced beams.

In this issue, we present a list of the reviewers that contributed to our Journal during the year 2014. We congratulate the authors and reviewers for the high quality achieved by our Journal.

Américo Campos Filho, José Luiz Antunes de Oliveira e Sousa, Roberto Caldas de Andrade Pinto and Romilde Almeida de Oliveira, Editors

A Revista IBRACON de Estruturas e Materiais está lançando o sexto e último número do volume de 2014. Esta edição traz cinco artigos sobre temas relevantes em materiais e estruturas de concreto. O primeiro artigo descreve um estudo sobre as propriedades de cinzas de casca de amendoim, visando à utilização como substituto parcial do cimento Portland em argamassas. O artigo seguinte apresenta um estudo de caso sobre os desafios e soluções para uma laje de subpressão para o novo Museu de Imagem e Som, em Copacabana, Rio de Janeiro. O terceiro artigo baseia-se nas propriedades reológicas do concreto bombeado. O objetivo é uma investigação sobre os efeitos das variáveis importantes para o projeto de concreto Portland nas características reológicas de pastas de cimento em concreto bombeado. Um modelo para prever o comportamento à flexão de lajes de concreto armado é descrito no quarto artigo, combinando modelo de dano de Mazars para simulação de fissuração do concreto, o modelo elastoplástico perfeito para escoamento e ruptura da armadura de aço, e a teoria clássica de laminados. O volume se encerra com um artigo sobre o desenvolvimento e análise do comportamento de compósitos cimentícios de elevado desempenho reforçados com fibras, aplicados como substrato de transição em vigas de concreto armado.

Neste número apresentamos uma lista dos colaboradores que contribuíram para a nossa Revista durante o ano de 2014. Parabenizamos os autores e revisores pela alta qualidade alcançada pela nossa Revista.

Américo Campos Filho, José Luiz Antunes de Oliveira e Sousa, Roberto Caldas de Andrade Pinto e Romilde Almeida de Oliveira, Editores

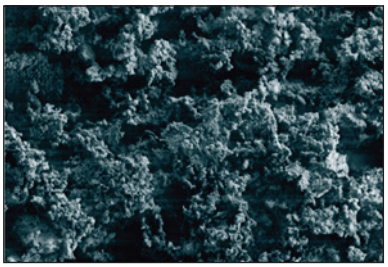

Cover: SEM microscopy images of cement past with 15% peanut husk ashes at 10 kX magnification

Courtesy: J. Kreiker, Córdoba, Argentina

Volume 7, Number 6
December 2014
ISSN: 1983-4195

REVISTA IBRACON DE ESTRUTURAS E MATERIAIS

IBRACON STRUCTURES AND MATERIALS JOURNAL

Contents

IBRACON

Ibracon Structures and Materials Journal
is published bimonthly
(February, April, June, August, October and December) by IBRACON.

IBRACON
Instituto Brasileiro do Concreto
Founded in 1972

R. Julieta do Espirito Santo Pinheiro, 68
Jardim Olímpia, São Paulo – SP
Brasil – 05542-120
Phone: +55 11 3735-0202
Fax: +55 11 3733-2190
E-mail: arlene@ibracon.org.br
Website: http://www.ibracon.org.br

Editors
Américo Campos Filho
(Brazil)

José Luiz Antunes de O. e Sousa
(Brazil)

Roberto Caldas de Andrade Pinto
(Brazil)

Romilde Almeida de Oliveira
(Brazil)

Cover design & Layout:
Ellementto-Arte
www.ellementto-arte.com

Aims and Scope

Aims and Scope

The IBRACON Structures and Materials Journal is a technical and scientifical divulgation vehicle of IBRACON (Brazilian Concrete Institute). Each issue of the periodical has 5 to 8 papers and, possibly, a technical note and/or a technical discussion regarding a previously published paper. All contributions are reviewed and approved by reviewers with recognized scientific competence in the area.

Objectives

The IBRACON Structures and Materials Journal´s main objectives are:

- Present current developments and advances in the area of concrete structures and materials;
- Make possible the better understanding of structural concrete behavior, supplying subsidies for a continuous interaction among researchers, producers and users;
- Stimulate the development of scientific and technological research in the areas of concrete structures and materials, through papers peer-reviewed by a qualified Editorial Board;
- Promote the interaction among researchers, constructors and users of concrete structures and materials and the development of Civil Construction;
- Provide a vehicle of communication of high technical level for researchers and designers in the areas of concrete structures and materials.

Submission Procedure

The procedure to submit and revise the contributions, as well as the formats, are detailed on IBRACON's WebSite (www.ibracon.org.br). The papers and the technical notes are revised by at least three reviewers indicated by the editors. The discussions and replies are accepted for publication after a revision by the editors and at least one member of the Editorial Board. In case of disagreement between the reviewer and the authors, the contribution will be sent to a specialist in the area, not necessarily linked to the Editorial Board.

Contribution Types

The periodical will publish original papers, short technical notes and paper discussions. Announcements of conferences and meetings, information about book reviews, events and contributions related to the area will also be available in the periodical's WebSite. All contributions will be revised and only published after the Editorial and Reviewers Boards approve the paper. Restrictions of content and space (size) are imposed to the papers. The contributions will be accepted for review in Portuguese, Spanish or English. The abstracts are presented in Portuguese or Spanish, and in English, independently of the language in which the paper is written. After the review process, papers originally written in Portuguese or Spanish should be translated into English, which is the official language of the IBRACON Structures and Materials Journal. Optionally, papers are also published in Portuguese or Spanish.

Original papers will be accepted as long as they are in accordance with the objectives of the periodical and present quality of information and presentation. The instructions to submit a paper are detailed in the template (available on IBRACON's WebSite).

The length of the papers must not exceed 20 pages.

A technical note is a brief manuscript. It may present a new feature of research, development or technological application in the areas of Concrete Structures and Materials, and Civil Construction. This is an opportunity to be used by industries, companies, universities, institutions of research, researchers and professionals willing to promote their works and products under development. The instructions to submit a technical note are detailed on IBRACON's WebSite.

A discussion is received no later than 3 months after the publication of the paper or technical note. The instructions to submit a discussion are detailed on IBRACON's WebSite. The discussion must be limited to the topic addressed in the published paper and must not be offensive. The right of reply is guaranteed to the Authors. The discussions and the replies are published in the subsequent issues of the periodical.

Internet Access

IBRACON Structural Journal Page in http://www.ibracon.org.br

Subscription rate

All IBRACON members have free access to the periodical contents through the Internet. Non-members have limited access to the published material, but are able to purchase isolated issues through the Internet. The financial resources for the periodical´s support are provided by IBRACON and by research funding agencies. The periodical will not receive any type of private advertisement that can jeopardize the credibility of the publication.

Photocopying

Photocopying in Brazil. Brazilian Copyright Law is applicable to users in Brazil. IBRACON holds the copyright of contributions in the journal unless stated otherwise at the bottom of the first page of any contribution. Where IBRACON holds the copyright, authorization to photocopy items for internal or personal use, or the internal or personal use of specific clients, is granted for libraries and other users registered at IBRACON.

Copyright

All rights, including translation, reserved. Under the Brazilian Copyright Law No. 9610 of 19th February, 1998, apart from any fair dealing for the purpose of research or private study, or criticism or review, no part of this publication may be reproduced, stored in a retrieval system, or transmitted in any form or by any means, electronic, mechanical, photocopying, recording or otherwise, without the prior written permission of IBRACON. Requests should be directed to IBRACON:

IBRACON

Rua Julieta do Espírito Santo Pinheiro, nº 68 ,Jardim Olímpia,
São Paulo, SP – Brasil CEP: 05542-120
Phone: +55 11 3735-0202 Fax: +55 11 3733-2190
E-mail: arlene@ibracon.org.br.

Disclaimer

Papers and other contributions and the statements made or opinions expressed therein are published on the understanding that the authors of the contribution are the only responsible for the opinions expressed in them and that their publication does not necessarily reflect the support of IBRACON or the journal.

Objetivos e Escopo

A Revista IBRACON de Estruturas e Materiais é um veículo de divulgação técnica e científica do IBRACON (Instituto Brasileiro do Concreto). Cada número do periódico tem 5 a 8 artigos e, possivelmente, uma nota técnica e/ou uma discussão técnica sobre um artigo publicado anteriormente. Todas as contribuições são revistas e aprovadas por revisores com competência científica reconhecida na área.

Objetivos

Os objetivos principais da Revista IBRACON de Estruturas e Materiais são:

- Apresentar desenvolvimentos e avanços atuais na área de estruturas e materiais de concreto;
- Possibilitar o melhor entendimento do comportamento do concreto estrutural, fornecendo subsídios para uma interação contribua entre pesquisadores, produtores e usuários;
- Estimular o desenvolvimento de pesquisa científica e tecnológica nas áreas de estruturas de concreto e materiais, através de artigos revisados por um corpo de revisores qualificado;
- Promover a interação entre pesquisadores, construtores e usuários de estruturas e materiais de concreto, e o desenvolvimento da Construção Civil;
- Prover um veículo de comunicação de alto nível técnico para pesquisadores e projetistas nas áreas de estruturas de concreto e materiais.

Submissão de Contribuições

O procedimento para submeter e revisar as contribuições, assim como os formatos, estão detalhados na página Internet do IBRACON (www.ibracon.org.br). Os artigos e as notas técnicas são revisadas por, no mínimo, três revisores indicados pelos editores. As discussões e réplicas são aceitas para publicação após uma revisão pelo editores e no mínimo um membro do Corpo Editorial. No caso de desacordo entre revisor e autores, a contribuição será enviada a um especialista na área, não necessariamente do Corpo Editorial.

Tipos de Contribuição

O periódico publicará artigos originais, notas técnicas curtas e discussões sobre artigos. Anúncios de congressos e reuniões, informação sobre revisão de livros e contribuições relacionadas à área serão também disponibilizadas na página Internet da revista. Todas as contribuições serão revisadas e publicadas apenas após a aprovação dos revisores e do Corpo Editorial. Restrições de conteúdo e espaço (tamanho) são impostas aos artigos. As contribuições serão aceitas para revisão em português, espanhol ou inglês. Os resumos serão apresentados em português ou espanhol, e em inglês, independentemente do idioma em que o artigo for escrito. Após o processo de revisão, artigos originalmente escritos em português ou espanhol deverão ser traduzidos para inglês, que é o idioma oficial da Revista IBRACON de Estruturas e Materiais. Opcionalmente, os artigos são também publicados em português ou espanhol.

Artigos originais serão aceitos desde que estejam de acordo com os objetivos da revista e apresentam qualidade de informação e apresentação. As instruções para submeter um artigo estão detalhadas em um gabarito (disponível no sítio do IBRACON).

A extensão dos artigos não deve exceder 20 páginas.

Um nota técnica é um manuscrito curto. Deve apresentar uma nova linha de pesquisa, desenvolvimento ou aplicação tecnológica nas áreas de Estruturas de Concreto e Materiais, e Construção Civil. Esta é uma oportunidade a ser utilizada por indústrias, empresas, universidades, instituições de pesquisa, pesquisadores e profissionais que desejem promover seus trabalhos e produtos em desenvolvimento. As instruções para submissão estão detalhadas na página de Internet do IBRACON.

Uma discussão é recebida não mais de 3 meses após a publicação do artigo ou nota técnica. As instruções para submeter uma discussão estão detalhadas na página de Internet do IBRACON. A discussão deve se limitar ao tópico abordado no artigo publicado e não pode ser ofensivo. O direito de resposta é garantido aos autores. As discussões e réplicas são publicadas nos números subseqüentes da revista.

Acesso via Internet

Página da Revista IBRACON de Estruturas e Materiais em http://www.ibracon.org.br

Assinatura

Todos os associados do IBRACON têm livre acesso ao conteúdo do periódico através da Internet. Não associados têm acesso limitado ao material publicado, mas podem adquirir números isolados pela Internet. O financiamento para suporte à revista é provido pelo IBRACON e por agências de financiamento à pesquisa. A revista não receberá qualquer tipo de anúncio privado que possa prejudicar a credibilidade da publicação.

Fotocópias

Fotocópias no Brasil, A Lei Brasileira de Direitos Autorais é aplicada a usuários no Brasil. O IBRACON detém os direitos autorais das contribuições na revista a menos que haja informação em contrário no rodapé da primeira página da contribuição. Onde o IBRACON detém os direitos autorais, autorização para fotocopiar itens para uso interno ou pessoal, ou uso interno ou pessoal de clientes específicos, é concedida para bibliotecas e outros usuários registrados no IBRACON.

Direitos autorais

Todos os direitos, inclusive tradução são reservados. Sob a Lei de Direitos Autorais No. 9610 de 19 de fevereiro de 1998, exceto qualquer acordo para fins de pesquisa ou estudo privado, crítica ou revisão, nenhuma parte desta publicação pode ser reproduzida, arquivada em sistema de busca, ou transmitida em qualquer forma ou por qualquer meio eletrônico, mecânico, fotocópia, gravação ou outros, sem a autorização prévia por escrito do IBRACON. Solicitações devem ser encaminhadas ao IBRACON:

IBRACON

Rua Julieta do Espírito Santo Pinheiro, nº 68 , Jardim Olímpia,
São Paulo, SP –Brasil CEP: 05542-120
Fone: +55 11 3735-0202 Fax: +55 11 3733-2190

E-mail: arlene@ibracon.org.br.

Aviso Legal

Artigos e outras contribuições e declarações feitas ou opiniões expressas aqui são publicadas com o entendimento que os autores da contribuição são os únicos responsáveis pelas opiniões expressas neles e que sua publicação não necessariamente reflete o apoio do IBRACON ou da revista.

Diretoria

Diretoria
Biênio 2013/2015

Diretor Presidente
Túlio Nogueira Bittencourt

Assessores da Presidência
Augusto Carlos de Vasconcelos
José Tadeu Balbo
Selmo Chapira Kuperman

Diretor 1º Vice-Presidente
Julio Timerman

Diretor 2º Vice-Presidente
Nelson Covas

Diretor 1º Secretário
Antonio Domingues de Figueiredo

Diretor 2º Secretário
Arcindo Vaqueiro Y Mayor

Diretor 1º Tesoureiro
Claudio Sbrighi Neto

Diretor 2º Tesoureiro
Carlos José Massucato

Diretor de Marketing
Hugo da Costa Rodrigues Filho

Diretor de Eventos
Luiz Prado Vieira Júnior

Assessor de Eventos
Maurice Antoine Traboulsi

Diretor Técnico
Inês Laranjeira da Silva Battagin

Diretor de Relações Institucionais
Ricardo Lessa

Diretor de Publicações e Divulgação Técnica
Paulo Helene

Diretor de Pesquisa e Desenvolvimento
Ana Elisabete Paganelli Guimarães A. Jacintho

Diretor de Cursos
Iria Lícia Oliva Doniak

Diretor de Certificação de Mão-de-obra
Roseni Cezimbra

Conselho Diretor
Biênio 2013/2015

Sócios Titulares Individuais

Inês Laranjeira da Silva Battagin
Cláudio Sbrighi Neto
Ana Elisabete Paganelli Guimarães A. Jacintho
Augusto Carlos de Vasconcelos
Nélson Covas
Vladimir Paulon
Antonio Laranjeiras
Enio Pazini Figueiredo
Júlio Timermam
Luis Prado Vieira Júnior

Sócios Titulares Mantenedores e Coletivos

ABCP – Associação Brasileira de Cimento Portland
POLI-USP – Escola Politécnica da Universidade de São Paulo
IPT – Instituto de Pesquisas Tecnológicas de São Paulo
L. A. FALCÃO BAUER
FURNAS
ABCIC – Associação Brasileira da Construção Industrializada em Concreto
GERDAU
ABESC – Associação Brasileira das Empresas de Serviços de Concretagem
CNO – Companhia Norberto Odebrecht
OTTO BAUMGART

Conselheiros Permanentes

Eduardo Antonio Serrano
Paulo Helene
Ronaldo Tartuce
Rubens Machado Bittencourt
Selmo Chapira Kuperman
Simão Priszkulnik

Acknowledgements

Acknowledgements / Agradecimentos

We acknowledge the following members for the collaboration in the reviewing process of the present and future volumes of the IBRACON Structures and Materials Journal.

Agradecemos a colaboração dos membros a seguir por sua participação no processo de avaliação deste e de futuros volumes da Revista IBRACON de Estruturas e Materiais.

Adriana Aparecida Ambrosio de Souza
Aldo Giuntini de Magalhães
Alexandre Duarte Gusmão
Aline Barboza
Almir Sales
Ana Catarina Evangelista
Ana Elisabete Paganelli Guimarães de Ávila Jacintho
André Teófilo Beck
Andriei José Beber
Anne Neiry de Mendonça Lopes
Ariela da Silva Torres
Armando Lopes Moreno Junior
Arnaldo Manoel Pereira Carneiro
Bernardo Fonseca Tutikian
Bruno do Vale Silva
Caio Gorla Nogueira
Caroline Luz
Cesar Fabiano Fioritti
Charlei Marcelo Paliga
Cintia Maria Ariani Fontes
Claudio Sbrighi Neto
Claudius de Sousa Barbosa
Daniel Veras Ribeiro
Dênio Ramam Carvalho de Oliveira
Dyorgge Silva
Edgar Bacarji
Edna Possan
Estela Oliari Garcez
Fábio Luís Gea dos Santos
Fernando Menezes Almeida Filho
Fernando Pelisser
Geilma Lima Vieira
Gerson Moacyr Sisniegas Alva
Gibson Rocha Meira
Gilson Natal Guimarães
Giovanna Oyamada
Giuliana Furtado Franca Bono
Guilherme Chagas Cordeiro
Gustavo Henrique Siqueira
Haroldo Bernardes
Humberto Varum
Ivo José Padaratz
Jardel Pereira Gonçalves
Jasson Rodrigues Figueiredo Filho
Jean Marie Désir
João Batista Marques de Sousa Junior
João Luiz Calmon Nogueira da Gama
João Rossignolo
Jorge Akasaki
José Julio de Cerqueira Pituba
José Luiz Pinheiro Melges
José Luiz Pinheiro Melges
José Marcio Calixto
José Renato Pessoa
José Tadeu Balbo
Karoline Moraes
Leandro Mouta Trautwein
Lidia Domingues Shehata
Luciana Tiemi Kataoka
Luísa Andréia Gachet Barbosa
Luiz Carlos de Almeida
Luiz Roberto Prudencio Junior
Marcelo Augusto da Silva Machado
Marcelo Henrique Farias de Medeiros
Maria Teresa Barbosa
Marta de Souza Lima Velasco
Maryangela Geimba de Lima
Mauricio de Pina Ferreira
Mauro de Vasconcelos Real
Mônica Leite
Mônica Pinto Barbosa
Nicole Hasparyk
Osvaldo Luís Manzoli
Paulo Andery
Paulo César Correia Gomes
Paulo Roberto Lima
Philippe Gleize
Rafael Giuliano Pileggi
Ricardo Amorim Einsfeld
Roberto Carlos Pavan
Roberto Chust de Carvalho
Roberto Dalledone Machado
Roberto Pettres
Rodrigo Gustavo Delalibera
Rogério Cattelan Antocheves de Lima
Ronald José Ellwanger
Ronaldo Barros Gomes
Ronaldson José de França Mendes Carneiro
Rosa Cristina Cecche Lintz
Selmo Kuperman
Sergio Hampshire de Carvalho Santos
Sérgio Percival Baroncini Proença
Sidiclei Formagini
Turibio José da Silva
Valdir Pignatta e Silva
Virgínia Maria Rosito d´Avila
Vladimir Antonio Paulon
Vladimir Guilherme Haach
Vladimir José Ferrari
Wayne Santos de Assis
William Taylor Matias Silva

Volume 7, Number 6 (December 2014) p. 905-912 • ISSN 1983-4195
REVISTA IBRACON DE ESTRUTURAS E MATERIAIS
IBRACON STRUCTURES AND MATERIALS JOURNAL

Study of peanut husk ashes properties to promote its use as supplementary material in cement mortars

Estudio de propiedades de las cenizas de cáscaras de maní para promover su uso como material suplementario en morteros cementicios

J. KREIKER [a]
jkreiker@ceve.org.ar

C. ANDRADA [b]
carina_andrada@hotmail.com

M. POSITIERI [b]
mpositieri@gmail.com

M. GATANI [a]
marianagatani@ceve.org.ar

E. Q. CRESPO [c]
equintana97@gmail.com

Abstract

The properties of peanut husk ashes as a potential supplementary material in cement mortars were studied in the laboratory. The ashes were prepared in an electric furnace at 500, 650 and 800 ºC during 180 minutes and used without further treatment. The characterization of ashes includes X-Ray fluorescence, X-Ray diffraction, SEM, and determination of pozzolanic activity by conductivity. The ashes were tested in mortars as partial substitute of Portland cement, in a rate of 15 % of substitution. The compression strength of mortars was evaluated between 7 and 120 days, for probes prepared using a proportion of cement:sand of 1:3 on weight with water/cement ratio of 0,5 v/v. It was observed that the calcinations conditions influenced the behavior of the ashes, giving better results the ashes obtained at 500 ºC. The compression tests showed values near to 70% at 7 days but higher than 80% after 28 days for mortars prepared with ashes, respect to the cement mortar reference.

Keywords: peanut husk ashes, supplementary materials for cement mortar.

Resumo

Se estudiaron en el laboratorio las propiedades de las cenizas de cáscaras de maní como un potencial material suplementario para morteros de cemento. Las cenizas fueron preparadas en un horno eléctrico a 500, 650 y 800 °C durante 180 minutos y utilizadas sin ningún acondicionamiento posterior. La caracterización de las cenizas incluye Fluorescencia de Rayos-X, Difracción de Rayos-X, Microscopia Electrónica de Barrido (SEM) y determinación de la actividad puzolanica por conductimetria. Las cenizas fueron ensayadas en morteros reemplazando un 15% de este material por cemento Portland. Se prepararon probetas usando una proporción cemento:arena 1:3 en peso con una relación agua/cemento 0,5 v/v. Las probetas fueron ensayadas para determinar la resistencia a la compresión a edades entre 7 y 120 días. Se observó que las condiciones de calcinación de las cáscaras de maní influyen en el comportamiento de las cenizas, siendo 500 °C la temperatura óptima de calcinación. Los ensayos de resistencia a la compresión arrojaron valores cercanos al 70 % respecto del patrón a los 7 días y mayores al 80% luego de 28 días para morteros preparados con cenizas.

Palavras-chave: cenizas de cáscaras de maní, material suplementario para morteros de cemento.

[a] *Experimental Centre for Economic Housing (CEVE) – National Council for Scientific and Technological Research (CONICET) – Economical Housing Association (AVE), Córdoba, Argentina;*
[b] *Center for Research, Development and Transfer of Materials and Quality (CINTEMAC), National Technological University, Córdoba Regional Faculty (UTN-FRC), Córdoba, Argentina;*
[c] *National Technological University, Córdoba Regional Faculty (UTN-FRC), Córdoba, Argentina.*

Received: 10 Feb 2014 • Accepted: 15 Sep 2014 • Available Online: 01 Dec 2014

© 2014 IBRACON

1. Introduction

Peanut husks (Arachis Hypogaea) are an abundant agroindustrial waste in the region of Córdoba, Argentina, concentrating the 95% of the country's peanut production. Almost 1 million tons were produced in 2011, generating around three hundred thousand tons of husks as waste (Cámara Argentina del Maní, 2012) [1]. Nowadays, peanut husks are used in the elaboration of panels [2], production of feed lots and for the manufacture of activated carbon [3]. The main use is as fuel in industrial processes, which generates an important amount of ashes used as landfill without added value, estimating a production of thirty tons per day of waste [4].

The cement industry is considered as highly contaminating, and several developments have been achieved in order to make the technologies of construction involving this binder material becomes more sustainable [5]. In this sense, the use of supplementary materials for cement has been widely recognized as a sustainable alternative. In general, ashes from industrial processes (fly ashes, silica fume, slag, etc.) have demonstrated very good properties as pozzolans, because they exhibit binder behavior. This sort of ashes have been studied for many years with interesting results regarding the physical and mechanical properties and the durability of mortars containing these materials as supplement [6, 7, 8, 9, 10, 11].

In addition, ashes from agro industrial wastes are also being used as supplementary binder materials, and many research works have been done upon these wastes, for instance rice husk ashes [12, 13, 14, 15, 16] , wheat straw ashes [17] , sugarcane bagasse ashes [18, 19, 20], palm oil ashes [21], dust wood ashes [22]. It has been demonstrated that cement added with these ashes have a similar or better behavior than normal concrete at ages beyond 28 days.

It is well known that the pozzolanic properties of the ashes will depend on its chemical composition, parameter associated to the nature of agro industrial waste, and to its morphology and crystallographic properties, parameters associated to its burnt conditions[23].

Very few studies have been done upon peanut husk ashes. Isolated examples explore the use of this waste for heavy metal removal [24], or in degumming and refining soy oil [25]. Also, none significant literature was found about its potential use as a supplementary material for mortars, finding only a description as a pozzolans type N [26] but with limited information about its characterization. The objective of this study was to characterize chemical and morphologically the peanut husk ashes prepared in laboratory controlled conditions and determine its pozzolanic behavior, in order to evaluate its potential use as a supplementary material for cement of mortars. This work includes the physical, chemical and morphological characterization of ashes prepared at 500, 650 and 800 ºC, the pozzolanic behavior for conductimetric method and the compression strength tests of mortars resulting of the replacement of a 15% of cement with ashes at different ages, for corroborate the results.

2. Materials and experimental program

2.1 Materials used

The peanut husks were provided by Maglione e Hijos S.R.L, from its production plant located on Las Junturas, Córdoba, Argentina. The husks were milled and only those retained on the 1 mm sieve were used. The Ashes were prepared calcinating husks in an electric furnace at 500, 650 y 800 ºC (PH-1, PH-2, PH-3, respectively), with a heating rate of 10 ºC/min, and kept at the scheduled temperature for 3 hours. At the end of this process, the ashes were cooled by opening the oven until reaching the room temperature, and used without further conditioning. Ordinary Portland Cement (OPC) type CPF 40 provided by Holcim conforming IRAM 50000 norms was used. Grade river sand with fineness modulus of 4.98 determined according IRAM 1505 norms, and specific gravity of 2.65 determined according IRAM 1520 norms, was aggregated. $Ca(OH)_2$ Anhedra (analytical grade) and H_2O MilliQ quality were used for conductivity tests. Cement mortars were made using water from line supply, without purification.

2.2 Testing procedures

2.2.1 Physical and chemical analysis of ashes

The ashes particle size distribution was determined by gravimetric assay according to IRAM 1505 norms, using a 0.001 g precision balance. The ashes specific gravity was determined according IRAM 1520 norms. The ashes mineralogical analysis was carried out by X-Ray diffraction (XRD) analyzing the samples prepared in random mounts in a Phillips X-Pert PRO PW3040/60 diffractometer, with Cu Kα X-ray radiation, Si monochromator, at 40 Kv and 30 mA, step scan at 0.3º/min and step size of 0.02 º 2θ. Peaks assignment was made by comparison using the data base of the software X`Pert Highscore . Microstructure morphology was observed with a scanning electron microscopy (SEM) using a *FE-SEM Σigma* apparatus. Chemical composition was determined by X-Ray fluorescence (XRF) using a Phillips PW 1400 equipment, and comparing the intensities of signals with standard references samples.

2.2.2 Pozzolanic activity by conductimetric test

The pozzolanic activity of ashes was evaluated according to the basic method which consist in evaluating the conductivity of a $Ca(OH)_2$ solution in presence of the pozzolanic material and the evolution of this parameter on time [27]. We used the modification proposed by Payá et al. [28] for ashes with high content of ions, which evaluate the conductivity by a period of 600 h. For this experience 200 mL of a $Ca(OH)_2$ solution with a conductivity value of approximately 7 mS/cm was kept at 40 ±1 ºC with continuous stirring. Then, 5 g of pozzolanic material were added to the solution, and the conductivity was registered over time (sample A). On the other hand, the same experience was carried out evaluating the conductivity of the pozzolanic material in MilliQ water (blank B). Finally the pozzolanic behavior of the material was estimated analyzing the graphic obtained by the difference between sample A and blank B (A-B).

2.2.3 Compressive strength

Compressive strength tests were carried out according to IRAM 1622 norms. Prismatic test specimens of 4x4x16 cm were made by replacing 15% of cement with previously described ashes: PH-1, PH-2, and PH-3. A binder:sand proportion of 1:3 on weight and

Figure 1 – Particle size distribution of peanut husk ashes

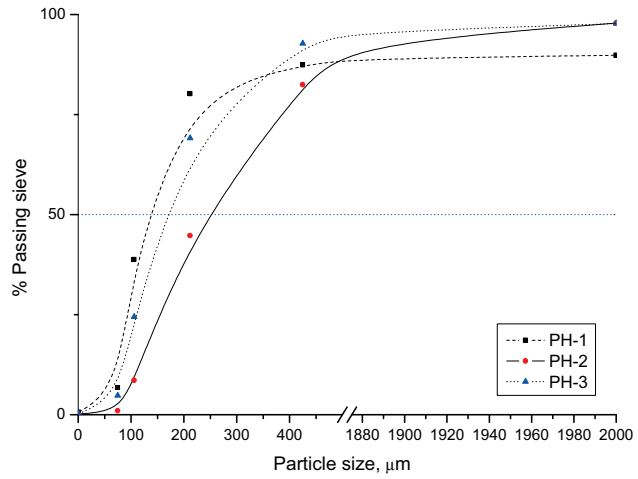

a water/cement (W/C) rate of 0.5, was used. The specimens were compacted using a vibrating table, and then covered overnight with wet plastic sheets. After twenty four hours, the probes were removed from their molds. Finally the probes were cured in water at 20 ºC until the point of test ages of 7, 14, 28, 60, 90 and 120 days. Compressive strength tests were carried out in a 30 t essay press, where each specimen was compressed and the maximum sustained load was registered. Three specimens were tested at each testing age and the average value was reported. The data is accepted when measurements have a CV<5% (coefficient of variation), and we apply de Grubbs Contrast to discard suspected point with a confidence interval of 95%.

Figure 3 – X-Ray diffraction of PH-2

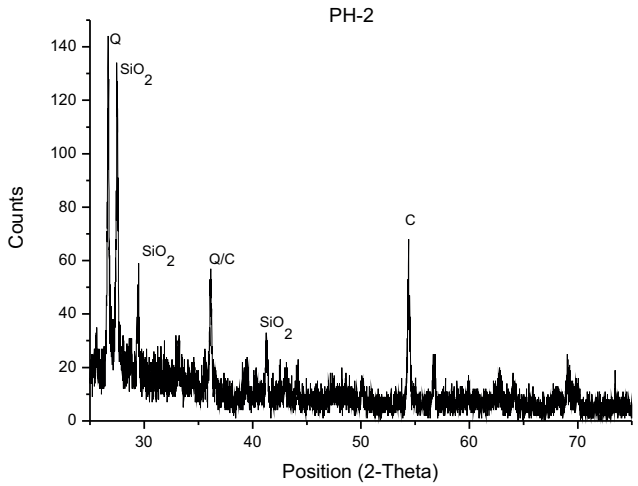

3. Results and discussions

3.1 Physical and chemical analysis of ashes

The ashes particle size distribution curves are shown in Fig. [1]. It is noted that the particles of ashes without grind, have a heterogeneous distribution and that the major percentage is around 100 and 200 mm. The specific gravity test of ashes PH-1, PH-2, PH-3 showed an average value of 0.39 g/cm^3.

The mineralogical analysis of ashes carried out by X-ray diffraction is shown in Fig. [2], Fig. [3] and Fig. [4], for PH-1, PH-2 and PH-3 respectively. Small quantities of crystal-phases, as Quartz (Q), Cristobalite

Figure 2 – X-Ray diffraction of PH-1

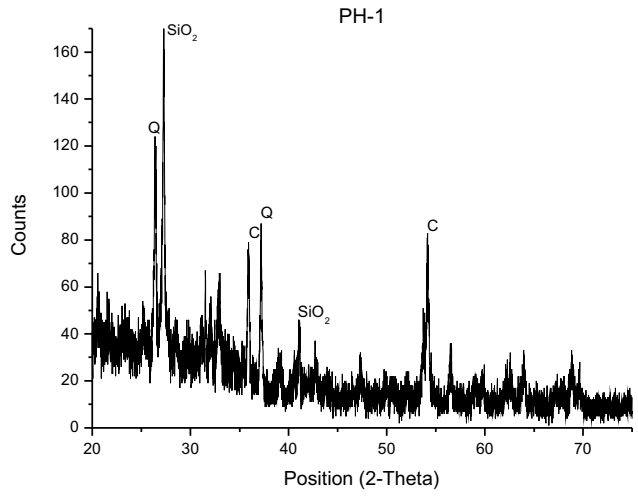

Figure 4 – X-Ray diffraction of PH-3

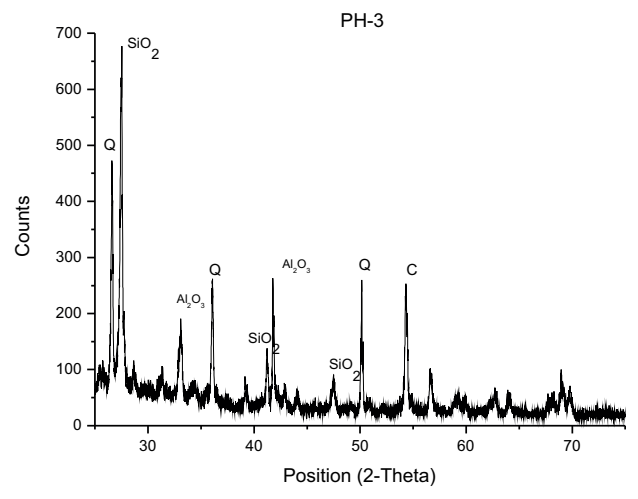

Figure 5 – SEM of PH-1 at 700 X and 10 KX

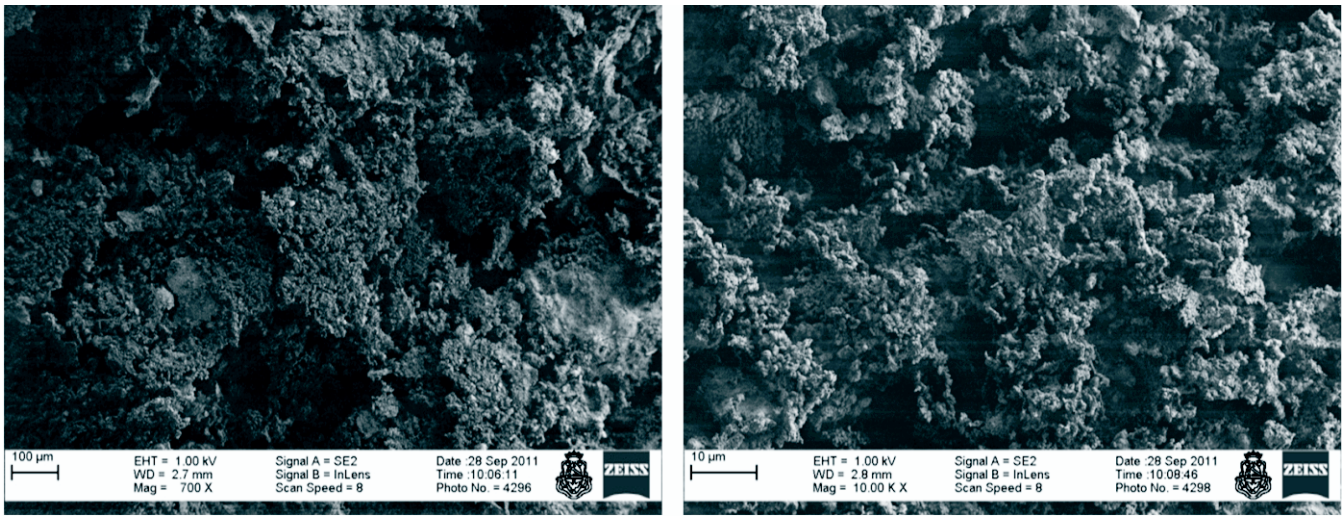

(C) and SiO_2, are present in all cases, but their intensities are more significant at 800 ºC, which is consistent with the reported by Martirena-Hernandez et al (2000) [13]. Crystal phases of Al_2O_3 were observed in PH-3 but not in PH-1 and PH-3. There are no significant crystallographic pattern differences between ashes obtained at 500 ºC and 650 ºC.

Fig. [5] shows the PH-1 SEM microscopy images with a 700 X and 10 KX magnifications. Due to the similar superficial characteristics of PH-2 and PH-3 with PH-1, their images are not shown. It is seen that unmilled ashes exhibit a heterogeneous surface at 700 X. And even presenting particles without a defined shape, they maintain some characteristic such as the husks structure. At 10 KX a more homogeneous surface with micropores is observed.

Table 1 – Composition % by mass, of ashes PH-1, PH-2 and PH-3

Oxides	PH-1	PH-2	PH-3
S_iO_2	34,1	35,8	36,6
A_i2O_3	11,6	10,8	10,3
F_e2O_3	1,9	1,95	2,2
CaO	13,1	13,7	18,1
K_2O	7,1	7,3	6,4
MgO	7,3	5,7	7,2
MnO	0,2	0,3	0,3
Sr ppm	570	555	548
Pb ppm	28	17	16
Zn ppm	168	151	143
Cu ppm	28	21	25
Ni ppm	8	6	6
Cr ppm	16	15	15
Ba ppm	1050	1059	1015

Chemical composition of ashes determined by X-Ray fluorescence is presented in Table [1].

The sum of silica, aluminium, and iron oxides contents is in all cases almost a 50% of the total, corresponding to a type C pozzolan, according to ASTM-C618 norms. The content of alkali oxides K_2O and Na_2O is higher than 1.5% permitted by norm, making it not advisable for some applications, because of the undesirable alkali-aggregate reaction in cement mortars [29, 30]. On the other hand, the high content of MgO might give expansive reactions [31], an undesirable property of cement mortars. The main disadvantage of this type of ashes is the low content of SiO_2 in comparison with other ashes from burnt agro-industrial wastes [32].

3.2 Pozzolanic activity by conductimetric test

The pozzolanic behavior of ashes was rudely determined by the reactivity in an unsaturated lime solution at 40 ºC. The graphics of conductivity versus time for PH-1, PH-2 and PH-3 in lime solution (A), in H_2O (B), and the difference between both graphics (A-B) are presented in Fig. [6], Fig. [7] and Fig. [8] , respectively. An important increment on conductivity for ashes in pure water is observed, probably due to the presence of CaO, K_2O, and other ions in smaller proportions, which are dissolved in water in these conditions. This effect was taken in account in the estimation of conductivity decrement for lime solution after the reaction with ashes. The difference between these graphics (A-B) showed clearly the reaction of consumption of Ca^{++}, typical for pozzolanic materials. In the period of time evaluated, the conductivity decreased up to 1-2 mS/cm in all cases, but it is worth noting a little difference on PH-1 conductivities, which might be attributed to a better pozzolanic behavior for this ashes prepared at 500 ºC, Fig. [9]. These observations agree with X-Ray diffraction graphics, which indicate the bigger

Figure 6 – Conductivity of ashes, graphics (A-B)

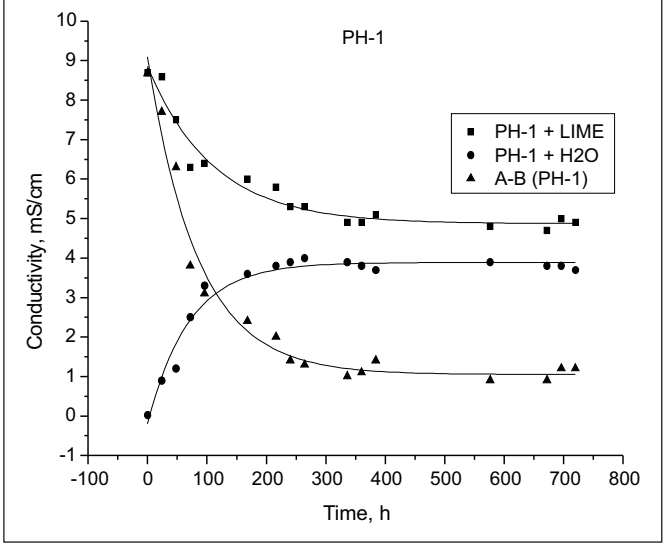

Figure 8 – Conductivity of ashes, graphics (A-B)

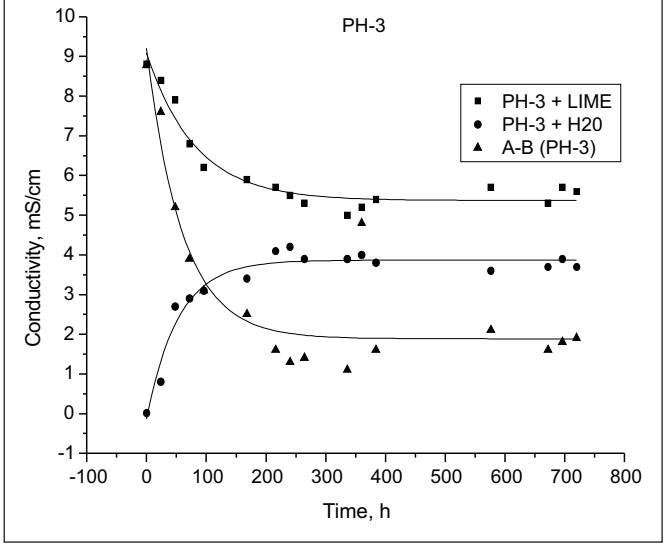

presence of amorphous silica at low temperatures meaning a better pozzolanic behavior, as was also reported by other authors[33].

3.3 Compressive strength

The Table 2 shows the results of compressive strength tests for mortars made with PH-1, PH-2 and PH-3, together with the specimen without ashes, M0.

The behavior of compressive strength is similar for MPH-2 and MPH-3 between 7 and 120 days. The compressive strength of MPH-1 is slightly minor than the others at shorter times, improving its behavior in longer periods, reaching a greater value than M0 at day 120, Fig. [10]. The Fig. [11] shows the behavior of mortars and the compression strength limit established by IRAM 1654 norms, for mortars with addition of pozzolanic material. The norm establishes as an acceptable behavior a value of 75% strength respect to reference mortar M0. MPH-2 and MPH-3 showed acceptable values, above 75% respect to M0 in all tests, with a behavior near to 85% at day 120. Despite that MPH-1 showed a value below 75% at day 7, its behavior at older ages increased significantly, reaching a value higher than M0 at day 120.

Figure 7 – Conductivity of ashes, graphics (A-B)

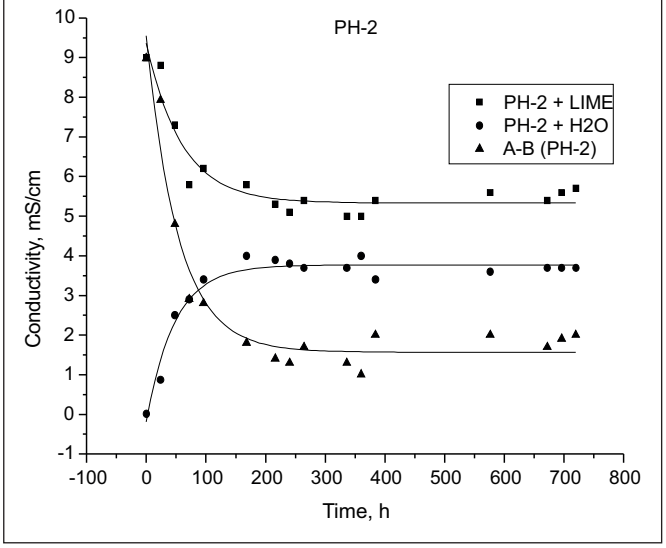

Figure 9 – Conductivity of ashes, graphics (A-B)

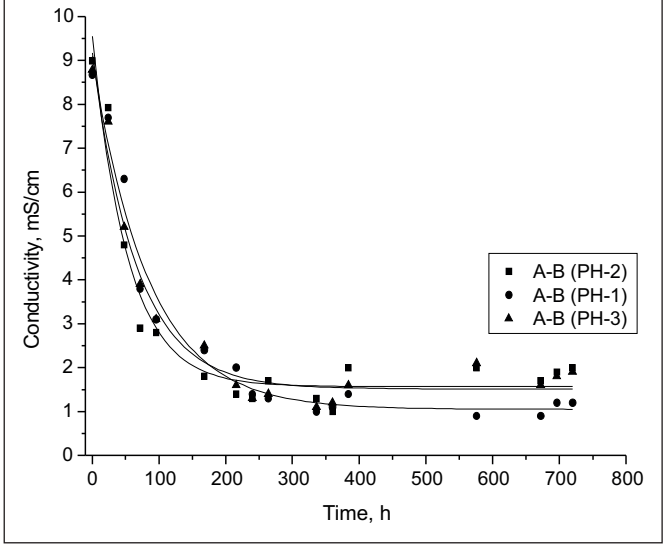

Table 2 – Compressive strength of probes at different ages

	Compressive strength (Mpa) at different ages (days)					
	7	14	28	60	90	120
M0	18.3	22.3	24.4	28.2	29.0	30.3
MPH-1	12.2	17.1	21.4	23.8	24.8	32.6
MPH-2	14.2	17.7	19.7	24.7	25.8	24.6
MPH-3	14.1	17.2	19.4	27.7	25.1	23.9

4. Conclusions

The ashes of peanut husks might be used as supplementary material for cement, because they have a chemical composition according to pozzolans type C, although the alkali content is a little high and could give unwanted reactions of the type alkali-aggregate in cement, therefore levels of addition should be low. The morphology of ashes depends on the burnt temperature of husks, therefore it is advisable to control this parameter to avoid the formation of crystalline phases in order to increase the reactivity of the ashes, being 500 ºC a suitable temperature for the calcinations. The ashes can be added to cement up to 15% without altering the mechanical properties of compressive strength of mortars and keeping the values permitted by the norm for Argentina.

The addition of peanut husk ashes to local manufacture of cement is presented as a potential alternative to decrease the environmental pollution associated with the production process, also adding value to an abundant regional waste, providing important economic and environmental benefits.

Additional studies on the mechanical and physical properties of mortars added with different dosages of peanut husk ashes are being carried out, and will be published in the future.

5. Acknowledgements

The authors wish to thank to the Experimental Center for Economical Housing (CEVE), the National Council of Scientific and Technological Research (CONICET), the Center for Research, Development and Transfer of Materials and Quality (CINTEMAC), and the Córdoba Regional Faculty of the National Technological University (UTN-FRC). The authors would like to thank to Diego Aguero from the CINTEMAC, to Ing. Liz Sablé from UTN-FRC, and to Arq. Eugenia Sipowicz from CEVE.

6. References

[01] Cámara Argentina del Maní. http://www.camaradelmani.com.ar/es/novedades. [accessed May. 21, 2012]

[02] Gatani M, Argüello R, Sesin S. Effect of chemical treatments

Figure 10 – Compression strength of cement mortars substituted with ashes

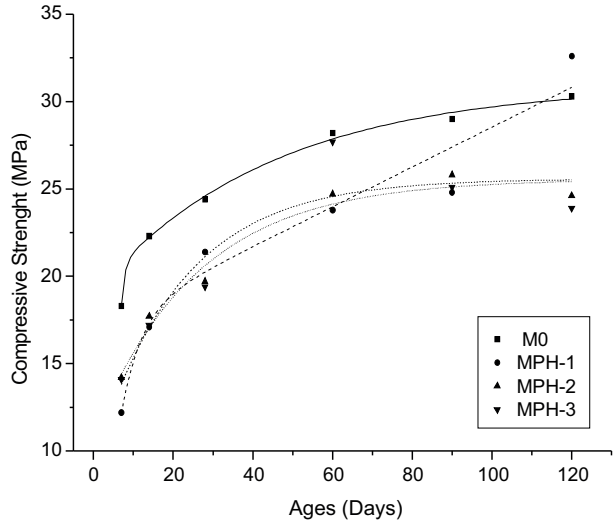

Figure 11 – Behavior of cement mortars substituted with ashes respect to M0

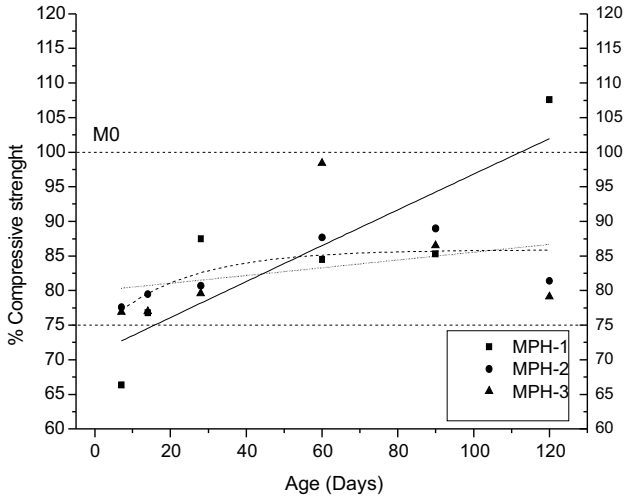

on the mechanical properties of peanut shell and cement blends. Materiales de Construcción, v. 60, n. 298, 2010; p. 137-47.

[03] Ravera MJA, Perez JD, Alonso R, Cotagro Coop. Agrop. Ltd. Procedimiento para obtener carbón activado y la instalación para llevarlo a cabo. AR Patent 45644A1, Novemeber 2005.

[04] Aceitera General Deheza. http://www.agd.com.ar/es/home.htm [accessed May. 21, 2011].

[05] Muller N, Harnish J. A blueprint for a climate friendly cement industry. Gland: WWF Lafarge Conservation Partnership 2008: 94p. http://assets.panda.org/downloads/english_report_lr_pdf.pdf {accessed Agost, 22, 2012).

[06] Hassan KE, Cabrera JG, Maliehe RS. The Effect of Mineral Admixtures on the Properties of High-Performance Concrete. Cement and Concrete Composites, v. 22, n.4, 2000; p. 267-271.

[07] Megat Johari MA, Brooks JJ, Kabir S, Rivard P. Influence of Supplementary Cementitious Materials on Engineering Properties of High Strength Concrete. Construction and Building Materials, v. 25, n. 5, 2011; p. 2639-2648.

[08] Shannag MJ. High Strength Concrete Containing Natural Pozzolan and Silica Fume. Cement and Concrete Composites, v. 22, n.6, 2000; p. 399-406.

[09] Lam L, Wong YL, Poon CS. Effect of Fly Ash and Silica Fume on Compressive and Fracture Behaviors of Concrete. Cement and Concrete Research, v. 28, n.2, 1998; p. 271-283.

[10] Papadakis VG, Antiohos S, Tsimas S. Supplementary Cementing Materials in Concrete: Part II: A Fundamental Estimation of the Efficiency Factor. Cement and Concrete Research, v. 32, n.10, 2002; p. 1533-1538.

[11] Papadakis VG, Tsimas S. Supplementary Cementing Materials in Concrete: Part I: Efficiency and Design. Cement and Concrete Research, v. 32, n.10, 2002; p. 1525-1532.

[12] Nair DG, Fraaij A, Klaassen AA, Kentgens APM. A Structural Investigation Relating to the Pozzolanic Activity of Rice Husk Ashes. Cement and Concrete Research, v. 38, n.6, 2008; p. 861-869.

[13] Cordeiro GC, Toledo Filho RD, Tavares LM, Fairbairn E, Hempel S. Influence of Particle Size and Specific Surface Area on the Pozzolanic Activity of Residual Rice Husk Ash. Cement and Concrete Composites, v. 33, n.5, 2011; p. 529-534.

[14] Kartini K. Rice ash pozzolanic material for sustainability. International Journal of Applied Science & Technology, v. 1, 2011; p. 169.

[15] Ganesan K, Rajagopal K, Thangavel K. Rice Husk Ash Blended Cement: Assessment of Optimal Level of Replacement for Strength and Permeability Properties of Concrete. Construction and Building Materials, v. 22, n.8, 2008; p. 1675-168.

[16] Chatveera B, Lertwattanaruk P. Evaluation of Sulfate Resistance of Cement Mortars Containing Black Rice Husk Ash. Journal of Environmental Management, v. 90, n.3, 2009; p. 1435-1441.

[17] Biricik H, Akoz F, Berktay I, Tulgar A .Study of Pozzolanic Properties of Wheat Straw Ash. Cement and Concrete Research, v. 29, n.5, 1999; p. 637-643.

[18] Martirena Hernandez J. F, Middendorf B, Gehrke M, Budelmann H. Use of Wastes of the Sugar Industry As Pozzolana in Lime-Pozzolana Binders: Study of the Reaction. Cement and Concrete Research, v. 28, n.11, 1998; p. 1525-1536.

[19] Frias M, Villar E, Savastano H. Brazilian Sugar Cane Bagasse Ashes From the Cogeneration Industry As Active Pozzolans for Cement Manufacture. Cement and Concrete Composites, v. 33, n. 4, 2011; p. 490-496.

[20] Ganesan K, Rajagopal K, Thangavel K. Evaluation of Bagasse Ash As Supplementary Cementitious Material. Cement and Concrete Composites, v. 29, n.6, 2007; p. 515-524.

[21] Foo KY, Hameed BH. Value-Added Utilization of Oil Palm Ash: A Superior Recycling of the Industrial Agricultural Waste. Journal of Hazardous Materials, v. 172, n. 2-3, 2009; p. 523-531.

[22] Cheah CB, Ramli M. The Implementation of Wood Waste Ash As a Partial Cement Replacement Material in the Production of Structural Grade Concrete and Mortar: An Overview. Resources, Conservation and Recycling, v. 55, n.7, 2011; p. 669-685.

[23] Martirena-Hernandez JF, Betancourt-Rodriguez S, Middendorf B, Rubio A, Martinez-Fernandez J, Machado Lopez J, Gonzales-Lopez R. Pozzolanic Properties of Residues of Sugar Industries. Materiales de Construcción, v. 50, n. 260, 2000; p. 71-78.

[24] Shih-Wei L, Chun-I L, LI-Hwa W. Kinetic study on lead (II) ion removal by adsorption onto peanut hull ash. Journal of the Taiwan Institute of chemical engineers, v. 42, n. 1, 2011; p. 166-72.

[25] Tse-Li L, Chun-I L. Performances of peanut hull ashes in bleacing water-degummed and alkali-refined soy oil. Journal of the Taiwan Institute of Chemical Engineers, v. 40, n.2, 2009; p. 168-73.

[26] Chaatveera B, Nimityongskul P. Use of coconut Husk Ash, Corn Ash and Peanut Shell Ash as Pozzolana. Journal of Science Technology, v. 16, n. 2, 1994; p. 1.

[27] Luxan MP, Madruga F, Saavedra J. Rapid Evaluation of Pozzolanic Activity of Natural Products by Conductivity Measurement. Cement and Concrete Research, v. 19, n. 1, 1989; p. 63-68.

[28] Paya J, Borrachero MV, Monzó J, Peris-Mora E, Amahjour F. Enhanced Conductivity Measurement Techniques for Evaluation of Fly Ash Pozzolanic Activity. Cement and Concrete Research, v. 31, n.1, 2001; p. 41-49.

[29] Gillot JE. Journal of Material in Civil Engineering, v. 4, 1995; p. 278.

[30] THAYLOR, H.F. Cement Chemistry. Ed. London Thomas Telford, 2 ed, 1997, 459p.

[31] Idorn GM. Expansive mechanisms in concrete. Cement and Concrete Research, v. 22, n. 6, 1992; p.1039-1046.

[32] Metha PK. Rice husk ash: a unique supplementary cementing material. Advances in Concrete Technology, v. 2, 1992; p. 407-431.

[33] Martirena-Hernandez JF, Betancourt-Rodriguez S, Middendorf B, Rubio A, Martinez-Fernandez J, Machado Lopez J, Gonzales-Lopez R. Pozzolanic Properties of Residues of Sugar Industries. Materiales de Construcción, v. 50, n. 260, 2000; p.71-78.

7. Norms

ASTM-C618 12a. American Society for Testing and Materials Standard Specification for Coal Fly Ash and Raw or Calcined Natural Pozzolan for Use in Concrete. ASTM-C618 annu. Book ASTM Stand. 04.02 (1997) 294-296.

IRAM 1505:2005 Instituto Argentino de Normalización y Certificación. Agregados. Análisis granulométrico. 12 Pages.

IRAM 1520:2002 Instituto Argentino de Normalización y Certificación. Agregados finos. Métodos de laboratorio para la determinación de la densidad relativa real, de la densidad relativa aparente y de la absorción de agua. 14 Pages.

IRAM 1622:2006 Instituto Argentino de Normalización y Certificación. Cemento Portland Métodos de determinación de las resistencias a compresión y flexión. 25 Pages.

IRAM 1654:2068 Instituto Argentino de Normalización y Certificación. Puzolanas. Métodos de ensayos generales. 32 Pages.

IRAM 50000:2010 Instituto Argentino de Normalización y Certificación. Cemento. Cemento para uso general. Composición, características. Evaluación de la conformidad y condiciones de recepción. 42 Pages.

Volume 7, Number 6 (December 2014) p. 913-921 • ISSN 1983-4195
REVISTA IBRACON DE ESTRUTURAS E MATERIAIS
IBRACON STRUCTURES AND MATERIALS JOURNAL

Watertightness in anti-flotation slabs. MIS-RJ Case

Estanqueidade de lajes de subpressão. Caso MIS-RJ




C. BRITEZ [a]
carlos.britez@concretophd.com.br

P. HELENE [b]
paulo.helene@concretophd.com.br

S. BUENO [c]
suelybueno@jkmf.com.br

J. PACHECO [d]
jessika.pacheco@concretophd.com.br

Abstract

It is common in coastal cities as Rio de Janeiro, that buildings located close to the shoreline have their basements below water table level. In most cases, the engineering solution for these buildings is to design a massive anti-flotation slab to satisfy, principally, the issues related to structural dimensioning and calculation hypothesis. On the other hand, the execution of this solution imply in significant construction problems related to reinforced concrete watertightness and durability. This paper presents a case study about challenges and solutions devised to execute an anti-flotation, 1m thick, 1200m³ reinforced concrete slab for the new Museu de Imagem e Som (MIS) – Sound and Image Museum, located at 50m from the seashore, at Copacabana in Rio de Janeiro, RJ. The results show that concrete proportions, concreting plan and pouring method adopted were decisive in obtaining a watertight structure, avoiding thus the employment of traditional waterproofing alternatives.

Keywords: anti-flotation slab, watertight concrete, watertight concrete structures, concrete at seashore.

Resumo

Tem sido comum em cidades litorâneas, como a do Rio de Janeiro, observar a construção de subsolos em edificações localizadas nas proximidades de orlas marítimas. Na maioria dos casos, a solução de engenharia envolvida nesses projetos é o uso de lajes de subpressão com o objetivo de garantir, principalmente, os aspectos relacionados com o dimensionamento estrutural e hipóteses de cálculo. No entanto, há complexidades significativas quanto à execução desse tipo de solução, no que tange aos aspectos de estanqueidade e durabilidade do concreto armado. Este artigo apresenta um estudo de caso sobre os desafios e as engenhosidades envolvidas para concretagem da laje de subpressão em concreto armado da nova sede do Museu de Imagem e do Som (MIS), com 1m de espessura e volume de 1200m³, situada a 50m da orla marítima, na região de Copacabana, Rio de Janeiro, RJ. Os resultados demonstraram que a composição do concreto, o plano de concretagem e os procedimentos executivos empregados foram decisivos para promover uma estrutura íntegra e com propriedades estanques, dispensando, nesse caso, alternativas tradicionais e convencionais de impermeabilização.

Palavras-chave: laje de subpressão, concreto estanque, estanqueidade estruturas de concreto, concreto em orla marítima.

[a] *Civil Engineering Construction Department at Escola Politécnica da Universidade de São Paulo. PhD Engenharia;*
[b] *Full Professor at Universidade de São Paulo. PhD Engenharia;*
[c] *Escritório Técnico Julio Kassoy e Mario Franco Eng. Civis Ltda. (JKMF);*
[d] *PhD Engenharia.*

Received: 13 Mar 2014 • Accepted: 19 Sep 2014 • Available Online: 01 Dec 2014

© 2014 IBRACON

1. Introduction

To make the new building for the Museu de Imagem e do Som (MIS) one more international architectural landmark for Rio de Janeiro city, known by the creativity of its artistic expressions and by the richness of its musical rhythms, the Secretaria de Estado e Cultura do Rio de Janeiro, together with Fundação Roberto Marinho (FRM), promoted recently an important international architectural contest, to choose a futurist design. The American architectural bureau Diller Scofidio + Renfro won the contest among other seven architectural bureaus selected for the final decision. The design was developed in Brazil by the renowned bureau Índio da Costa Arquitetura, Urbanismo, Design e Transporte (ICA).

Located at Atlântica avenue, at Copacabana, just at 50m from the beach, the new MIS headquarters will substitute the old museum premises. The MIS, opened in 1965, is installed simultaneously in two places, at Praça XV, located in downtown Rio, and at Lapa. The new building will also host the Carmen Miranda Museum, which is now located at Flamengo neighborhood (CORBIOLI, 2011)[1].

It should be noted that the American architects proposed a museum as a vertical boulevard, with seven stories, a continuous external promenade and a display of sequential ramps and floors. The building will have a total area of seven thousand square meters approximately, including foyers, box office, wardrobe, exposition rooms, auditorium, didactical activities room, shop, cafeteria, panoramic restaurant, bar, terrace, piano bar, belvedere, administration areas, storage spaces for collections, parking and load/unload facilities. The new MIS premises, shown in Figure 1, are being built by the construction company Rio Verde. Construction works are being managed by the company Engineering.

The building has 2 basement floors and a technical mezzanine also located below grade, besides the superior floors. As the building is being built very close to the sea shore (50m), very special procedures and engineering techniques were required to design a watertight anti-flotation slab, with considerable volume (1200m³) and thickness (1m).

Other problems are, besides ensuring technical parameters related to watertightness and high concrete strength (characteristic compressive strength was specified at f_{ck} 50MPa at 28 days), weather factors (hot weather, concreting commonly occur at temperatures about 35ºC) and logistic (the concrete batch plant is approximately 30km afar from the working site, mixing trucks drive through a tourist route, with heavy traffic. At working days and hours, mixing trucks take at last 1 hour to transport the concrete).

The anti-flotation slab was executed during November 2012 and January 2013, at an elevation about 10m under sea level. Concrete mix proportions, as well as some execution details, mainly those related to watertightness will be described below. A substantial part of procedures employed is included in Brazilian current standards (ABNT NBR 6118:2007 [2]; ABNT NBR 12655:2006 [3]; ABNT NBR 14931:2004 [4]) and in international literature (KOSMATKA; WILSON, 2001 [5]; KENNEDY, 2005 [6]; LAMOND; PIELERT, 2006 [7]). However, most part of procedures was based on directives supported by the reference paper published by Helene, Terzian e Sardinha (1980) [8].

2. Watertightness concept

It is important to explain that concrete, as a material, is capable of promoting sufficient conditions for a very low permeability which means that it can be considered watertight. As it can promote an efficient barrier against water penetration, concrete is largely employed to build large reservoirs, pools, dams, water and effluent treatment plants, etc.

Nevertheless, most problems of employing this potentially "watertight" material, arose from the difficulty of obtaining the watertightness of structures, which depends not only on the material, but mainly on proceedings. Thus, besides a material of adequate quality, the procedures related to good engineering practices are needed to avoid honeycombs, defective compaction, unpredicted fissures, construction joints or defective joints through which water may percolate.

The watertightness of a concrete structure may be understood as the capacity of this structure to avoid percolation of liquids through

Figure 1 – Future MIS headquarters, Copacabana, Rio de Janeiro, RJ, Images by Diller Scofidio + Renfro for the international contest. (Courtesy of ICA)

walls, joints or slabs that contain those liquids. It mainly involves issues related to good construction practices and requiring special care during execution.

Thus, it can be understood that to build a successful, watertight anti-flotation slab, at least two aspects shall be carefully and deeply considered:

- The first one is related to the material (concrete) that shall be resistant, sound, of very low permeability and durable;
- The second one is related to special cares and procedures that constitute the set of good construction practices in order to get a final watertight structure.

However, experience has proven that bigger and most frequent failures in liquid retaining structures are related more to execution techniques and procedures (good construction practices) than to material quality.

3. Design data, materials and procedures adopted for MIS

3.1 Historical and basic design data

Initially, the solution proposed by the structural design bureau, Escritório Técnico Julio Kassoy e Mario Franco Eng. Civis Ltda. (JKMF), for MIS foundation, consisted in diaphragm walls for lateral retention, cast-in-place piles with steel profiles and structure construction downwards from grade up to reach foundation level, when direct foundations, columns and a 30cm thick anti-flotation slab with tiebacks anchors into earth. Notwithstanding, it was verified that this procedure would be rather slow.

Them it was studied a second alternative, drilling provisional tiebacks anchored to the soil in three lateral faces of the site, where no buildings existed at neighbor land plots. In this way it would be possible to reach the foundation level and build the structure upwards at a much higher speed. Main columns would have direct foundations. This method was adopted and at one of the lateral sides of the plot (where neighbor buildings existed), provisional slabs were built working as horizontal beams, which would enable proceed with excavation as those slabs attained required design strength.

As the site is very close to the sea, and the foundation design was given a prize (Prêmio Milton Vargas 2012), during excavation procedures the well points for water table depressing had several clogging problems and also soil breakouts with the consequent flooding of the excavation. Under these conditions it became more and more unfeasible the execution of direct foundations, as the soil did not remain stable when excavated to execute the foundations. The designed method became a painful procedure.

It was then decided to study a radier type foundation, excavating the whole construction site to a single level, with a 1,0m thick slab that would work as a foundation slab for the columns as well as an anti-flotation slab. It was verified too that 1,0m thickness will be insufficient for all “embedded footings” inside this anti-flotation slab. Even with a concrete strength of 50MPa, stresses inside the slab would be too high for that thickness. To solve this problem, the inferior radier elevation was lowered and the columns with higher loads had their footing height increased up to 47cm. The cross section of some columns was also increased in order to reduce the slab punching shear stresses. As this was the adopted solution, the major challenge consisted in finding a proceeding that could assure concrete integrity, avoiding pathological manifestations that may jeopardize the stress distribution and the structural performance.

In short, the MIS anti-flotation slab was conceived as a trapeze in plan view, measuring approximately 51m long (parallel to Atlântica Avenue), with sides 25m and 20m, respectively. The four sides are embedded into diaphragm walls with variable thickness depending on direction, neighbor constructions and soil conditions. The characteristic design compressive concrete strength is f_{ck} 50MPa, the slab volume is approximately 1200m³ and the mean thickness is 1m. The slab was reinforced as a “cage” and at intermediate thirds in height (at 33cm each), a complementing reinforcing mesh was added, having 1 ø 12,5mm each 30cm of spacing in both directions. The steel/concrete ratio of the anti-flotation slab excepting footing and complementary reinforcing is 72kg/m³. Considering footing and already mentioned complementing reinforcing, this ratio increases to 105kg/m³.

3.2 Concrete mix and employed ingredients

The concrete mix for the anti-flotation slab was developed by PhD Engenharia (Concrete technology consultancy company for Fundação Roberto Marinho) from an extensive laboratory program, jointly with Votorantim Cimentos / Engemix S. A. (concrete supplier). Prototypes were tested at construction site in secondary structures, in order to verify fresh concrete conditions and hardened concrete strengths. The standard ABNT NBR 12655:2006 “Concreto de cimento Portland – preparo, controle e recebimento – Procedimento” prescriptions were followed, specially item 5.2.2.2 “Condições especiais de exposição”, as well as minimal design specifications:

- f_{ck} ≥ 50MPa (at 28 days), as specified in concrete structural design;
- water/cement ratio ≤ 0,4 (linked to aggressiveness class);
- mortar ratio from 52 to 55% (related to pouring height and workability);
- slump from 16 to 25cm (fluid concrete: related to segregation and bleeding issues);
- silica fume addition (at least 5%) (high strength concrete and AAR prevention);
- waterproofing admixture, acting by integral crystallization, promoting self-healing of fissures (dosing ratio depending on concentration/supplier).

It should be observed that the waterproofing admixture, acting by integral crystallization that promotes self-healing of fissures was dosed per manufacturer’s technical instructions, including the recommendation of obligatory visits of the their technical representative, who went several times to the concrete batch plant to verify procedures. In this case, it was employed 1,0% by cement weight of XYPEX NF 500 (concentrated), supplied by MC-Bauchemie Brasil.

It is also important to stress that the chosen mix proportions were developed having in mind the ingredients that are available at Rio de Janeiro (which are not the most appropriate for a fluid, high strength concrete, with consequently high elasticity modulus, as per design specifications). The worst problem for the ingredients was the high fineness modulus of sands. Grain grade curves submitted by Engemix, normally employed at Caju batching plant, showed lack of fines in both sands (natural and artificial) which corresponds to higher fineness modulus (between 2,3 and 2,9 respectively).

The mix proportions as well as the suppliers of the ingredients for the anti-flotation slab concrete are described in Table 1. It can be observed that no water was employed, besides that existing in sands (to be subtracted from the whole amount of ice). All mixing water was replaced by ice cubes with initial specified temperature of -10ºC (delivered by refrigerator trucks with a Thermo King type refrigeration unit). The technical specification to accept concrete at working site asked for a 20ºC temperature. In reality, that temperature went up to 25ºC in very hot days. As concreting batches had maximum volumes of about 150m³ and the slab had a high reinforcement ratio with well distributed rebars through the 1m thickness, the temperature difference in hot days did not imply in fissures of thermal origin. The mean time of arrival, acceptance and discharge of mixing trucks was 12 minutes, which is rather quick.
In order to not slowing down the concrete production before concreting events, based on a large data obtained from the concrete batch plant about sand humidity, it was admitted the weighted average of 5% as a constant for both sands (natural and artificial) and, consequently, the amount of ice was also constant for each mixing truck. This amount was calculated as 130kg per cubic meter, with the explicit exception written in the technical specification of a corrective procedure in case of rainy days or if very high humidity batches of sand were detected by the control technicians at the concrete mix plant.

3.3 Execution recommendations

The whole technical specification was elaborated based on reference paper "Considerações sobre estanqueidade de estruturas de concreto" published by Helene, Terzian and Sardinha (1980) [8]. Besides basic guidelines exposed in the paper about lean concrete/structural concrete interface treatment, assurance of rebar recover and placing, other procedures were essential to assure the watertightness of the structure, the main one was related to concreting joints and the other with proceedings. Besides general recommendations, the Contractor Rio Verde team, which was responsible for project execution, was given specific technical guidelines about proceedings for anti-flotation slab by PhD consultants.

3.3.1 Concreting joints

Principally, due to time limits for mixing trucks circulation at Copacabana coastal avenue, as well as existing legislation related to noise produced by construction sites, it was not possible to program slab concreting in a single, continuous event, what would be ideal (and feasible) by the use of special additives and procedures. Concreting, thus, was divided into 10 different phases (determined by the structural designer).
When casting a concrete watertight structure, construction joints or concreting joints are one of the most sensible points which ask for more attention. Execution shall be planned in a way to minimize nonconformities at these points.
At all concreting joints, it was recommended to use poultry wire mesh as an incorporated formwork, structured by the steel reinforcement existing at the joint, together with hydro swelling tapes. Reinforcement design included an "C" clamp shaped bar each 25cm, designed to work as a support to tie the mesh, all the way up every joint (at one of the sides). Thus, a vertical joint was obtained, allowing concrete to be duly vibrated through the whole slab and principally next to concreting joints, which are the most critical places. The typical detail of the poultry wire mesh used as an incorporated formwork and of the hydro swelling tape at the slab, can be seen in the perspective of Figure 2.
It should be noted that the ideal location for the hydro swelling tape should be as close to the wire mesh bottom as possible. However, when the reinforcement for the next concreting phase is already completed, this place is almost inaccessible. The tape was then placed at a higher region, approximately 30cm below the slab up-

Table 1 – Concrete mix proportions for the anti-flotation slab by weight, dry materials for 1m³ of concrete. Designed for a characteristic compressive strength f_{ck} of 50MPa at 28 days.

Mix proportions	Designed for f_{ck}=50MPa
Cement per m³ (CP III-40 RS – Votoran Moagem Santa Cruz)	448kg
Sílica fume addition (Silmix)	30kg
Water/cement+additions (cementing materials) ratio	0,35
Water (from sand humidity only, mean value fixed at 5%) + ice	168kg
Medium sand, natural (Areal D. Lucia)	650kg
Artificial sand, crushed sand type II (A 21 Mineração)	73kg
Crushed stone 0 (A 21 Mineração)	162kg
Crushed stone 1 (A 21 Mineração)	921kg
Waterproofing admixture, acting by integral crystallization (XYPEX NF 500 concentrado, MC-Bauchemie)	4,5kg
Polyfunctional plasticizer admixture (MIRA RT 75, Grace)	4,0kg
Superplasticizer admixture (Tecflow 9040, Rheoset/Grace)	2,9kg
100% of ice replacing free mixing water (humid aggregates, sand humidity weighted average is 5%)	130kg (ice)

per face, as can be seen in Figure 2. The same procedure (tapes) was implemented at reinforcing slabs intersection with diaphragm walls. Figure 3 exemplifies actual situation at worksite before, during and after concreting a generic phase.

The hydro swelling tape was put in place only a few minutes before concreting the phase juxtaposed to the already concreted phase. As these phases were not concreted in sequence with previous phases, the time interval was at least 7 days. A wooden barrier was also placed at the bottom of the poultry wire mesh to prevent cement slurry leakage. Obviously, there was a normal controlled leakage of cement slurry through the wire mesh (a very small amount), because the employed concrete was of the fluid type, but nothing that could jeopardize the objective of having a rough surface with the incorporated wire mesh. The ideal condition for the next phase concreting would be a dry, saturated and quite rough surface. Thus, the joint vertical face was saturated before concreting the juxtaposed phase. As the hydro swelling tape has a controlled, slow initial action, there were no problems in this procedure that could damage the tape, which activates in contact with water.

At the concreting joint region an hexagonal galvanized mesh, Ø 0,56mm, ½" opening with three twists, poultry wire was utilized, supplied by Fábrica de Telas São Jorge. Two superimposed and dislocated meshs were employed at each joint in order to reduce the mesh opening. The utilized hydro expansive tape has more flexibility to fit the concrete substrate contours and not needing a grove to be placed. It is of PENEBAR SW 55 type (controlled swelling water-stop) made by PENETRON Brasil, and installed as per manufacturer specifications. The supplier also supervised this procedure in loco, as the tape could not touch the rebars and its installation asked for a special care.

3.3.2 Concreting procedures

3.3.2.1 Concreting plan

The anti-flotation slab concreting plan was in accordance with detailed design specification, wich divided it in 10 different phases and with concreting joints layout as already indicated. Related to this, it can be observed that the designed layout, due to time-schedule reasons and reinforcement characteristics, did not obey the ideal shrinking joints procedure, in other words, all slabs vertical faces (corresponding to each phase) remain "free" to move and dilate, including in regions where slabs intersect with reinforcing walls built above diaphragm walls.

Thus, it was planned that no juxtaposed concreting phases were held together, which provided the maximum possible number of free slab sides. Besides this, it was recommended a minimal time interval of one week between juxtaposed concreting phases, which did not mean cast two phases simultaneously, if not

Figure 2 – Typical detail at concreting joint region, showing the poultry wire mesh as an incorporated formwork and hydro swelling tape

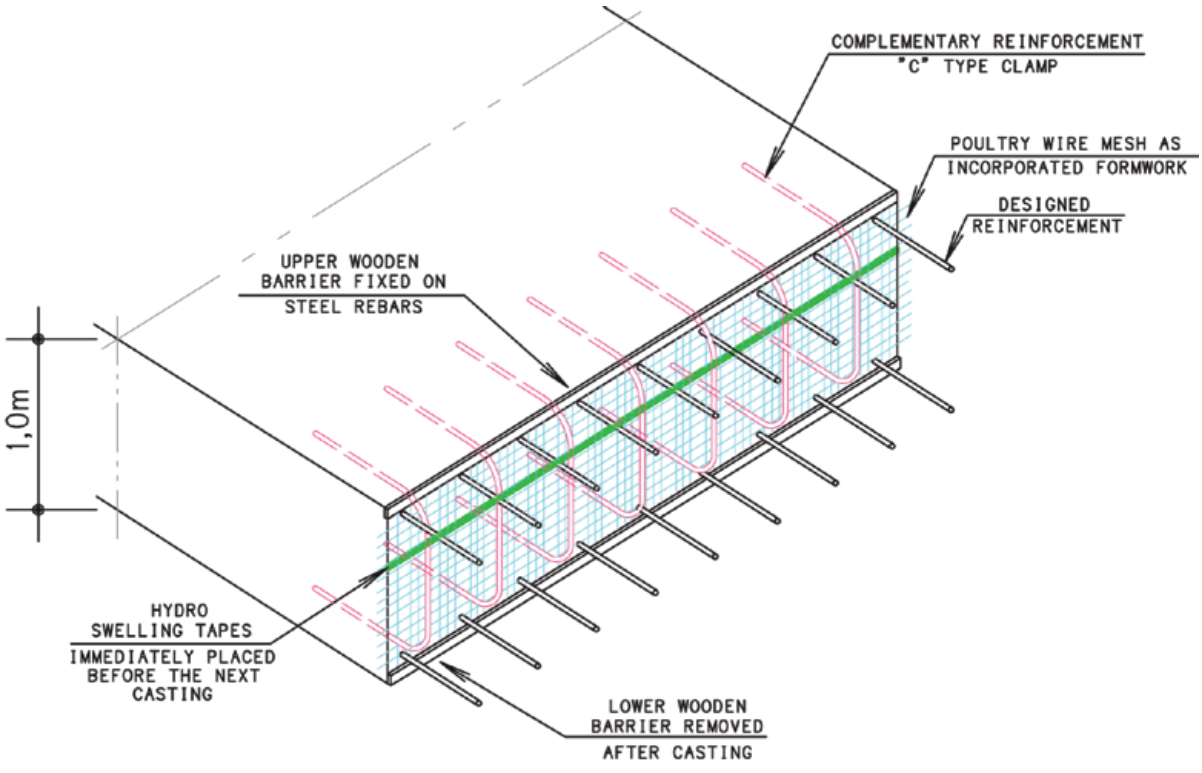

Figure 3 – Typical details of anti-flotation slab concreting joints along the 10 concrete placing phases

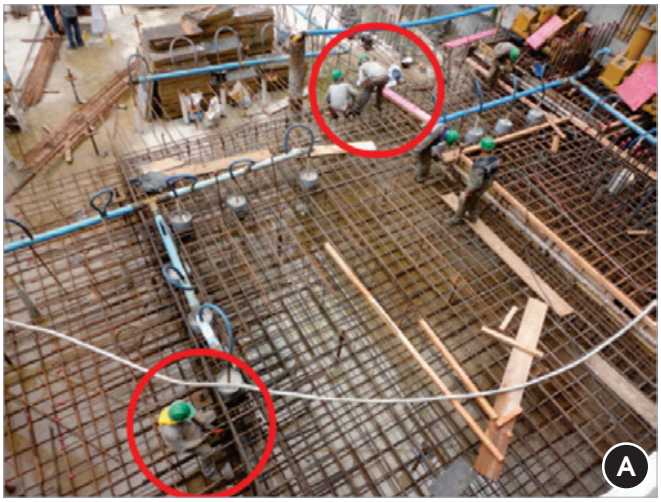

Detail of preplacement step: poultry wire mesh adjustment at designed joint

Detail of concreting joint with poultry wire mesh and external reinforcement support

Detail of poultry wire mesh performance during concrete placing: minimal cement slurry leakage

Detail of concreting joint before hydro swelling tape placing: vertical and rough surface, the next slab reinforcement not yet finished

Detail of hydro swellin flexible tape already placed for next concreting procedure: reinforcement for next concreting phase is totally completed

Detail of finishing obtained by upper wooden support barrier, wire mesh just underneath, will yet be cut

Figure 4 – Not juxtaposed (intercalated) concreting phases

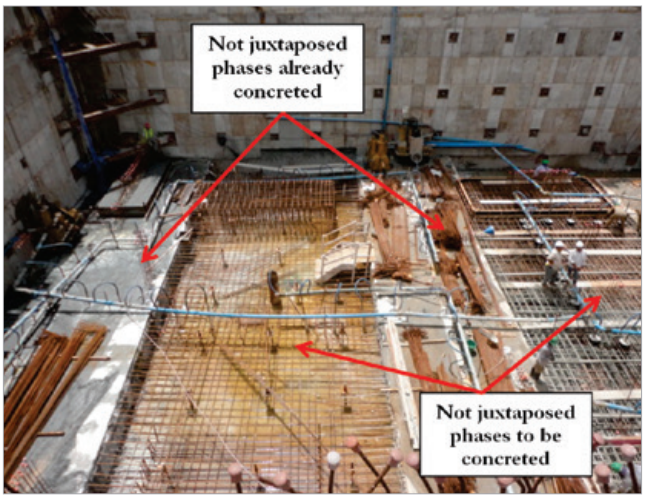

juxtaposed. In this way, the temperatures originated by cement hydration exothermal reactions should be decreasing and, consequently, deformations associated to this phenomenon will be minimized. These measures, notwithstanding, had no impact on project time-schedule, enabling an effective production of approximately 20m³/h, which means that 1200m³ of concrete were placed in 60 hours divided into 10 different concreting events. This concreting plan, in not juxtaposed (intercalated) phases, can be observed in Figure 4.

3.3.2.2 Concreting procedures and technological control

It was recommended that the first layer be carefully poured to ensure that concrete could pass through the inferior reinforcing mesh. For this case it was also recommended the consolidation by vibration with lesser diameter heads (2"), and instructions for special cares to be taken were given (for instance, not to lean the vibrator head on rebars, specially at edges, where a higher concentration of reinforcing bars is found). Once poured the first layer, covering bottom rebars, subsequent layers were vibrated from sub-layer previously vibrated (this limitation was also defined by the vibrator head length).

Basically, concrete was placed in three horizontal sub-layers of approximately 0,33m (33cm) high all the way in each phase, without caring of construction joints, in order to get an uniform layer. Concrete was continually placed in a preferred direction from the poultry wire mesh to the opposite side, foreseeing that hardening would be quicker at mesh region, in order to avoid higher pressures at these more fragile points, and returning to the initial point (not yet concreted) to pour the next sub-layer, and so on. In exceptional cases of an accidental interruption due to mixing trucks flux or to intense traffic from batch plant to working site, it was recommended to re-consolidate (re-vibrate) the concrete before beginning new pouring, and that interruption could not be greater than 1h.

During all concreting phases, at least two vibrator operators for concreting events were predicted, with a minimum of three extra vibrators, as one of them could fail during operation, what could impair concrete quality. It was also recommended to employ vibrators with 2" and 3" diameter heads, the lesser diameter ones being the most appropriate to be used at regions where higher steel ratios were concentrated (bottom and edges).

All concrete batches were carefully consolidated and cured. Detailed consolidation procedures can be consulted in well-established literature (KOSMATKA; WILSON, 2001 [5]; KENNEDY, 2005 [6]; LAMOND; PIELERT, 2006 [7]) and also in the standard ABNT NBR 14931:2004 "Execução de Estruturas de Concreto. Procedimento" [4]. Some relevant points to be remarked, employed in concreting this MIS anti-flotation slab, were:

- Concrete was consolidated (vibrated) always vertically (never in tilted or horizontal directions);
- Concrete was consolidated (vibrated) at the most possible points of each slab in every concreting phase;
- Extra care was taken to avoid excess or lack of consolidation;
- Vibrator head was introduced quickly and drawn slowly (to avoid possible air packs);
- The head length was always greater than the thickness of the layer to be concreted;

Figure 5 – Detail of concreted phase, joint to the reinforcing wall, with a curing mat over the surface and of curing procedure (mat being soaked)

Figure 6 – Anti-flotation slab already finished and beginning of formwork erection of 2nd basement columns (some of them already concreted)

- Extra care was taken to avoid vibrating the rebars;
- A minimum distance, related to the depth penetrated by the vibrator head, was maintained to define the points to be consolidated (the depth penetrated by the head was the same as the distance for next point to be vibrated).

Regarding curing, it is possible to asset that this was one of the most important steps in concreting procedure. If curing would not be efficient and correct, it could make the concrete inadequate, even if all previous steps had been well executed. For the anti-flotation slab, a high pressure cleaner, the WAP type was utilized, with its nozzle regulated to obtain a water spray, as a nebulizer mist, in order to cover the already concreted part and also the phase being concreted. It shall be remarked that there is no problem in having this mist during concreting.

After some hardening of concrete (by touch), the whole surface was covered with a mat soaked with water, which was maintained pressed against the surface of the concreted phase, sprayed with drinking water each 2h at most. This mat was always saturated at the end of the working time to ensure that it would remain humid during night and again early in the following morning, at beginning of work. This careful curing procedure was maintained at least for 7 days (up to the probable next phase concreting date). The curing procedure (a mat being soaked) can be seen in Figure 5. The curing mat employed was 100% polyester with an adhered perforated polyethylene film, manufactured by BIDIM, line Bidim CC-10 type.

4. Results

4.1 Watertightness

With the recomendations met described in previous chapter, technicians from the Contractor (Rio Verde), Project management firm (Engineering Co.) and from Concrete consultant firm (PhD Engenharia) were responsible for visually verifying possible fissures originated by shrinking or by thermal stress in each concreted phase. In

Figure 7 – Results of concrete compressive strength at 28 days

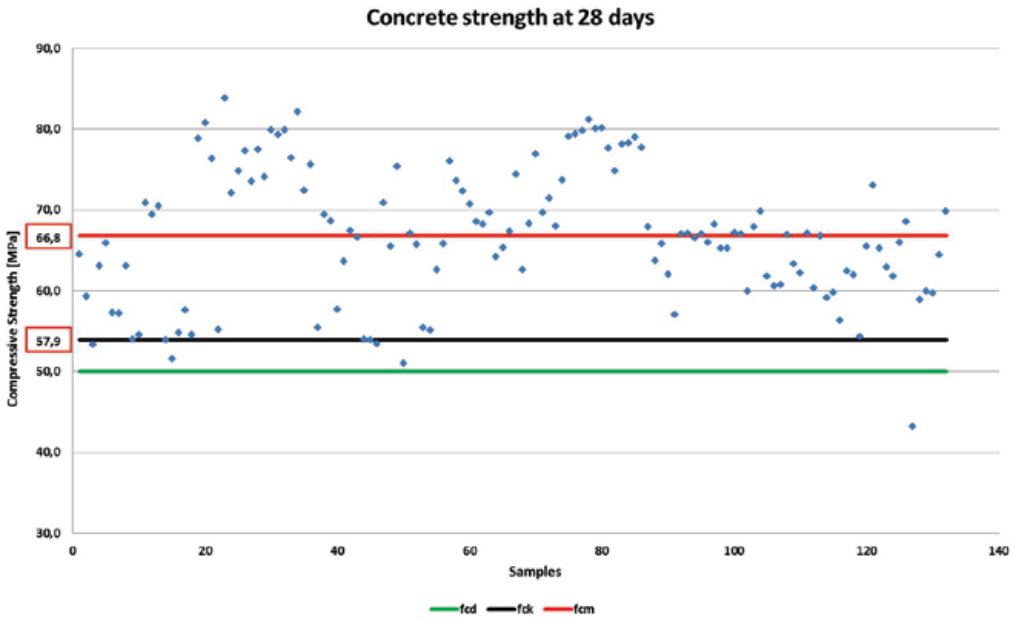

this context, it shall be remarked that during and after finishing the ten phases, no fissures of any kind were detected through which water could percolate. The already finished anti-flotation slab can be seen in Figure 6, with formwork for 2nd basement columns already erected.

4.2 Concrete technological control

An exhaustive concrete technological control was established for the slab –total sampling (100%) – as mentioned above. Of all mixing trucks, only one was identified as having compressive strength below design specification, with a value of 43,2MPa. This value was submitted to the structural engineer, who approved it, by new calculation, not being needed any additional structural reinforcement.
Graph at Figure 7 presents the results of concrete compressive strength at 28 days old. It can be seen that there was an excessive dispersion, which probably was associated to errors when pouring cylinders or during compressive rupture test, in short, related to technological control procedures. Later on, by means of a more refined statistical analysis, the anomalous results were abandoned.

5. Final considerations

1. It can be considered that an adequate design, the study and development of an appropriated concrete mix, as well as rigorous procedures utilized for concreting the MIS anti-flotation slab described here, were determinant to obtain a watertight, seamless structural element in spite of adverse soil, weather and logistic conditions. It can also be understood that the propositions presented in this paper may be considered as a good alternative for similar cases, as a quicker and less costly option, which in specific cases, may replace the use of traditional waterproofing solutions;
2. It can be also considered that this paper enabled to stress the fact that the appropriate employment of simple and less costly procedures, described in Brazilian standards and in well-established literature, associated to good engineering and building practices, are favorable to get a final, satisfactory result. Many of the procedures described in this paper are in agreement with the prescriptions of our national standards.

6. Acknowledgements

The authors wish to acknowledge Fundação Roberto Marinho for their kindly permission to publishing this paper. Our grateful thanks are also extended to Architectural Bureau Indio da Costa, to Rio Verde and to Engineering Co. for their help in offering valuable data and particularly to Eng. Bruno Lery Santos (Rio Verde) for his support and willingness in transmitting informations.

7. References

[01] CORBIOLI, N. Museu da Imagem e do Som, Rio de Janeiro. São Paulo, PROJETODESIG, ed. 372, Fevereiro de 2011. Disponível em <http://www.arcoweb.com.br/arquitetura/diller-scofidio-renfro-museu-rio-16-03-2011.html>. Acesso em 21/06/2012 às 17:52h.

[02] ASSOCIAÇÃO BRASILEIRA DE NORMAS TÉCNICAS. NBR 6118: Projeto de estruturas de concreto: Procedimento. Rio de Janeiro, 2007. 221p.

[03] ASSOCIAÇÃO BRASILEIRA DE NORMAS TÉCNICAS. NBR 12655: concreto de cimento Portland - Preparo, controle e recebimento: Procedimento. Rio de Janeiro, 2006. 18p.

[04] ASSOCIAÇÃO BRASILEIRA DE NORMAS TÉCNICAS. NBR 14931: execução de estruturas de concreto: Procedimento. Rio de Janeiro, 2004. 53p.

[05] KOSMATKA, Steven H; WILSON, Michelle L. Design and control of concrete mixtures. 15ª edição. Illinois: Portland Cement Association, 2011.

[06] KENNEDY, Lindsay K., ed. The Contractor's Guide to Quality Concrete Construction. 3ª ed. American Society of Concrete Contractors - ASCC, 2005.

[07] LAMOND, Joseph F., PIELERT, James H., eds. Significance of Tests and Properties of Concrete & Concrete-Making Materials. Pensilvânia: American Society for Testing & Materials - ASTM, 2006.

[08] HELENE, P. R. L.; TERZIAN, P. R.; SARDINHA, V. L. A. Considerações sobre estanqueidade de estruturas de concreto. In: Anais do 2º Simpósio Brasileiro de Impermeabilização. Rio de Janeiro: Instituto Brasileiro de Impermeabilização, 1980, p. 176-97.

Volume 7, Number 6 (December 2014) p. 922-939 • ISSN 1983-4195

REVISTA IBRACON DE ESTRUTURAS E MATERIAIS

IBRACON STRUCTURES AND MATERIALS JOURNAL

Study of cement pastes rheological behavior using dynamic shear rheometer

Estudo do comportamento reológico de pastas cimentícias utilizando reômetro de cisalhamento dinâmico





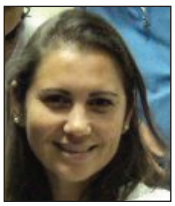


J. E. S. L.TEIXEIRA [a]
jamilla.teixeira@ufes.br

V. Y. SATO [a]
yumisato2003@hotmail.com

L. G. AZOLIN [a]
lu_gagno@hotmail.com

F. A. TRISTÃO [a]
fernandoavancini@ct.ufes.br

G. L. VIEIRA [a]
geilma.vieira@gmail.com

J. L. CALMON [a]
calmonnt@npd.ufes.br

Abstract

Concrete, in its fresh state, has flow characteristics that are crucial to its proper launch and densification. These characteristics are usually measured through empirical testing as the slump test, but this test does not quantify completely the material behavior. Since this material is characterized as a Bingham fluid, it is essential the study of its rheological behavior to verify its properties even in fresh state. The use of classical rheology has been employed by the scientific community to obtain rheological parameters determinants to characterize this material, such as yield stress, plastic viscosity and evolution of shear stress to shear rate. Thus, this present study aims to determine the rheological behavior of different cement pastes produced with cement CP III 40 RS, varying between them the hydration periods (20 and 60 min), the water-cement ratio (0.40, 0.45 and 0.50) and the use or not of additive. Samples were assayed by flow test to determine the rheological parameters showing the effect of the variables mentioned above in these parameters.

Keywords: rheology, cement paste, viscosity, shear stress.

Resumo

O concreto, em seu estado fresco, possui características de fluidez que são determinantes para seu correto lançamento e adensamento. Estas características são geralmente medidas através de ensaios empíricos como o abatimento de tronco de cone, porém este ensaio não quantifica totalmente o comportamento do material. Sendo o material caracterizado como fluido binghamiano, é fundamental o estudo de seu comportamento reológico para a verificação de suas propriedades ainda no estado fresco. O uso da reologia clássica tem sido empregado pela comunidade científica de forma a obter parâmetros reológicos determinantes na caracterização deste material, tais como a tensão de escoamento, viscosidade plástica e evolução da tensão de cisalhamento com a taxa de cisalhamento. Dessa forma, o presente trabalho tem como objetivo verificar o comportamento reológico de diferentes pastas cimentícias produzidas com o cimento CP III 40 RS e variando-se entre elas o tempo de hidratação (20 e 60 min), a relação água-cimento (0,40; 0,45 e 0,50) e com e sem incorporação de aditivo. Amostras foram ensaiadas através de ensaios de fluxo para determinação dos parâmetros reológicos, mostrando o efeito das variáveis acima mencionadas nestes parâmetros.

Palavras-chave: reologia, pasta de cimento, viscosidade, tensão de cisalhamento.

[a] *Department of Civil Engineering, Federal University of Espírito Santo, Vitória – ES – Brasil.*

Received: 14 Jun 2013 • Accepted: 20 Oct 2014 • Available Online: 01 Dec 2014

© 2014 IBRACON

1. Introduction

It is known that Portland concrete is one of the most used materials around the world. There are several applications of this material in different areas of civil construction sector. Basically, concrete can be defined as a composite material made with hydraulic binder (Portland Cement), coarse and fine particles (aggregates), water and air, and can also contain additions and chemical additives to improve and/or modify some of its properties. The properties of this composite are directly affected by the properties of its constituents and the study of those is fundamental to determine the ideal characteristics of the concrete to be used in construction sites.

An appropriate concrete application requires, among other characteristics, good material workability. This characteristic depends on several factors, such as mixture design, equipment used to its placement, the finishing method applied, as well as the local conditions. Concrete needs to have enough cohesion and proper viscosity to make possible its transportation to the job site without having to deal with undesired situations, such as segregation of its constituents, which can affect its quality.

Therefore, concrete is a material that needs special care in all stages of its application, from the developments of specifications to its correct placement and complete cure, because many times this composite has structural function. The Brazilian standard NBR 7212 (ABNT, 1984) limits the time of transportation of concrete from mixing to its placement to a maximum of 150 minutes. If this time is exceeded, the concrete could lose workability because of water evaporation and the setting time due to the hydration process of cement particles.

To the technical control of concrete and to verify its workability in fresh state, a commonly used test is performed, the so called Slump Test, according to the Brazilian standard NBR NM 67 (ABNT, 1998). However, some concrete rheological properties, such as viscosity, shear stress, yield stress, and others cannot be obtained directly from this test. The use of better controlled equipment such as rheometers can give more precise information with respect to this fluid. Rheology is a branch of physics that studies the deformation and flow of materials, in an attempt to understand the relation among stress, rate of deformation and time. There is a concern about the mechanics of deformable bodies that can be in solid, liquid or gaseous state (MARTINS, 2004; COSTA, 2006; SCHRAMM, 2006). The study of rheology, in practice, is applied to materials that show more complex flow behavior than simple fluids (liquid and gas) or ideal elastic solids, even though, depending on the conditions in which the test is performed, the material can demonstrate simple or complex behavior (CASTRO, 2007).

According to De Larrard et al. (1996), the use of rheometers is beneficial not only to obtain a large number of parameters but also to evaluate physical quantities that may be scientific related to different stages of concrete use. Reis (2008) stated that shear stress is directly related to the results of slump tests. Another parameter evaluated is the apparent viscosity, which indicates the increment in stress that needs to be imposed to produce certain rate of deformation. In practice, the apparent viscosity is associated to the material capacity to be placed, pumped, segregated and finished, and therefore can differentiate a concrete that is workable to the one that is hard to work, having difficult pumping behavior and presenting surface voids in the structural elements when the formwork is removed (CASTRO et al., 2011).

When the workability is evaluated considering rheological parameters, the concrete production control can be made in a more accurate manner. The rheological assessment can show not only if a test result is satisfactory but also can identify the factors that can influence negatively the concrete workability during test (CASTRO, 2007).

To determine the rheological parameters of cement pastes, such as yield stress, apparent viscosity, and the effects of material consolidation associated to the hydration of cement particles, the literature suggests the use of some tests, such as the flow test, oscillatory tests (time sweep and strain sweep) and Vane tests (SATO et al., 2012; LISBÔA, 2004; CAVALCANTI, 2006; VENÂNCIO, 2008; SAAK et al., 2001; BETIOLI et al., 2009). Even though there are several studies trying to understand the behavior of concrete in its fresh state, the use of tools and tests based on rotational rheology are not many.

Concrete in its fresh state can be considered a fluid, and therefore, basic principles of rheology can be applied to this material (METHA, 1986). The main factors that cause concrete incompatibility are the amount of C_3A; the type and amount of sulfates in the cement; water-soluble alkalis (Na+, K+), either from cement particles or additives; type and design procedure of both materials, such as mineral mixtures; the cement paste temperature and the water-to-cement ratio. Some researchers related the sensibility of rheological parameters to the factors above-mentioned (FERRARIS, 1996; ZHANG, 2001; CHEN, STRUBLE, ZHANG, 2006).

For the rheological analysis of cement pastes and mortars, some parameters need to be carefully defined. The time and energy spent during the mixing process for sample preparation, for example, influence significantly the rheological properties of those materials. França, Cardoso and Pileggi (2011 and 2012) mentioned that the greater the mixing time, the more efficient is the mixing process due to the high energy involved in the process, producing therefore a more disperse material (small size of mobile units, particles or agglomerates), homogeneous, stable and a more fluid like behavior. The mixing method used to produce cement pastes should simulate the shearing effects that occurs when concrete is produced. Bhattacharja and Tang (2000) also reported the use of a high shearing mixer to prepare cement pastes in order to simulate the effects of shearing.

Taking into account the need of o broader evaluation of concrete properties in its fresh state, this study aims at analyzing the rheological properties of cement pastes by performing flow test using dynamic shear rheometer as the main testing equipment. Thus, the rheological properties of pastes produced with different water-cement ratios, with and without additives, will be analyzed so as to verify the effects of these constituents on rheological behavior of cement pastes.

2. Objectives

The present study aims at verifying the rheological behavior different cement pastes produced by mixing water and Portland cement, with and without additives, so as to assess the influence of these constituents on the study rheological parameters (yield stress, apparent viscosity, rheological profile of the material and effects of this material associated to cement hydration).

The composition of these pastes used different water-cement ratios (0.40; 0.45 and 0.50), with and without additives. Also, the

Figure 1 – Granulometric curve of portland cement CP III 40 RS

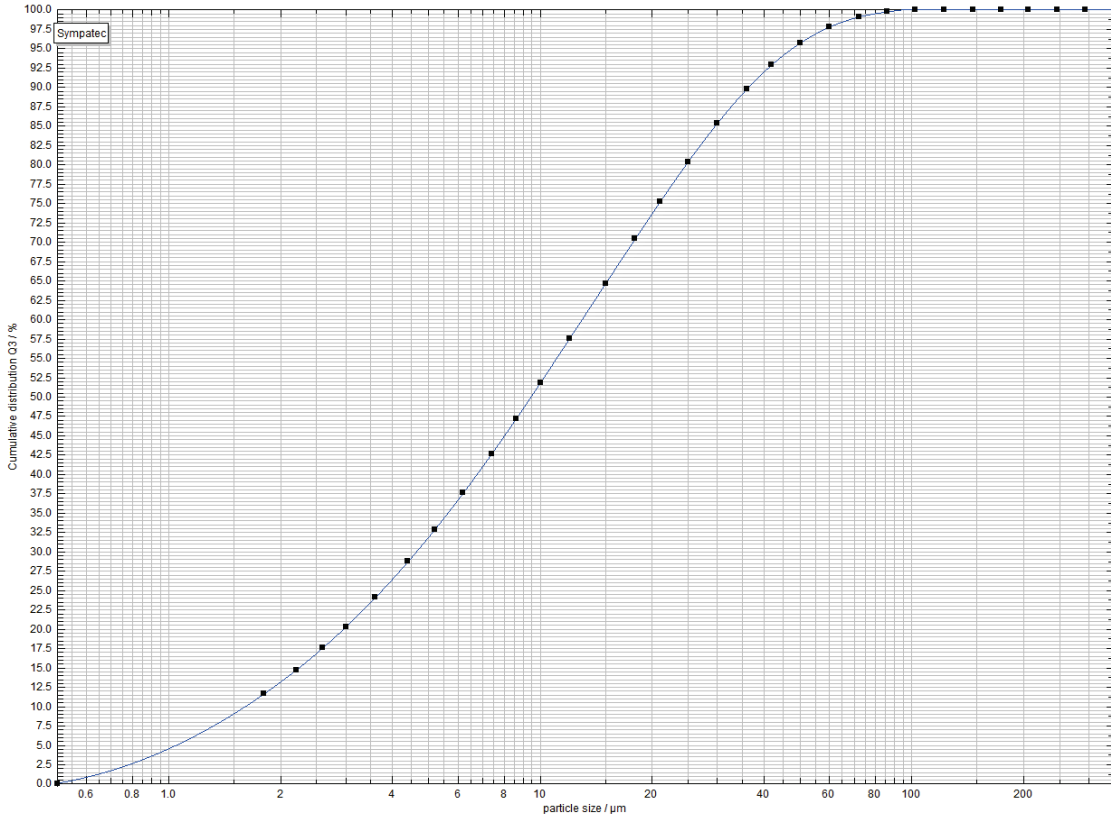

pastes were tested at different hydration times (20 and 60 min.) in order to allow verifying the effect of cement hydration on rheological properties of the study cement pastes.

3. Materials and methods

3.1 Materials

In order to be carried out, this study used CP III 40 RS cement, classified as blast furnace Portland, resistant to sulfates as per Standard NBR 5735 (Brazilian Association of Technical Standards – ABNT, 1991). For the granulometric classification of the material, we used a laser diffraction granulometer (model Sympatec®) with lenses able to read between 1.8 to 350 mm. Figure 1 shows the granulometric distribution curve obtained for the study cement.
The additive incorporated into the study cement pastes was GLENIUM® 51 (by BASF S. A.), which is as polycarboxylate ether superplasticizer. The water used in this study was taken directly from the water concessionaire's local network.

3.2 Composition and preparation of cement pastes

This study analyzed samples of cement pastes with three different water/cement (w/c) ratios, with and without additives. Table 1 presents the w/c ratio values and the amount of additive for each sample used in the flow test.

3.2.1 Mixing procedures

Since there is no standard procedure for mixing cement pastes to be used in rheological property determination using a dynamic shear rheometer, this study adopted the procedure for mixing cement pastes provided by standard NBR 13276 (ABNT, 2005), which

Table 1 – W/c ratios and amount of additive in the pastes analyzed

Cement paste	w/c ratio	Additive
Paste 1	0.40	–
Paste 2	0.45	–
Paste 3	0.50	–
Paste 4	0.40	0.2 %
Paste 5	0.45	0.2 %
Paste 6	0.50	0.2 %

Table 2 – Process of mixing materials

Procedure	Initial time (s)	Final time (s)
Putting cement and water together	0	30
Mixer use	30	60
Cleaning and wait	60	120
Mixer use	120	150

concerns preparation of mix and mortar consistency index for settling and coating walls and ceilings. The mixes were determined on an electronic digital scale with 0.01g accuracy. A mechanical mixer was employed to ensure homogenization of the sample.

In compliance with NBR 13276 (ABNT, 2005), first the amount of water and cement were separately weighed with 1.0g approximation. Then, water was added to the specific portion of cement corresponding to the w/c under study for a continuous period of 30 seconds. After putting the materials together, they were blended in the mixer for 30 seconds, then the machine was turned off. The mixer was cleaned, we waited for 60 seconds and, finally, it was turned on again and material was mixed for another 30 seconds so as to obtain a homogeneous paste. In pastes composed also by the additive, it was added to the paste after mixing as mentioned above. The new mix was homogenized using a spatula for 30 seconds. Table 2 shows the stages for preparing the cement pastes.

After all the mixing process, the samples were kept in air-tight containers until the tests were carried. This was not to lose humidity to the ambient. Before each test, the paste was mixed again in the following way: 30 seconds using mixer, 15 seconds using spatula, and 30 seconds using the mixer again, so as to keep homogeneity.

Figure 2 – Slope from 0 to 100s -1 in 2 minutes and to 0 again in 2 more minutes (Betioli et al., 2009)

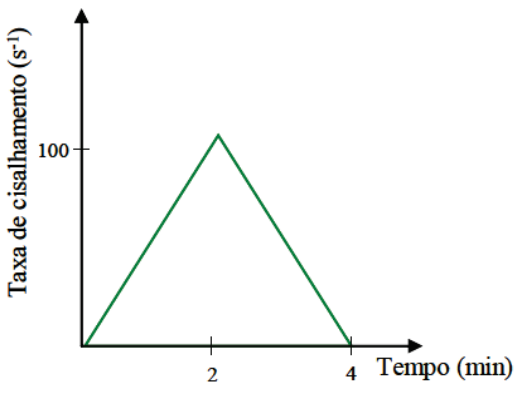

3.3 Flow test

Through flow-test, we can obtain shear stress at a particular shear rate. The test consists in applying an increasing shear rate with acceleration from 0 to 100 s^{-1} in 2 minutes, flowed by deceleration to 0 in another 2 minutes, as shown in Figure 2.

From the variation of these parameters, one can trace the rheological profile of materials, and determine important rheological properties such as apparent viscosity (h_{ap}), yield stress (s_0) and hysteresis area (AH, Portuguese acronym). Apparent viscosity of cement pastes was evaluated at the maximum shear rate applied, which was 100 s^{-1} in this study. Yield stress was approximate by extrapolating the shear stress curve and shear rate, until 0 s^{-1}. Another parameter analyzed with flow test results was hysteresis area (AH). This area is formed by acceleration and deceleration curves in the shear stress vs. shear rate graph (OLIVEIRA et al., 2000; BETIOLI et al., 2012), and it indicates that the level of system structuring/destructuring.

Shear cycles were carried out at pre-defined times within the cement dormancy induction interval, which shows less heat release (KIRCHHEIM, 2008). In this interval, the cement hydration reactions are considered controlled, which allows us to consider the conservation of mass at the moment of testing. Silva (2001) determined an induction period between 20 and 110 minutes from the intersection of the horizontal section with two lines: The line traced in the pre-induction period and the extrapolation of acceleration regression line, as shown in Figure 3.

Thus, the cement pastes were tested at two different cement hydration times (20 and 60 min) within the material induction interval, so as to analyze the effects of cement hydration on rheological properties of cement pastes.

In order to carry out the flow tests, we used a dynamic shear rheometer. The geometry chosen for flow test was parallel-plate geometry, which has 40 mm diameter and 1mm spacing. For

Figure 3 – Heat release rate during 6 hydration hours. The interval of induction period takes place between 20 and 110, approximately (Silva, 2001)

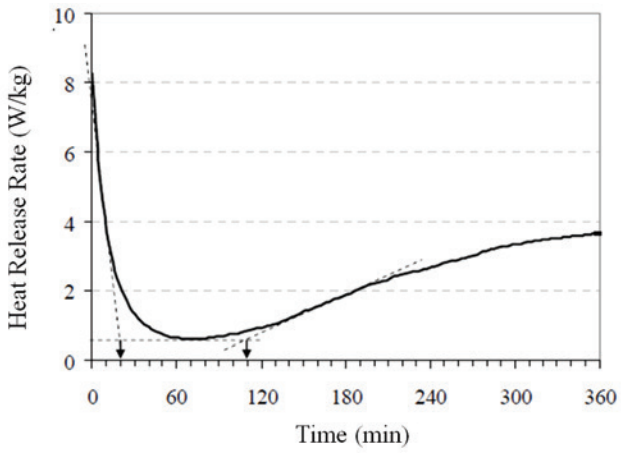

each study paste, three samples were tested. For making the shear stress vs shear rate; and viscosity vs shear rate graphs, we employed the arithmetic mean of the sample values. In the analysis of graphs, we verified the effects of water-cement ratio, additive addition, cement and hydration of rheological behavior. In order to avoid water evaporation and keep the sample temperature at 25º C during the test, a protective device (Peltier plate) was used. A textured sticker was applied to the surface of each plate so as to prevent the sample from slipping, as seen in Figure 4.

4. Results and discussion

Figures 5 and 6 show shear stress and apparent viscosity referring to shear rate for cement pastes (with and without additive) for each hydration time (20 and 60 min) analyzed in this study.

One can see that the study cement pastes need an initial shear stress (σ0) to start yielding. After overcoming this yield stress, the pastes showed non-linear behavior, which shows a behavior tendency of a Herschel-Bulkley fluid, also known as generalized Bingham.

By analyzing the hysteresis areas between the acceleration and deceleration curves of the shear stress vs. shear rate graph, one can see that at 20 minutes of hydration, this area is virtually null. This can indicate the dispersion status of samples. Not so significant hysteresis areas little show that the mixing process adopted was enough to obtain a homogeneous sample, with total breakdown of agglomerates. On the other hand, at 60 minutes, there is a trend of restructuring of these agglomerates and, therefore, breakdown takes place during imposed shear cycles.

The action of additive is seen through the levels of shear stress in the samples. According to Oliveira et al. (2003 apud FRANÇA, CARDOSO and PILEGGI, 2012), the required levels of stress for mixing concrete are reduced when using additives, because they allow better dispersion of particles.

Figure 6 shows that for all the pastes, apparent viscosity obtained from the relationship between shear stress and shear rate decreased as shear rate increased, which shows the thixotropic nature of this material. In pastes that received additives, the addition effects on rheological behavior were evident, such as decrease in apparent viscosity, as seen in Figure 6 compared to pastes without additive (Figure 5). When adding this material, the pastes became more fluid and more susceptible to excessive deformation if submitted to shear stress. This makes measuring shear stress values more difficult using the equipment adopted in this study.

Tables 3 and 4 show the apparent viscosity and yield stress values obtained at 20 and 60 minutes of hydration, respectively.

It is seen that pastes without additive and w/c ratio 0.40, 0.45 and 0.5 increased, respectively, of 4, 9 and 7 times their yield stress at hydration age of 60 minutes compared to age 20 minutes. The increase in hydration time made pastes show a more agglomerated structure because of the process of hydrating cement particles. Therefore, more stress is required to start paste yielding. This phenomenon is reflected on the increase of yield stress. As expected, the pastes without additive showed higher yield strength compared to pastes with additive, which was also reflected on apparent viscosity of the study pastes. Addition of polycarboxylate plasticizing admixtures causes cement particles to disperse, increasing flow, a phenomenon known as electrical repulsion. Thus, pastes with additives become more fluid, which results in significant reduction of yield stress and apparent viscosity values compared to pastes with the same water-cement ratio.

Figure 7 shows the correlation between yield stress and water-cement obtained in this study.

We can see the trend of correlation between the parameters analyzed using exponential function, both for pastes with and without additive. Coefficients of determination (R^2) of 0.99 and 0.96 for

Figure 4 – Geometry of parallel plates with and peltier and textured adhesive

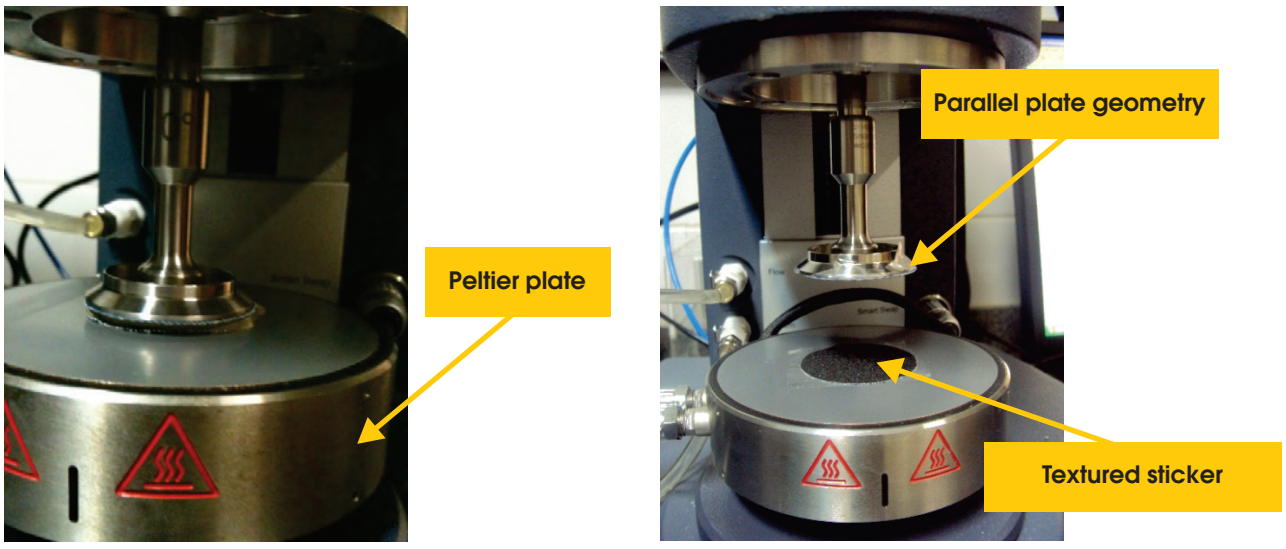

Figure 5 – Shear stress vs. shear rate in cement pastes: (a) without additive and (b) with additive, tested at hydration times 20 and 60 minutes.

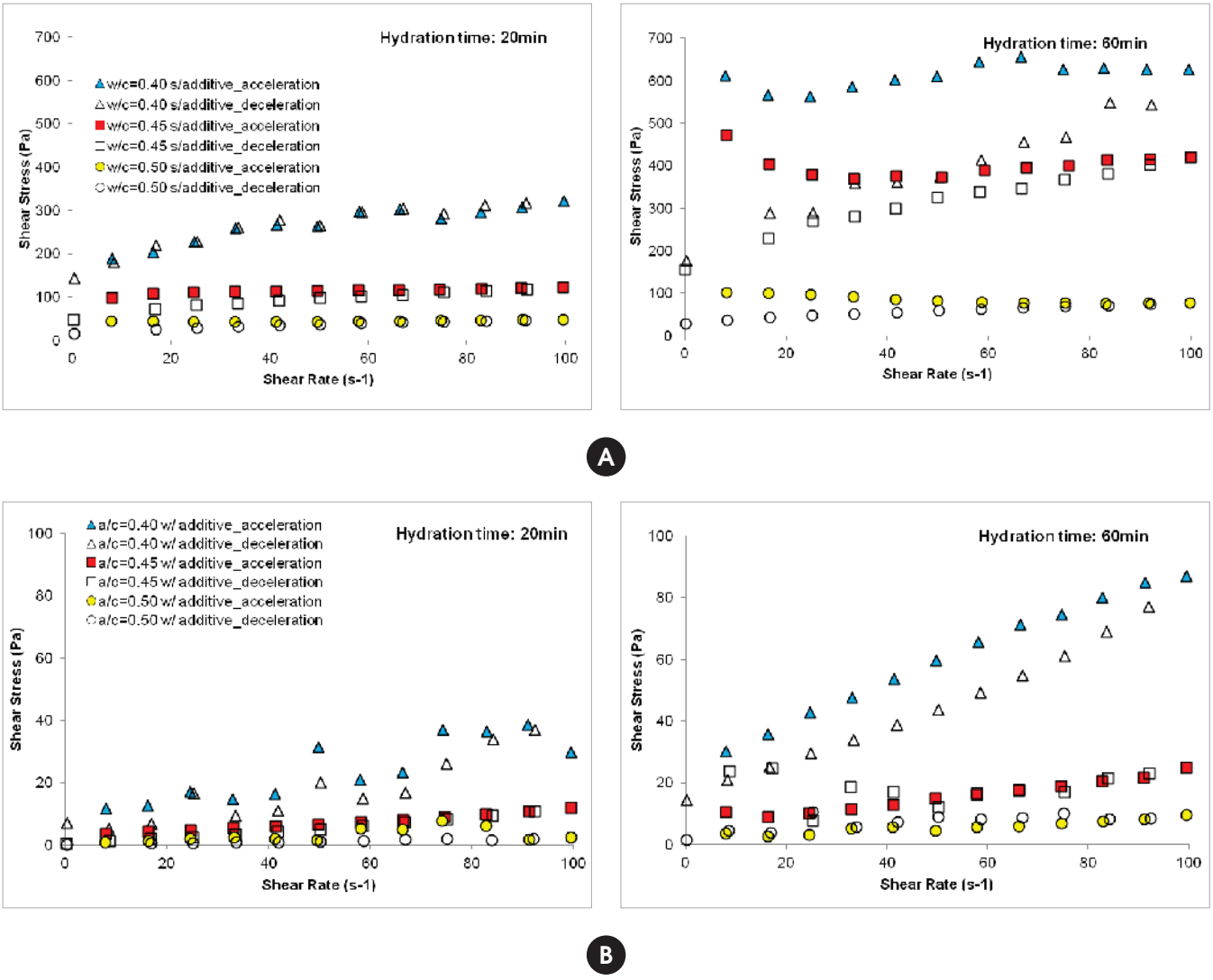

Table 3 – Rheological properties of cement pastes after hydration of 20 min

w/c	η_{ap} (Pa.s)		σ_0 (Pa.s)	
	Without additive	With additive	Without additive	With additive
0.4	3.2	0.29	143	8.5
0.45	1.2	0.11	47	2.48
0.5	0.48	0.02	15	0.2

Table 4 – Rheological properties of cement pastes after hydration of 60 min

w/c	η_{ap} (Pa.s)		σ_0 - Acceleration (Pa.s)	
	Without additive	With additive	Without additive	With additive
0.4	6.3	0,87	576	27
0.45	4	0.2	441	8
0.5	0.8	0.1	100	3

pastes without and with additives, respectively, show strong negative correlation between yield stress and water-cement ratio. The use of this type of correlation, based on analysis of rheological parameters can lead to measuring workability in a more scientific way.

5. Conclusions

In order to better understand the influence of important variable in dosing cement mixes (w/c ratio, cement hydration, and use of chemical admixtures) on cement-based materials, we adopted rheological tests. The rheological behavior of cement pastes is complex because many factors interfere in their properties, such as type of cement and its reactive nature, water-cement ratio used, presence of additives, and mixing conditions (speed, length, confinement), among others.

The flow test is an effective tool to determine rheological properties of cement pastes in laboratory, because it is possible to induce samples to a high shearing magnitude. This resulted in different values of rheological properties (apparent viscosity and yield stress).

Apparent viscosity showed to be higher in pastes with lower water-cement ratio among the samples without additive. The pastes using additive showed apparent viscosity with little variation.

Yield stress for pastes without additives increased significantly with hydration age.

This study shows the need of further investigations on rheological characterization of cement pastes due to the large range of products that can be used to produce them.

6. Acknowledgements

The authors are grateful to Capes (Coordination for the

Figure 6 – Apparent viscosity vs. shear rate in cement pastes: (a) without additive and (b) with additive, tested at hydration times 20 and 60 minutes

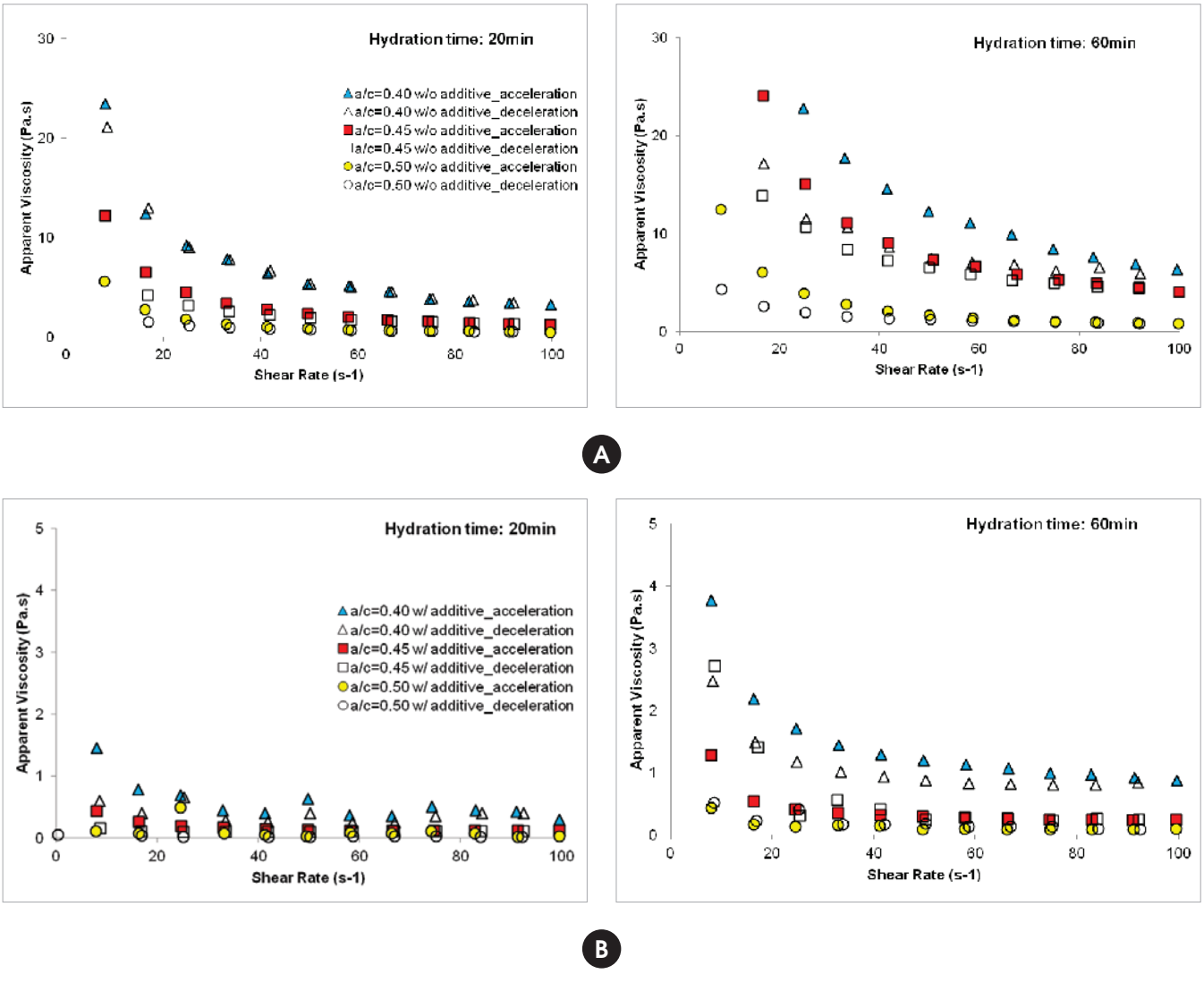

Figure 7 – Correlation between yield stress and water-cement ratio at hydration time of 20 min

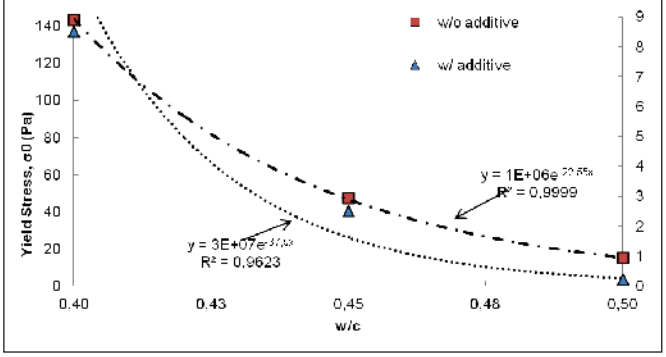

Improvement of Higher Education Personnel) and CNPq (Brazilian National Council for Scientific and Technological Development) for financial support, and to *Laboratório de Ensaios em Materiais de Construção –LEMAC* (Laboratory for Testing Construction Materials) at Technology Center at Federal University of Espírito Santo (UFES), Brazil for their technical support and infrastructure for carrying out this study.

7. References

[01] ASSOCIAÇÃO BRASILEIRA DE NORMAS TÉCNICAS. NBR 13276: Preparo da mistura e determinação do índice de consistência da argamassa para assentamento e revestimento de paredes e tetos, 2005.

[02] _____. NBR 5735: Cimento Portland de Alto Forno. Rio de Janeiro, 1991.

[03] _____. NBR 7212: Execução de concreto dosado em central. Rio de Janeiro, 1984.

[04] _____. NBR NM 67: Concreto - Determinação da consistência pelo abatimento do tronco de cone. Rio de Janeiro, 1998.

[05] BARNES, H. A.; HUTTON, J. F.; WALTERS, K. An introduction to rheology. 3. ed. Amsterdam: Elsevier, 1993.

[06] BETIOLI, A. M.; JOHN, V. M.; GLEIZE, P. J. P., PILEGGI, R. G. Caracterização reológica de pasta cimentícia: associação de técnicas complementares. Ambiente Construído, Porto Alegre, v. 9, n. 4, p. 37-48, out./dez. 2009.

[07] BETIOLI, A. M. , GLEIZE, P. J. P., JOHN, V. M. , PILEGGI, R. G. Effect of EVA on the fresh properties of cement paste. Cement & Concrete Composites Vol. 34, 255–260, 2012.

[08] BHATTACHARJA, S.; TANG, F. J. Rheology of cement paste in concrete with different mix designs and interlaboratory evaluation of the mini-slump cone test, PCA R&D, Serial No. 2412, Portland Cement Association, Skokie, Illinois, 2000.

[09] CASTRO, A. L. Aplicação de conceitos reológicos na tecnologia dos concretos de alto desempenho. 2007. 302f. Tese (Doutorado) - Escola de Engenharia de São Carlos / Instituto de Física de São Carlos/ Instituto de Química de São Carlos - Universidade de São Paulo, São Carlos, 2007.

[10] CASTRO A. L., LIBÓRIO J. B. L., PANDOLFELLI V. C. Reologia de concretos de alto desempenho aplicados na construção civil – Revisão. Revista Cerâmica, São Carlos, v. 57, p. 63-75, 2011.

[11] CAVALCANTI, D. J. H. Contribuição ao estudo de propriedades do concreto auto-adensável visando sua aplicação em elementos estruturais. 2006. 141f. Dissertação (Mestrado) – Programa de Pós-Graduação em Engenharia Civil, Universidade Federal de Alagoas, Maceió, 2006.

[12] CHEN, C.; STRUBLE, L. J.; ZHANG, H. Using dynamic rheology to measure cement-admixture interactions. Journal of ASTM International, West Conshohocken, v. 3, mar. 2006.

[13] COSTA, M. R. M. M. Análise comparativa de argamassas colantes de mercado através de parâmetros reológicos. 2006. 131f. Tese (Doutorado) – Escola Politécnica da Universidade de São Paulo, São Paulo, 2006.

[14] De LARRARD, F.; SEDRAN, T.; HU, C.; SZITKAR, J. C.; JOLY, M.; DERKX, F. Evolution of the workability of superplasticized concretes: assessment with the BTRHEOM rheometer. In: International Rilem Conference – Production Methods and Workability of Concrete, 1996, Paisley/Scotland. Proceedings… London: E & FN Spon, 1996, p. 377-388.

[15] FERRARIS, C. F.. Measurements of rheological properties of high performance concrete: state of the art report. Journal of Research of the National Institute of Standards and Technology, Gaithersburg, v. 104, n. 5, p. 461-478, 1996.

[16] FRANÇA, M. S.; CARDOSO, F. A.; PILEGGI, R. G. Avaliação do comportamento de mistura de argamassas através de reometria rotacional. Ambiente Construído, v. 12, n. 2, p. 165-174, 2012.

[17] FRANÇA, M. S.; CARDOSO, F. A.; PILEGGI, R. G. Influência do tempo de mistura nas propriedades reológicas de argamassas. In: Simpósio Brasileiro de Tecnologia de Argamassas, 9., 2011, Belo Horizonte. Anais... Belo Horizonte: SBTA, 2011.

[18] GHIO, V. A.; MMONTEIRO P. J.; DEMSETZ, L. A. The rheology of fresh cement paste containing polysaccharide gums. Cement Concrete Research, Philadelphia, v. 24, n. 2, p. 243-249, 1994.

[19] HACKLEY, V. A.; FERRARIS, C. F. Guide to rheological nomenclature: measurements in ceramic particle systems. NIST special publication, v. 946, 2001.

[20] KIRCHHEIM, A.P. Aluminatos tricálcicos cúbico e ortorrômbico: análise da hidratação in situ e produtos formados. 2008. 265f. Tese (Doutorado) – Programa de Pós-Graduação em Engenharia Civil, Universidade Federal do Rio Grande do Sul, Porto Alegre. 2008.

[21] LISBÔA, E. M. Obtenção do concreto auto-adensável utilizando resíduo do beneficiamento do mármore e granito e estudo de propriedades mecânicas. 2004. 121f. Dissertação (Mestrado) – Programa de Pós-Graduação em Engenharia Civil, Universidade Federal de Alagoas, Maceió, 2004.

[22] MARTINS, A. L. P. Estudo das propriedades reológicas do muco brônquico de pacientes sob fisioterapia respiratória. 2004. 70f. Dissertação (Mestrado) - Programa de Pós-Graduação em Fisioterapia. Universidade Federal de São Carlos, São Carlos, 2004.

[23] METHA, P. K. Concrete: structure, properties, and materials. Prentice-Hall, Inc, Englewood Cliff, New Jersey, p. 449, 1986.

[24] NONAT, A.; MUTIN, J. C.; LECOQ, X.; JIANG, S. P. Physico-chemical parameters determining hydration and particle in-

teractions during the setting of silicate cements. Solid State Ionics, v. 101-103, n. 2, p. 923-930, nov. 1997.

[25] OLIVEIRA, I. R., STUDART, A. R., PILEGGI, R. G., PANDOLFELLI, V. C. Dispersão e empacotamento de partículas: Princípios e aplicações em processamento cerâmico. Fazendo Arte Editorial. 2000.

[26] RAMACHANDRAN, V. S.; BEAUDOIN, J. J. Handbook of analytical techniques in concrete science and technology: principles, techniques, and applications, Book 2001.

[27] REIS, J. F. A. Determinação de parâmetros reológicos de concretos através do ensaio de abatimento de tronco de cone modificado: estudo de caso. 2008. 177f. Dissertação (Mestrado) – Programa de Pós-Graduação em Engenharia Mecânica, Universidade Estadual Paulista, Ilha Solteira, 2008.

[28] SAAK, A. W.; JENNINGS, H. M.; SHAH, S. P. The influence of wall slip on yield stress and viscoelastic measurements of cement paste. Cement and Concrete Research, Philadelphia, v. 31, n. 2, p. 205-212, fev. 2001.

[29] SATO, V. Y.; EVANGELISTA, K. T. C.; TEIXEIRA, J. E. S. L.; TRISTÃO, F. A. Estudo das propriedades reológicas de pastas de cimento de concretos bombeados. In: Congresso Brasileiro do Concreto, 54., 2012, Maceió. Anais... Maceió: IBRACON, 2012.

[30] SCHRAMM, G. Reologia e reometria: fundamentos teóricos e práticos. 2. ed. São Paulo: Artiliber, 2006.

[31] SILVA, D. A. Efeitos dos polímeros HEC e EVA na microestrutura de pastas de cimento portland. 2001. 246f. Tese (Doutorado em Ciência e Engenharia dos Materiais) – Departamento de Engenharia dos Materiais, Universidade Federal de Santa Catarina, Florianópolis, 2001.

[32] TATTERSALL, G.H.; BANFILL P.F.G. The Rheology of Fresh Concrete, Pitman, p. 356, 1983.

[33] VENÂNCIO, P. B. F. Dosagem de argamassa para estaca raiz. 2008. 173f. Dissertação (Mestrado) – Departamento de Engenharia Civil e Ambiental, Universidade de Brasília, Brasília, 2008.

[34] ZHANG, H. Using Dynamic Rheology to Explore the Microstructure and Stiffening of Cementitious Materials, Ph.D. Thesis, University of Illinois at Urbana-Champaign, 2001.

Volume 7, Number 6 (December 2014) p. 922-939 • ISSN 1983-4195

REVISTA IBRACON DE ESTRUTURAS E MATERIAIS

IBRACON STRUCTURES AND MATERIALS JOURNAL

Study of cement pastes rheological behavior using dynamic shear rheometer

Estudo do comportamento reológico de pastas cimentícias utilizando reômetro de cisalhamento dinâmico





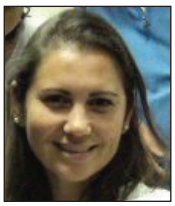


J. E. S. L.TEIXEIRA [a]
jamilla.teixeira@ufes.br

V. Y. SATO [a]
yumisato2003@hotmail.com

L. G. AZOLIN [a]
lu_gagno@hotmail.com

F. A. TRISTÃO [a]
fernandoavancini@ct.ufes.br

G. L. VIEIRA [a]
geilma.vieira@gmail.com

J. L. CALMON [a]
calmonnt@npd.ufes.br

Abstract

Concrete, in its fresh state, has flow characteristics that are crucial to its proper launch and densification. These characteristics are usually measured through empirical testing as the slump test, but this test does not quantify completely the material behavior. Since this material is characterized as a Bingham fluid, it is essential the study of its rheological behavior to verify its properties even in fresh state. The use of classical rheology has been employed by the scientific community to obtain rheological parameters determinants to characterize this material, such as yield stress, plastic viscosity and evolution of shear stress to shear rate. Thus, this present study aims to determine the rheological behavior of different cement pastes produced with cement CP III 40 RS, varying between them the hydration periods (20 and 60 min), the water-cement ratio (0.40, 0.45 and 0.50) and the use or not of additive. Samples were assayed by flow test to determine the rheological parameters showing the effect of the variables mentioned above in these parameters.

Keywords: rheology, cement paste, viscosity, shear stress.

Resumo

O concreto, em seu estado fresco, possui características de fluidez que são determinantes para seu correto lançamento e adensamento. Estas características são geralmente medidas através de ensaios empíricos como o abatimento de tronco de cone, porém este ensaio não quantifica totalmente o comportamento do material. Sendo o material caracterizado como fluido binghamiano, é fundamental o estudo de seu comportamento reológico para a verificação de suas propriedades ainda no estado fresco. O uso da reologia clássica tem sido empregado pela comunidade científica de forma a obter parâmetros reológicos determinantes na caracterização deste material, tais como a tensão de escoamento, viscosidade plástica e evolução da tensão de cisalhamento com a taxa de cisalhamento. Dessa forma, o presente trabalho tem como objetivo verificar o comportamento reológico de diferentes pastas cimentícias produzidas com o cimento CP III 40 RS e variando-se entre elas o tempo de hidratação (20 e 60 min), a relação água-cimento (0,40; 0,45 e 0,50) e com e sem incorporação de aditivo. Amostras foram ensaiadas através de ensaios de fluxo para determinação dos parâmetros reológicos, mostrando o efeito das variáveis acima mencionadas nestes parâmetros.

Palavras-chave: reologia, pasta de cimento, viscosidade, tensão de cisalhamento.

[a] *Department of Civil Engineering, Federal University of Espírito Santo, Vitória – ES – Brasil.*

Received: 14 Jun 2013 • Accepted: 20 Oct 2014 • Available Online: 01 Dec 2014

© 2014 IBRACON

1 Introdução

É sabido que o concreto é um dos materiais mais utilizados no mundo. Sua aplicação abrange diversas áreas da construção civil. Basicamente, pode-se definir o concreto como um material compósito formado pela mistura de um aglomerante (cimento), agregados miúdos, agregados graúdos, água e ar, podendo conter adições e aditivos químicos para melhorar ou modificar algumas de suas propriedades. As propriedades desse material compósito são influenciadas pelas propriedades de seus constituintes e o estudo destas é de grande importância para a determinação das características ideais do concreto a ser utilizado em obra.

Para a utilização do concreto é desejável que este tenha, entre outras características, trabalhabilidade adequada. Essa característica é dependente de vários fatores, tais como do projeto de misturas, dos equipamentos a serem utilizados no lançamento do material, do acabamento a se realizar e das condições locais. O concreto deve ter coesão e viscosidade adequada, para que seja possível realizar seu transporte sem que ocorram situações indesejadas que prejudiquem sua qualidade, como a segregação de seus constituintes.

Assim, o concreto é um material que exige atenção especial, desde a fase de especificação até a cura, pois muitas vezes possui função estrutural. A norma NBR 7212 (ABNT, 1984) determina que o tempo limite para executar o lançamento do concreto seja de 150 minutos a partir da sua mistura. Caso esse tempo seja ultrapassado, o concreto poderá apresentar perda de trabalhabilidade por perda de água por evaporação e início da pega devido às reações de hidratação do cimento.

Para o controle tecnológico do concreto e a verificação da sua trabalhabilidade no seu estado fresco, um ensaio comumente utilizado em campo é o teste de abatimento de tronco de cone (Slump test), normatizado na NBR NM 67 (ABNT, 1998). Contudo, algumas propriedades reológicas do concreto, tais como viscosidade, tensão de cisalhamento, tensão de escoamento, entre outras, não são possíveis de se obter através desse ensaio. Entretanto, o emprego de equipamentos automatizados e controlados, tais como os reômetros, garante a obtenção de informações mais precisas a respeito do fluido estudado.

A reologia é o ramo da física que analisa os efeitos provocados um material através de aplicações de uma tensão ou deformação, procurando entender as relações entre tensão, deformação, taxa de deformação e tempo. Há uma preocupação quanto à mecânica de corpos deformáveis que podem estar no estado sólido, líquido ou gasoso (MARTINS, 2004; COSTA, 2006; SCHRAMM, 2006). O estudo da reologia, na prática, está voltado para os materiais que apresentam propriedades do escoamento mais complexas do que as de um fluido simples (líquido ou gás) ou as de um sólido elástico ideal, apesar de que, dependendo das condições que o ensaio é realizado, o material terá um comportamento simples ou complexo (CASTRO, 2007).

Segundo De Larrard et al. (1996), a finalidade de se utilizar um reômetro não é apenas medir o maior número de parâmetros possíveis, mas avaliar quantidades físicas que possam estar cientificamente relacionadas aos vários estágios de utilização do concreto. Reis (2008) afirma que essa tensão de cisalhamento está diretamente relacionada com o ensaio de abatimento de tronco de cone. Outro parâmetro reológico analisado é a viscosidade aparente, que aponta o acréscimo de tensão que deve ser imposta para produzir uma determinada taxa de cisalhamento. A viscosidade aparente se associa, na prática, às capacidades de aplicação, bombeamento, segregação do material e acabamento, facilitando a distinção entre um concreto trabalhável de um que apresenta um comportamento “pegajoso”, com dificuldades para bombear e apresentando vazios na superfície do elemento estrutural quando a forma é retirada (CASTRO et al., 2011).

Quando a trabalhabilidade é avaliada quanto aos parâmetros reológicos, o controle da produção do concreto é feito de uma forma mais criteriosa. Além de mostrar se o ensaio obteve um resultado apropriado ou não – o que os ensaios padrões são incapazes de realizar – essa avaliação também pode identificar quais os fatores que estão influenciando para a falha do ensaio de se atingir a trabalhabilidade desejada (CASTRO, 2007).

Para a determinação dos parâmetros reológicos da pasta cimentícia, tais como tensão de escoamento, viscosidade aparente, perfil reológico do material e, ainda, os efeitos da consolidação desse material associados à hidratação do cimento, a literatura propõe alguns testes como, por exemplo, ensaio de fluxo, ensaio oscilatório (varredura de tempo e varredura de deformação) e ensaio de palheta ou Vane test (SATO et al., 2012; LISBÔA, 2004; CAVALCANTI, 2006; VENÂNCIO, 2008; SAAK et al., 2001; BETIOLI et al., 2009). Apesar do número cada vez crescente de estudos que visam à análise do comportamento do concreto em seu estado fresco, o uso de ferramentas e ensaios baseados na reologia rotacional ainda é incipiente.

O concreto no seu estado fresco pode ser considerado um fluido e, por conseguinte, os princípios básicos da reologia podem ser aplicados a este material (METHA, 1986). Os fatores mais importantes que causam incompatibilidades de concreto podem ser resumidos como a quantidade de C3A; o tipo e a quantidade de sulfato de rolamento no cimento; álcalis solúveis em água (Na+, K+), tanto a partir do cimento quanto do aditivo; o tipo e a dosagem de ambos, como misturas minerais; a temperatura de pasta de cimento e a relação água/cimento. Alguns pesquisadores (FERRARIS, 1996; ZHANG, 2001; CHEN, STRUBLE, ZHANG, 2006) relataram a sensibilidade dos parâmetros reológicos para os fatores acima mencionados.

Para a análise dos parâmetros reológicos de pastas e argamassas cimentícias, alguns parâmetros devem ser cuidadosamente definidos. O tempo e a energia de mistura na fabricação de misturas, por exemplo, influenciam significativamente nas propriedades reológicas do material. Em sua pesquisa, França, Cardoso e Pileggi (2011 e 2012) mencionam que quanto maior o tempo de mistura, mais eficiente é o processo de mistura devido à maior energia envolvida no processo, produzindo um material disperso (menor o tamanho das unidades móveis, partículas ou aglomerados), homogêneo, estável e um comportamento mais fluido. A mistura de pasta de cimento deve imitar o cisalhamento que é submetido no concreto. Bhattacharja e Tang (2000) também relataram a utilização de um misturador de alto cisalhamento para preparação da pasta de cimento simulando o efeito de cisalhamento.

Levando em consideração a necessidade de uma avaliação mais abrangente das propriedades do concreto no seu estado fresco, esta pesquisa busca fazer a análise das propriedades reológicas de pastas cimentícias através da realização de ensaio de fluxo utilizado o reômetro de cisalhamento dinâmico como principal equipamento de ensaio. Assim, propriedades reológicas de pastas produzidas com diferentes relações água-cimento com e sem incorporação de

Figura 1 – Curva granulométrica do cimento Portland CP III 40 RS

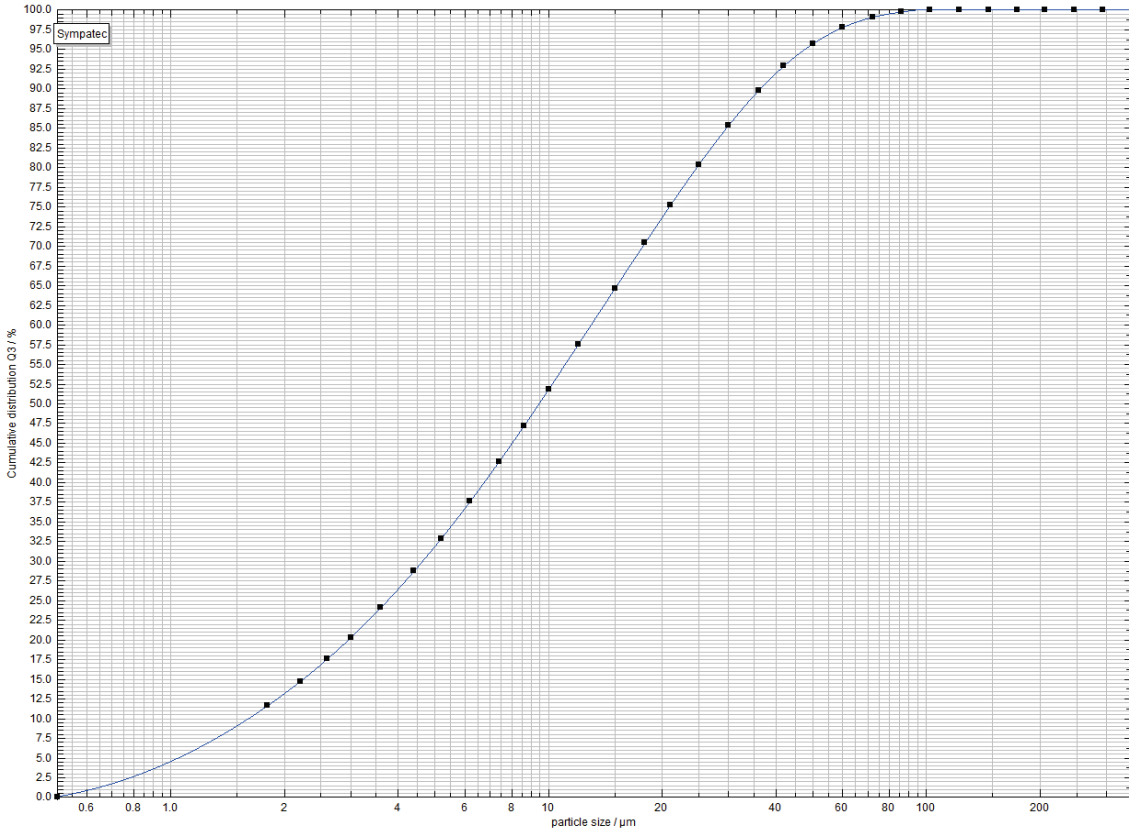

aditivos serão analisadas para verificar os efeitos destes constituintes no comportamento reológico de pastas cimentícias.

2. Objetivos

O presente trabalho tem como objetivo verificar o comportamento reológico de diferentes pastas cimentícias produzidas através da mistura de água e cimento Portland, com e sem incorporação de aditivos, de forma a se verificar a influência destes constituintes nos parâmetros reológicos analisados (tensão de escoamento, viscosidade aparente, perfil reológico do material e efeitos da consolidação desse material associados à hidratação do cimento).
Na composição dessas pastas foram utilizadas diferentes relações água-cimento (0,40; 0,45 e 0,50), com e sem incorporação de aditivo. Além disso, as pastas foram ensaiadas em diferentes tempos de hidratação (20 e 60 min), para que também fosse possível a verificação do efeito da hidratação do cimento nas propriedades reológicas das pastas cimentícias estudadas.

3. Materiais e métodos

3.1 Materiais

Para a realização desta pesquisa utilizou-se o cimento CP III 40 RS, classificado como cimento Portland de Alto Forno resistentes à sulfatos de acordo com a norma NBR 5735 (ABNT, 1991). Para caracterização granulométrica do material, foi realizado ensaio utilizando um granulômetro (modelo Sympatec®) de difração a laser, cuja lente realiza leituras em materiais na faixa de 1,8 a 350 mm. A Figura 1 mostra a curva de distribuição granulométrica obtida para o cimento utilizado neste estudo.
O aditivo incorporado nas pastas cimentícias estudadas foi o GLENIUM® 51 (da empresa BASF S. A.), que é um superplastificante à base de éter policarboxílico. A água utilizada neste trabalho foi obtida diretamente da rede de água da concessionária.

Tabela 1 – Relações a/c e quantidade de aditivo nas pastas analisadas

Pasta cimentícia	Relação a/c	Aditivo
Pasta 1	0,40	–
Pasta 2	0,45	–
Pasta 3	0,50	–
Pasta 4	0,40	0,2 %
Pasta 5	0,45	0,2 %
Pasta 6	0,50	0,2 %

Tabela 2 – Processo de mistura dos materiais

Procedimento	Tempo inicial (s)	Tempo final (s)
Junção de cimento com a água	0	30
Mistura com mixer	30	60
Limpeza e espera	60	120
Mistura com mixer	120	150

3.2 Composição e preparação das pastas cimentícias

Nesta pesquisa foram analisadas amostras de pastas cimentícias com três relações a/c distintas, com e sem acréscimo de aditivo. Na Tabela 1 são apresentados os valores de relação a/c e a quantidade de aditivo determinada para cada amostra utilizada no ensaio de fluxo.

3.2.1 Procedimento de mistura

Como ainda não há um método normatizado de mistura para a produção de pastas cimentícias a serem utilizadas na determinação das propriedades reológicas utilizando reômetro de cisalhamento dinâmico, foi adotado na presente pesquisa o procedimento de mistura das pastas cimentícias segundo a norma NBR 13276 (ABNT, 2005) que se trata do preparo da mistura e determinação do índice de consistência da argamassa para assentamento e revestimento de paredes e tetos. As massas dos materiais foram estabelecidas numa balança eletrônica digital de precisão de 0,01g. Utilizou-se um misturador mecânico para garantir a homogeneização da amostra. De acordo com a NBR 13276 (ABNT, 2005), primeiramente, pesou-se separadamente a quantidade de água e cimento com aproximação de 1,0g. Em seguida acrescentou-se na água a porção específica de cimento correspondente à relação a/c estudada, de modo contínuo num período de 30 segundos. Após a junção dos materiais, estes foram misturados com um mixer por 30 segundos e então o equipamento foi desligado. Limpou-se o mixer e esperaram-se mais 60 segundos e, por fim, ligou-se o equipamento e misturou-se por mais 30 segundos de forma a obter um a pasta homogênea. Nas pastas compostas também pelo aditivo, este foi incorporado à pasta após o término da mistura mencionada anteriormente, e a nova mistura foi homogeneizada com a espátula por 30 segundos. A Tabela 2 mostra as etapas executadas para preparação das pastas cimentícias.

Após todo o processo de mistura, as amostras foram mantidas em recipientes herméticos até a realização dos ensaios para que não houvesse perda de umidade para o meio. Antes de cada ensaio, a pasta era misturada novamente da seguinte forma: 30 segundos com o mixer, 15 segundos com a espátula e 30 segundos com o mixer novamente, a fim de manter sua homogeneidade.

3.3 Ensaio de fluxo

Através do ensaio de fluxo é possível obter a tensão de cisalhamento a uma dada taxa de cisalhamento. O ensaio consiste na aplicação de uma taxa crescente de cisalhamento com aceleração de 0 a 100 s-1 em 2 min seguida de uma desaceleração até 0, em mais 2 min, como ilustrada na Figura 2.

A partir da variação desses parâmetros, pode-se traçar o perfil reológico dos materiais e assim determinar importantes propriedades reológicas, tais como viscosidade aparente (η_{ap}), tensão de escoamento (σ_0) e área de histerese (AH). A viscosidade aparente das pastas cimentícias foi avaliada na máxima taxa de cisalhamento aplicada, que neste estudo foi de 100 s^{-1}. A tensão de escoamento foi aproximada pela extrapolação da curva de tensão de cisalhamento *vs* taxa de cisalhamento, até a taxa 0 s-1.

Figura 2 – Rampa de 0 a 100 s-1 em 2 minutos e até 0 s-1 em mais 2 minutos (Betioli et al., 2009)

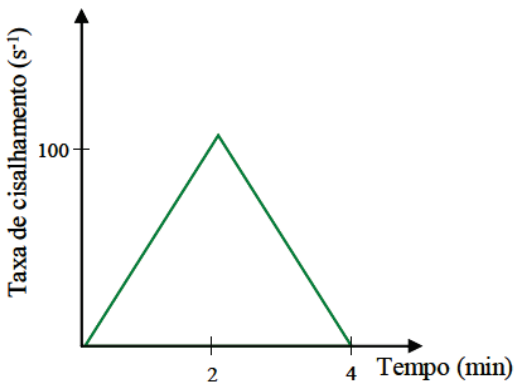

Figura 3 – Taxa de calor liberado durante 6 h de hidratação. O intervalo do período de indução ocorre entre 20 min e 110 min, aproximadamente (Silva, 2001)

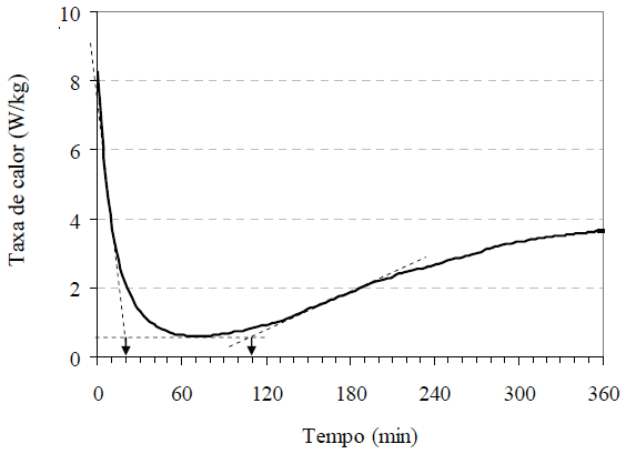

Outro parâmetro analisado com os resultados do ensaio de fluxo é a área de histerese (AH). Esta área é formada através das curvas de aceleração e desaceleração no gráfico de tensão de cisalhamento *vs* taxa de cisalhamento (OLIVEIRA *et al*., 2000; BETIOLI *et al*., 2012) e indica o grau de estruturação/desestruturação do sistema.
Os ciclos de cisalhamento foram realizados em tempos predefinidos dentro do intervalo de indução ou dormência do cimento, o qual apresenta menor liberação de calor (KIRCHHEIM, 2008). Neste intervalo as reações de hidratação do cimento são consideradas controladas, o que permite considerar a conservação da massa no momento do ensaio. Silva (2001) determinou o período de indução entre 20 min e 110 min a partir das intersecções do trecho horizontal com duas retas: a reta traçada no período de pré-indução e a extrapolação da linha de regressão do período de aceleração, como apresentado na Figura 3.
Dessa forma, as pastas cimentícias foram ensaiadas em dois tempos distintos de hidratação do cimento (20 min e 60 min) dentro do intervalo de indução do material para análise dos efeitos da hidratação do cimento nas propriedades reológicas das pastas cimentícias. Para a realização dos ensaios de fluxo foi utilizado um reômetro de cisalhamento dinâmico. A geometria escolhida para o ensaio de fluxo foi a geometria de placas paralelas, que possui diâmetro de 40 mm e espaçadas de 1 mm. Para cada pasta estudada, foram ensaiadas três amostras. Na composição dos gráficos de tensão de cisalhamento *vs* taxa de cisalhamento e viscosidade *vs* taxa de cisalhamento utilizou-se a média aritmética dos valores das amostras. A partir da análise dos gráficos verificaram-se os efeitos da relação água-cimento, da incorporação do aditivo e da hidratação do cimento em seu comportamento reológico. Para evitar a evaporação da água e manter a temperatura da amostra em 25o C durante o ensaio, utilizou-se um dispositivo protetor (placa peltier). Foi fixado na superfície de cada placa um adesivo texturizado para impedir o deslizamento da amostra, como ilustrado na Figura 4.

4. Resultados e discussão

As Figura 5 e 6 ilustram a tensão de cisalhamento e a viscosidade aparente em função da taxa de cisalhamento para as pastas cimentícias (com e sem aditivo) químico para cada tempo de hidratação (20 e 60 min) analisado neste estudo.
É possível perceber que as pastas cimentícias estudadas necessitam de uma tensão de cisalhamento inicial (s0) para iniciar o escoamento. Após superar esta tensão de escoamento, as pastas apresentam um comportamento não linear, mostrando uma tendência de comportamento de um fluido Herschel-Bulkley, também conhecido como Bingham generalizado.
Ao se analisar as áreas de histereses entre as curvas de aceleração e desaceleração do gráfico tensão de cisalhamento *vs* taxa de cisalhamento, é possível perceber que aos 20 minutos de hidratação, esta área é praticamente nula. Isso pode indicar o estado de dispersão das amostras. Áreas de histereses pouco significativas indicam que o processo de mistura adotado foi suficiente para a obtenção de uma amostra homogênea com a quebra de todos os aglomerados.Já aos 60 minutos de hidratação, percebe uma tendência de reestruturação destes aglomerados e dessa, forma, essa quebra se dá nos ciclos de cisalhamento impostos.
A ação do aditivo é percebida pela redução dos n´veis de tensão de cisalhamento das amostras. Segundo Oliveira *et al.* (2003 *apud* França, Cardaso e Pilegi, 2012), os níveis de tensão requeridos para mistura de concretos são reduzidos ao se utilizar aditivos, pois estes possibilitam uma melhor dispersão das partículas.
Observa-se (Figura 6) que em todas as pastas a viscosidade aparente, obtida através da relação entre a tensão de cisalhamento e taxa de cisalhamento, diminui com o aumento da taxa de cisalhamento, mostrando a natureza tixotrópica do material. Nas pastas que obtiveram o acréscimo do aditivo ficaram evidentes os efeitos da adição destes no comportamento reológico das pastas, como a

Figura 4 – Geometria de placas paralelas com peltier e adesivo texturizado

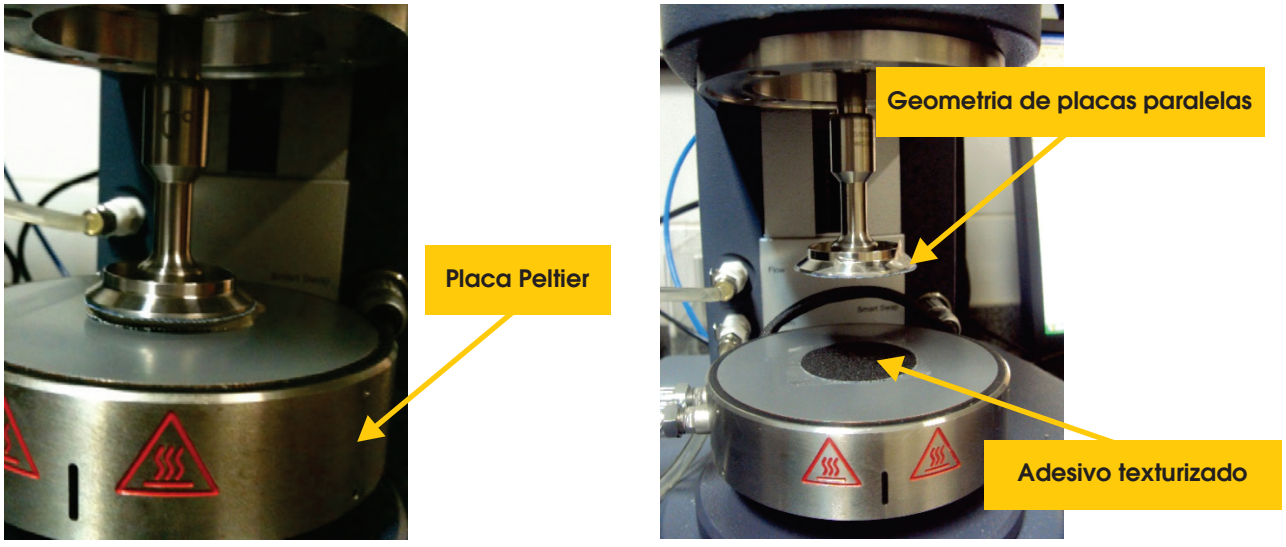

Figura 5 – Tensão de cisalhamento vs taxa de cisalhamento em pastas cimentícias: (a) sem aditivo e (b) com aditivo, ensaiadas nos tempos de hidratação de 20 e 60 minutos

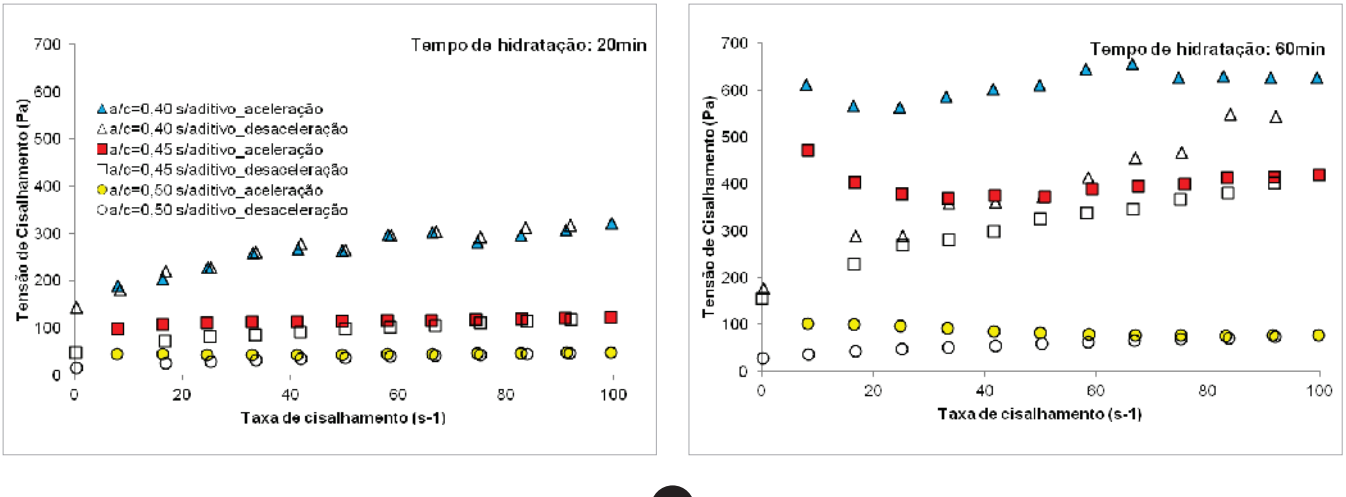

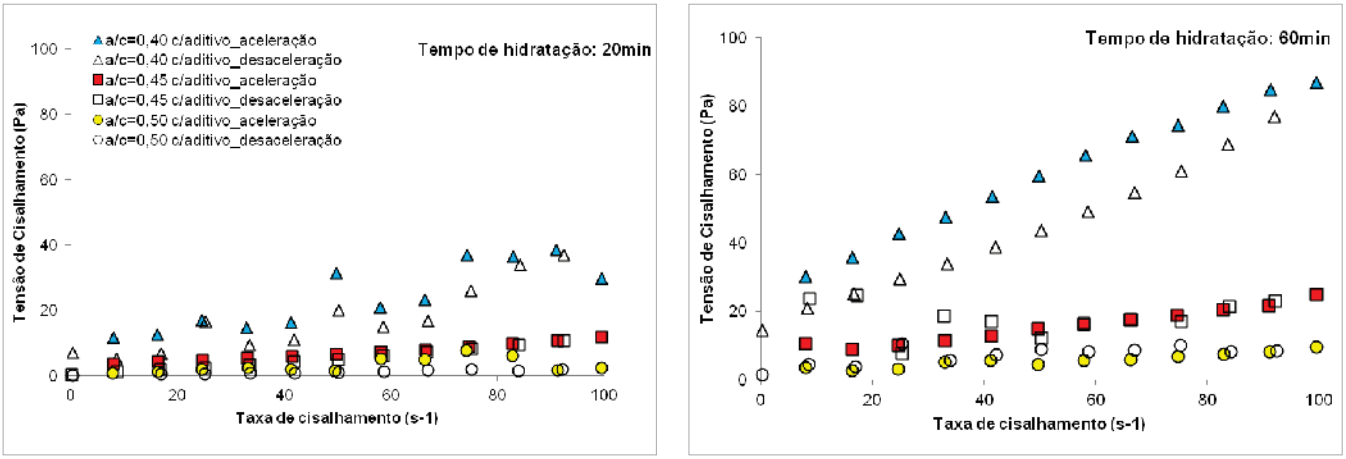

Tabela 3 – Propriedades reológicas das pastas cimentícias após tempo de hidratação de 20 min.

a/c	η_{ap} (Pa.s)		σ_0 (Pa.s)	
	Sem aditivo	Com aditivo	Sem aditivo	Com aditivo
0,4	3,2	0,29	143	8,5
0,45	1,2	0,11	47	2,48
0,5	0,48	0,02	15	0,2

Tabela 4 – Propriedades reológicas das pastas cimentícias após tempo de hidratação de 60 min.

a/c	η_{ap} (Pa.s)		σ_0 – Aceleração (Pa.s)	
	Sem aditivo	Com aditivo	Sem aditivo	Com aditivo
0,4	6,3	0,87	576	27
0,45	4	0,2	441	8
0,5	0,8	0,1	100	3

diminuição da viscosidade aparente, como mostrado na Figura 6, quando comparadas as pastas sem aditivos (Figura 5). Com a adição deste material, as pastas se tornaram mais fluidas, e mais susceptíveis a deformações excessivas quando submetidas a tensões de cisalhamento, tonando mais difícil à medição de valores de tensão de cisalhamento com o equipamento utilizado nesta pesquisa.

A Tabela 3 e 4 apresenta os valores da viscosidade aparente e das tensões de escoamento obtidas para os tempos de 20 min e 60 min de hidratação, respectivamente.

É possível verificar que pastas sem aditivo e relação a/c de 0,40; 0,45 e 0,5 sofreram, respectivamente, um incremente de 4, 9 e 7 vezes nas suas tensões de escoamento quando atingiram a idade de hidratação de 60 min em comparação com a idade de hidratação de 20 min. O incremento no tempo de hidratação fez com que as pastas apresentassem uma estrutura mais aglomerada, devido ao processo de hidratação das partículas de cimento, sendo portanto necessário a aplicação de uma maior tensão para iniciar o escoamento da pasta, fenômeno este refletido no incremento de valor da tensão de escoamento. Como esperado, as pastas sem aditivo exibiram maiores resistências ao escoamento quando comparadas às pastas com aditivos, valores estes que também refletiram nas viscosidades aparentes das pastas estudadas. A adição de aditivos plastificantes a base de policarboxilato causam dispersão das partículas de cimento, aumentando assim sua fluidez, efeito conhecido como repulsão elétrica. Assim, as pastas com aditivos se tornam mais fluidas, resultando numa expressiva diminuição dos valores de tensão de escoamento e viscosidade aparente quando comparamos pastas com mesma relação água-cimento.

A Figura 7 ilustra a correlação entre a tensão de escoamento e a relação água-cimento obtida neste estudo.

Figura 6 – Viscosidade aparente vs taxa de cisalhamento em pastas cimentícias: (a) sem aditivo e (b) com aditivo, ensaiadas nos tempos de hidratação de 20 e 60 minutos

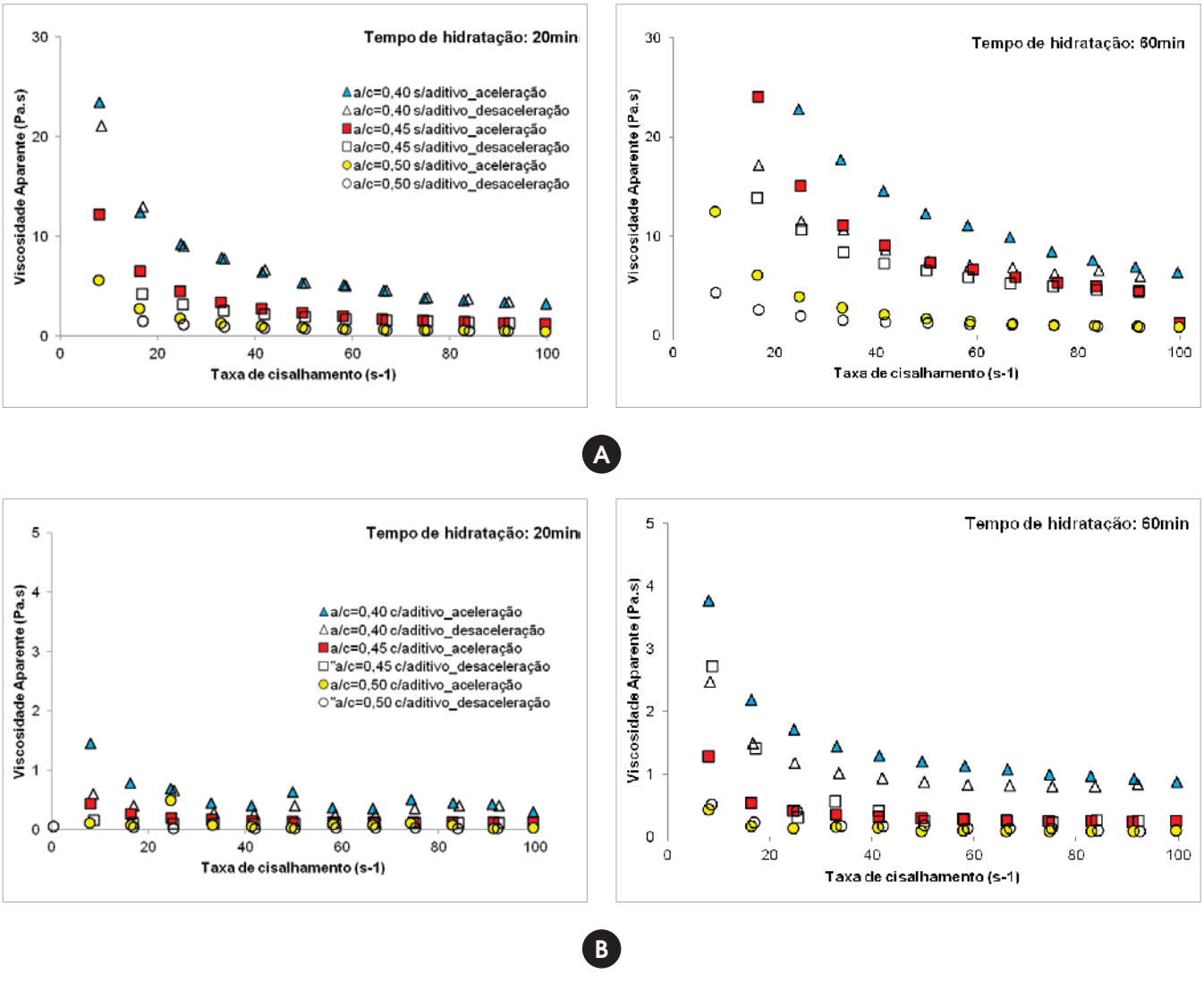

Figura 7 – Correlação entre a tensão de escoamento e relação água-cimento em tempo de hidratação de 20 minutos

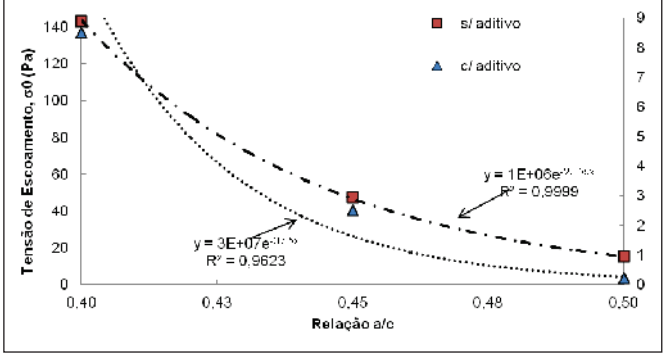

É possível perceber uma tendência de correlação entre os parâmetros analisados utilizando uma função exponencial, tanto para pastas com e sem uso de aditivo. Os coeficientes de determinação (R^2) de 0,99 e 0,96 para as pastas sem e com aditivos, respectivamente, mostram uma correlação negativa forte entre a tensão de escoamento com a relação água-cimento. O uso deste tipo de correlação, com base em análise de parâmetros reológicos pode levar a medidas do grau de trabalhabilidade de uma maneira mais científica.

5. Conclusões

Para uma melhor compreensão da influência de variáveis importantes na dosagem de misturas cimentícias (relação a/c, hidratação do cimento e uso de aditivos químicos) no comportamento de materiais à base de cimento, utilizou-se ensaios reológicos. O comportamento reológico pastas cimentícias é complexo, pois diversos fatores interferem nas suas propriedades como, por exemplo, o tipo de cimento e sua natureza reativa, a relação água/cimento utilizada, a presença de aditivos, as condições de mistura (velocidade, tempo, confinamento), entre outros.

O ensaio de fluxo é uma ferramenta eficaz para a determinação das propriedades reológicas de pastas cimentícias em laboratório uma vez que é possível solicitar as amostras com alta magnitude de cisalhamento. O que resultou em diferentes valores das propriedades reológicas (viscosidade aparente e tensão de escoamento).

Observou-se que a viscosidade aparente é maior em pastas com menor relação água/cimento entre as amostras sem incorporação de aditivo. As pastas que tiveram incorporação de aditivo mostraram viscosidades aparentes com pouca variação.

Verificou-se que as tensões de escoamento das pastas sem aditivo cresceram significativamente com a idade de hidratação.

Mostra-se necessária a realização de mais pesquisas para caracterização reológica de pastas cimentícias considerando o grande número de materiais que podem ser utilizados na confecção as mesmas.

6. Agradecimentos

Os autores agradecem à CAPES e ao CNPq pelo aporte financeiro, e ao Laboratório de Ensaios em Materiais de Construção (LEMAC) do Centro tecnológico da Universidade Federal do Espírito Santo pelo apoio técnico e por disponibilizar a infraestrutura necessária para a realização desta pesquisa.

7. Referências

[01] ASSOCIAÇÃO BRASILEIRA DE NORMAS TÉCNICAS. NBR 13276: Preparo da mistura e determinação do índice de consistência da argamassa para assentamento e revestimento de paredes e tetos, 2005.

[02] _____. NBR 5735: Cimento Portland de Alto Forno. Rio de Janeiro, 1991.

[03] _____. NBR 7212: Execução de concreto dosado em central. Rio de Janeiro, 1984.

[04] _____. NBR NM 67: Concreto - Determinação da consistência pelo abatimento do tronco de cone. Rio de Janeiro, 1998.

[05] BARNES, H. A.; HUTTON, J. F.; WALTERS, K. An introduction to rheology. 3. ed. Amsterdam: Elsevier, 1993.

[06] BETIOLI, A. M.; JOHN, V. M.; GLEIZE, P. J. P., PILEGGI, R. G. Caracterização reológica de pasta cimentícia: associação de técnicas complementares. Ambiente Construído, Porto Alegre, v. 9, n. 4, p. 37-48, out./dez. 2009.

[07] BETIOLI, A. M. , GLEIZE, P. J. P., JOHN, V. M. , PILEGGI, R. G. Effect of EVA on the fresh properties of cement paste. Cement & Concrete Composites Vol. 34, 255–260, 2012.

[08] BHATTACHARJA, S.; TANG, F. J. Rheology of cement paste in concrete with different mix designs and interlaboratory evaluation of the mini-slump cone test, PCA R&D, Serial No. 2412, Portland Cement Association, Skokie, Illinois, 2000.

[09] CASTRO, A. L. Aplicação de conceitos reológicos na tecnologia dos concretos de alto desempenho. 2007. 302f. Tese (Doutorado) - Escola de Engenharia de São Carlos / Instituto de Física de São Carlos/ Instituto de Química de São Carlos - Universidade de São Paulo, São Carlos, 2007.

[10] CASTRO A. L., LIBÓRIO J. B. L., PANDOLFELLI V. C. Reologia de concretos de alto desempenho aplicados na construção civil – Revisão. Revista Cerâmica, São Carlos, v. 57, p. 63-75, 2011.

[11] CAVALCANTI, D. J. H. Contribuição ao estudo de propriedades do concreto auto-adensável visando sua aplicação em elementos estruturais. 2006. 141f. Dissertação (Mestrado) – Programa de Pós-Graduação em Engenharia Civil, Universidade Federal de Alagoas, Maceió, 2006.

[12] CHEN, C.; STRUBLE, L. J.; ZHANG, H. Using dynamic rheology to measure cement-admixture interactions. Journal of ASTM International, West Conshohocken, v. 3, mar. 2006.

[13] COSTA, M. R. M. M. Análise comparativa de argamassas colantes de mercado através de parâmetros reológicos. 2006. 131f. Tese (Doutorado) – Escola Politécnica da Universidade de São Paulo, São Paulo, 2006.

[14] De LARRARD, F.; SEDRAN, T.; HU, C.; SZITKAR, J. C.; JOLY, M.; DERKX, F. Evolution of the workability of superplasticized concretes: assessment with the BTRHEOM rheometer. In: International Rilem Conference – Production Methods and Workability of Concrete, 1996, Paisley/Scotland. Proceedings… London: E & FN Spon, 1996, p. 377-388.

[15] FERRARIS, C. F.. Measurements of rheological properties of high performance concrete: state of the art report. Journal of

Research of the National Institute of Standards and Technology, Gaithersburg, v. 104, n. 5, p. 461-478, 1996.

[16] FRANÇA, M. S.; CARDOSO, F. A.; PILEGGI, R. G. Avaliação do comportamento de mistura de argamassas através de reometria rotacional. Ambiente Construído, v. 12, n. 2, p. 165-174, 2012.

[17] FRANÇA, M. S.; CARDOSO, F. A.; PILEGGI, R. G. Influência do tempo de mistura nas propriedades reológicas de argamassas. In: Simpósio Brasileiro de Tecnologia de Argamassas, 9., 2011, Belo Horizonte. Anais... Belo Horizonte: SBTA, 2011.

[18] GHIO, V. A.; MMONTEIRO P. J.; DEMSETZ, L. A. The rheology of fresh cement paste containing polysaccharide gums. Cement Concrete Research, Philadelphia, v. 24, n. 2, p. 243-249, 1994.

[19] HACKLEY, V. A.; FERRARIS, C. F. Guide to rheological nomenclature: measurements in ceramic particle systems. NIST special publication, v. 946, 2001.

[20] KIRCHHEIM, A.P. Aluminatos tricálcicos cúbico e ortorrômbico: análise da hidratação in situ e produtos formados. 2008. 265f. Tese (Doutorado) – Programa de Pós-Graduação em Engenharia Civil, Universidade Federal do Rio Grande do Sul, Porto Alegre. 2008.

[21] LISBÔA, E. M. Obtenção do concreto auto-adensável utilizando resíduo do beneficiamento do mármore e granito e estudo de propriedades mecânicas. 2004. 121f. Dissertação (Mestrado) – Programa de Pós-Graduação em Engenharia Civil, Universidade Federal de Alagoas, Maceió, 2004.

[22] MARTINS, A. L. P. Estudo das propriedades reológicas do muco brônquico de pacientes sob fisioterapia respiratória. 2004. 70f. Dissertação (Mestrado) - Programa de Pós-Graduação em Fisioterapia. Universidade Federal de São Carlos, São Carlos, 2004.

[23] METHA, P. K. Concrete: structure, properties, and materials. Prentice-Hall, Inc, Englewood Cliff, New Jersey, p. 449, 1986.

[24] NONAT, A.; MUTIN, J. C.; LECOQ, X.; JIANG, S. P. Physico-chemical parameters determining hydration and particle interactions during the setting of silicate cements. Solid State Ionics, v. 101-103, n. 2, p. 923-930, nov. 1997.

[25] OLIVEIRA, I. R., STUDART, A. R., PILEGGI, R. G., PANDOLFELLI, V. C. Dispersão e empacotamento de partículas: Princípios e aplicações em processamento cerâmico. Fazendo Arte Editorial. 2000.

[26] RAMACHANDRAN, V. S.; BEAUDOIN, J. J. Handbook of analytical techniques in concrete science and technology: principles, techniques, and applications, Book 2001.

[27] REIS, J. F. A. Determinação de parâmetros reológicos de concretos através do ensaio de abatimento de tronco de cone modificado: estudo de caso. 2008. 177f. Dissertação (Mestrado) – Programa de Pós-Graduação em Engenharia Mecânica, Universidade Estadual Paulista, Ilha Solteira, 2008.

[28] SAAK, A. W.; JENNINGS, H. M.; SHAH, S. P. The influence of wall slip on yield stress and viscoelastic measurements of cement paste. Cement and Concrete Research, Philadelphia, v. 31, n. 2, p. 205-212, fev. 2001.

[29] SATO, V. Y.; EVANGELISTA, K. T. C.; TEIXEIRA, J. E. S. L.; TRISTÃO, F. A. Estudo das propriedades reológicas de pastas de cimento de concretos bombeados. In: Congresso Brasileiro do Concreto, 54., 2012, Maceió. Anais... Maceió: IBRACON, 2012.

[30] SCHRAMM, G. Reologia e reometria: fundamentos teóricos e práticos. 2. ed. São Paulo: Artiliber, 2006.

[31] SILVA, D. A. Efeitos dos polímeros HEC e EVA na microestrutura de pastas de cimento portland. 2001. 246f. Tese (Doutorado em Ciência e Engenharia dos Materiais) – Departamento de Engenharia dos Materiais, Universidade Federal de Santa Catarina, Florianópolis, 2001.

[32] TATTERSALL, G.H.; BANFILL P.F.G. The Rheology of Fresh Concrete, Pitman, p. 356, 1983.

[33] VENÂNCIO, P. B. F. Dosagem de argamassa para estaca raiz. 2008. 173f. Dissertação (Mestrado) – Departamento de Engenharia Civil e Ambiental, Universidade de Brasília, Brasília, 2008.

[34] ZHANG, H. Using Dynamic Rheology to Explore the Microstructure and Stiffening of Cementitious Materials, Ph.D. Thesis, University of Illinois at Urbana-Champaign, 2001.

Volume 7, Number 6 (December 2014) p. 940-964 • ISSN 1983-4195

IBRACON

REVISTA IBRACON DE ESTRUTURAS E MATERIAIS

IBRACON STRUCTURES AND MATERIALS JOURNAL

Finite Difference Energy Method for nonlinear numerical analysis of reinforced concrete slab using simplified isotropic damage model

Análise não linear numérica via MDFE de lajes de concreto armado utilizando a mecânica do dano



M. V. A. LIMA [a]
mveniciosalmeida@gmail.com

J. M. F. LIMA [a]
lima.jmf@gmail.com

P. R. L. LIMA [a]
lima.prl@pq.cnpq.br

Abstract

This work presents a model to predict the flexural behavior of reinforced concrete slabs, combining the Mazars damage model for simulation of the loss of stiffness of the concrete during the cracking process and the Classical Theory of Laminates, to govern the bending of the structural element. A variational formulation based on the principle of virtual work was developed for the model, and then treated numerically according to the Finite Difference Energy Method, with the end result a program developed in Fortran. To validate the model thus proposed have been simulated with the program, some cases of slabs in flexure in the literature. The evaluation of the results obtained in this study demonstrated the capability of the model, in view of the good predictability of the behavior of slabs in flexure, sweeping the path of equilibrium to the rupture of the structural element. Besides the satisfactory prediction of the behavior observed as positive aspects of the model to its relative simplicity and reduced number of experimental parameters necessary for modeling.

Keywords: reinforced concrete slabs, damage mechanics, finite difference energy method.

Resumo

Neste trabalho é apresentado um modelo para previsão do comportamento à flexão de lajes de concreto armado, combinando o modelo de dano de Mazars, para simulação da perda de rigidez do concreto durante o processo de fissuração e a Teoria Clássica de Laminados, para reger a flexão do elemento estrutural. Uma formulação variacional com base no princípio dos trabalhos virtuais foi desenvolvida para o modelo, sendo em seguida tratada numericamente segundo o Método das Diferenças Finitas Energéticas (MDFE), tendo como resultado final um programa desenvolvido em Fortran. Para validar o modelo proposto, foram simulados com o programa dois casos de lajes sob flexão, encontrados na literatura. A avaliação dos resultados obtidos nas análises demonstrou a potencialidade do modelo, tendo em vista a boa capacidade de previsão do comportamento de lajes sob flexão, varrendo a trajetória de equilíbrio até a ruptura do elemento estrutural. Além da satisfatória previsão do comportamento observou-se, como aspectos positivos do modelo, a sua relativa simplicidade e o número reduzido de parâmetros experimentais necessários à modelagem.

Palavras-chave: laje de concrero armado, mecânica do dano, método das diferenças finitas energéticas.

[a] *Universidade Estadual de Feira de Santana, Programa de Pós-graduação em Engenharia Civil e Ambiental, Feira de Santana, Bahia, Brasil.*

Received: 25 Sep 2013 • Accepted: 11 Jul 2014 • Available Online: 01 Dec 2014

© 2014 IBRACON

1. Introduction

The concrete structures are used throughout the world with many different applications, as bridges, buildings, roads, etc. However, the reduction of natural resources and the large consumption of energy in production of cement and steel have required the use of structures using the full potential of these materials. Despite the design codes permitting the use of simplify models to calculate the reinforced concrete structures, only with the development of more sophisticated methods will be possible to obtain an optimized structure. Using an appropriate numerical method, that incorporates the nonlinearity of the physical material, will be possible to predict with more accuracy the structural behavior of structures under bending, identifying their state of cracking and deformation.

Since 1904, the finite difference method (FDM) has been used in solving differential equations for structural analysis of continuous beams or plates loaded in plane or out of plane [1]. As a computational method the FDM, together with finite element method (FEM), originated in the engineering literature in the mid 1950s. Many ideas and techniques are common to both methods, and in some cases they coincide. Nevertheless, with its more systematic use of the variational approach, its greater geometric flexibility, and the way it more easily lends itself to error analysis, the FEM has become the dominating approach both among numerical analysts and in applications [2]. However, recent studies have demonstrated the capability of the FDM in the analysis of reinforced concrete structures: structural analysis of slab [3], tensile members [4], frames [5] and columns [6] of reinforced concrete has been developed using physical or geometrical nonlinearity approach to evaluate the cracking, ultimate load, spalling, steel-concrete bond-slip, deflection and buckling. The results indicate that: i) the comparisons with experimental results confirm the validity of the method and ii) the finite difference analysis procedure is both fast-running and accurate and most suitable for design office application, combining the speed of analysis and the detail and accuracy of FE analysis [7].

An evolution of the finite difference method is the Finite Difference Energy Method (FDEM). Finite difference analysis divides a member into discrete segments to find an approximate solution to the differential equations of member motion. The segments in partial difference analysis are divided by nodes, with the displacement at each node expressed in terms of the difference in displacement of adjacent nodes. In FDEM these differences are used directly in equations associated to principle of virtual work or to principle of potential energy. This fact leads to some advantages over the traditional approach of the finite difference method with lower order derivatives and higher accuracy. With the variational principle, the boundary condition is taken care automatically and the matrix of equilibrium equations is symmetric (in the case of elements without damage), which yield considerable savings in computational effort. By relying on energy equations, the method has a similar structure with the finite element method (FEM): the discretization is conceived in terms of nodal degrees of freedom and it uses the same kinematic boundary conditions. One advantage of this method with respect to the FEM is a reduction of degrees of freedom by node what demonstrates the great potential to mechanical analysis of complex structures.

In fact, structural applications of FDEM have emerged in 1950s, with Houbolt [8], Griffin and Varga [9] and Bushnell [10]. In Brazil the FDEM has been used since 1980s to analyze of isotropic beams, plates and shells [11-14]. Recently the FDEM, in association with Damage Mechanics, was used to modeling of reinforced concrete beams and fiber concrete beams [15] resulting in good agreements with experimental results. This qualifies the model for analysis of more complex structures such as reinforced concrete slabs.

The application of nonlinear models for the study of reinforced concrete slabs is less reported in the technical literature, when compared with studies on beams. However, some important contributions to the theoretical prediction of the bending behavior of slabs can be verified as the association between elastoplastic model and FEM [16-17]. The use of Mazars [18] with Boundary Element Method [19] alone or combined with FEM [20] has also been reported. Fracture Mechanic model and FEM were used by Bandeira [21] to analyze reinforced concrete slabs with commercial software DIANA. All results indicate that, with the use of non-linear models for modeling the stress-strain behavior of concrete, it is possible to predict satisfactorily the structural behavior of reinforced concrete slabs under bending.

The main objective of this work is to verify the application of the FDEM to nonlinear analysis of reinforced concrete slabs using the Damage Model of Mazars [18]. Another nonlinear models, based at experimental results, has been used to describe the stress-strain behavior of concrete [22-24] but the application of Mazars´s Model showed a good performance to analyze of reinforced concrete beams [25-26] and requires few experimental parameters. Two reinforced concrete slabs evaluated experimentally by Taylor et al. [27] and McNeice [28] were used to validate the proposed model.

2. Analytical formulation

2.1 Damage model

The damage model proposed by Mazars [18] has easy implementation, when compared with anysotropic model, for example. This is because the damage variable D is associated with the extension deformation of concrete according to the following hypotheses:

a) The damage process of concrete occurs in elastic state;
b) The concrete is considered isotropic before and after the damage;
c) It is supposed that the damage begins when the equivalent strain reaches a reference strain value ε_{d0}, determined in uniaxial tensile tests in relation to the maximum stress.

In this analysis, the stress in a given main direction $i\left(i = 1, 2\ and\ 3\right)$ can be represented by positive and negative:

$$\sigma_i^+ = \sigma_i \text{ if } \sigma_i > 0 \text{ and } \sigma_i^+ = 0 \text{ if } \sigma_i \leq 0 \quad (1a)$$

$$\sigma_i^- = \sigma_i \text{ if } \sigma_i < 0 \text{ and } \sigma_i^- = 0 \text{ if } \sigma_i \geq 0 \quad (1b)$$

Thus the tensile and compressive strains can be represented using Hooke´s Law:

$$\varepsilon_{ti} = \frac{1+\upsilon}{E}\sigma_i^+ - \frac{\upsilon}{E}\sum_{j=1}^{3}\sigma_j^+ \quad (2a)$$

$$\varepsilon_{ci} = \frac{1+\upsilon}{E}\sigma_i^- - \frac{\upsilon}{E}\sum_{j=1}^{3}\sigma_j^- \quad (2b)$$

where υ is the coefficient of Poisson of concrete.

The extension state is locally characterized by an equivalent strain that is expressed by:

$$\bar{\varepsilon} = \sqrt{\left(\varepsilon_1^+\right)^2 + \left(\varepsilon_2^+\right)^2 + \left(\varepsilon_3^+\right)^2} \quad (3)$$

Where ε_i, main strain components, and ε_i^+ +, the positive parts, with $i = 1, 2\ and\ 3$, are defined by (4) and (5), respectively:

$$\varepsilon_i = \varepsilon_{ti} + \varepsilon_{ci} \quad (4)$$

$$\varepsilon_i^+ = \frac{1}{2}\left(\varepsilon_i + |\varepsilon_i|\right) \quad (5)$$

According Mazars [18] the damage process starts when the tensile strain exceeds the deformation ε_{do}, referred to the maximum stress of an uniaxial tension test (Equation 6).. As the concrete behaves differently in tension and compression, the damage variable D is obtained by combining properly the variables D_{ct} and D_{cc}, related to tension and compression, respectively, as follows:

$$\bar{\varepsilon} - \varepsilon_{do} \le 0 \quad (6)$$

$$D_c = \alpha_t D_{ct} + \alpha_c D_{cc} \quad (7)$$

where:

$$\alpha_t = \frac{\sum_{i=1}^{3}\varepsilon_{ti}^+}{\varepsilon_v^+} \quad (8a)$$

$$\alpha_c = \frac{\sum_{i=1}^{3}\varepsilon_{ci}^+}{\varepsilon_v^+} \quad (8b)$$

with

$$\varepsilon_{ti}^+ = \frac{1}{2}\left(\varepsilon_{ti} + |\varepsilon_{ti}|\right) \quad (9a)$$

$$\varepsilon_{ci}^+ = \frac{1}{2}\left(\varepsilon_{ci} + |\varepsilon_{ci}|\right) \quad (9b)$$

$$\varepsilon_v^+ = \sum_{i=1}^{3}\left(\varepsilon_{ti}^+ + \varepsilon_{ci}^+\right) \quad (9c)$$

and: $0 \le \alpha_t \le 1; 0 \le \alpha_c \le 1; e\ \alpha_t + \alpha_c = 1$.
D_{ct} and D_{cc} are defined as:

$$D_{ct} = 1 - \frac{\varepsilon_{do}\left(1 - A_t\right)}{\bar{\varepsilon}} - \frac{A_t}{exp\left[B_t\left(\bar{\varepsilon} - \varepsilon_{do}\right)\right]} \quad (10a)$$

$$D_{cc} = 1 - \frac{\varepsilon_{do}\left(1 - A_c\right)}{\bar{\varepsilon}} - \frac{A_c}{exp\left[B_c\left(\bar{\varepsilon} - \varepsilon_{do}\right)\right]} \quad (10b)$$

where A_t, B_t, A_c and B_c are experimental parameters defined related to stress-strain curves of concrete under tension or compression, respectively.
The constitutive relation of damaged concrete can defined thus as:

$$\sigma = E_c\left(1 - D_c\right)\varepsilon \quad (11)$$

where E_c represents the elastic modulus of concrete undamaged.

2.2 Flexural model

The Classical laminated plate theory was used to model the reinforced concrete slab. In comparison, the discrete approach to modeling concrete and steel reinforcement include a large number of functions and material parameters and involve tedious programming and computational effort due higher degrees of freedom [17]. However, layered approach is more simple since the materials are represented by layers and the strain and stress of concrete and reinforcement through the thickness of the cross-section can be monitored progressively, in this manner providing an accurate representation of the structural behavior. Layered approach in FEM have been widely used to analysis of reinforced concrete structures [17, 24, 29-31] with relative success.
Similar to the Euler-Bernoulli beam theory and the plate theory, the classical laminated plate theory is only valid for thin laminates with small displacement in the transverse direction. It shares the same classical plate theory assumptions: [32-33]:

1) The layers are perfectly bonded together;
2) The laminate is thin compared to the lateral dimensions and is loaded in its plane;
3) A straight line originally normal to the undeformed mid-surface remains straight and rotates so as to remain straight and normal to the deformed mid-surface plane;
4) A line normal to the mid-surface of the plate is inextensible (does not stretch);
5) Linear geometric analysis is considered with smalls deflections and rotations when compared to unity. The Kirchhoff's thin plate approximations can be used here to derive relationships between in-plane and out-of-plane displacements, curvatures, twists, and strains;
6) The material of each layer is linearly elastic and has three planes of material symmetry (i.e, orthotropic). In fact, the classical plate theory usually assumes that the material is isotropic, while a fiber reinforced composite laminate with multiple layers may have more complicated stress-strain relations.
7) Loads are applied in mid-surface plane.

Figure 1 – Undeformed and deformed geometries of an edge of a plate under the Kirchhoff assumptions

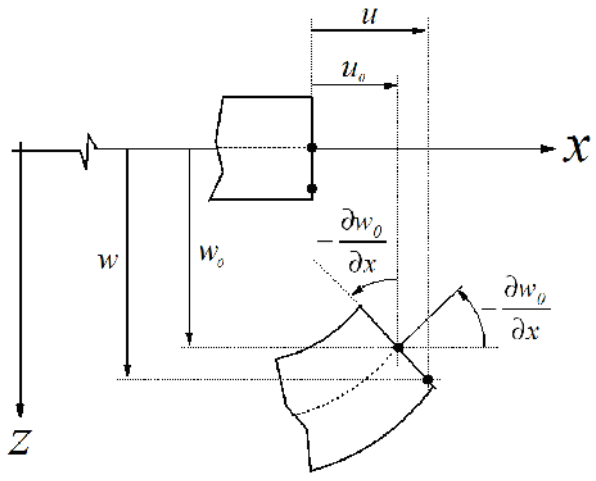

Based assumptions 1 to 5 the deformations u, v and w can be described entirely in terms of the deformation of the mid-surface plane u_0, v_0 and w_0 (Figure 1):

$$u(x,y,z) = u_0(x,y) - z\frac{\partial w_0}{\partial x} \quad (12a)$$

$$v(x,y,z) = v_0(x,y) - z\frac{\partial w_0}{\partial y} \quad (12b)$$

$$w(x,y,z) = w_0(x,y) \quad (12c)$$

where $\frac{\partial w_0}{\partial x}$ and $\frac{\partial w_0}{\partial y}$ are rotations of a normal the mid-plane about the x and y axes, respectively.
Based in assumption 5, by substitution of these displacements relation into the strain-displacement equations of the classical theory of elasticity, the following relations are obtained:

$$\varepsilon_x = \frac{\partial u_0}{\partial x} - z\frac{\partial^2 w_0}{\partial x^2} \quad (13a)$$

$$\varepsilon_y = \frac{\partial v_0}{\partial y} - z\frac{\partial^2 w_0}{\partial y^2} \quad (13b)$$

$$\gamma_{xy} = \frac{\partial u_0}{\partial y} + \frac{\partial v_0}{\partial x} - 2z\frac{\partial^2 w_0}{\partial x \partial y} \quad (13c)$$

$$\varepsilon_z = 0 \quad (13d)$$

$$\gamma_{xz} = 0 \quad (13e)$$

$$\gamma_{yz} = 0 \qquad (13f)$$

Each lamina in the laminate is assumed to be in plane stress state so that the constitutive relation for a typical lamina k, assuming nonlinearity of material, can be written as:

$$\begin{bmatrix}\sigma_x\\ \sigma_y\\ \tau_{xy}\end{bmatrix} = \begin{bmatrix}\bar{Q}_{11} & \bar{Q}_{12} & \bar{Q}_{16}\\ \bar{Q}_{12} & \bar{Q}_{22} & \bar{Q}_{26}\\ \bar{Q}_{16} & \bar{Q}_{26} & \bar{Q}_{66}\end{bmatrix}\begin{bmatrix}\varepsilon_x\\ \varepsilon_y\\ \gamma_{xy}\end{bmatrix} \qquad (14)$$

The elements of $[\bar{Q}]$ are related to the engineering constants E, G and υ, according assumption 6, as follows. Transformation of lamina stress and strain from the 1-2 axes to the rotated x - y axes (orientation θ) is shown here in matrix notation.

$$\bar{Q}_{11} = Q_{11}\cos^4\theta + 2\left(Q_{12} + 2Q_{66}\right)\text{sen}^2\theta\cos^2\theta + Q_{22}\text{sen}^2\theta \qquad (15a)$$

$$\bar{Q}_{12} = \left(Q_{11} + Q_{22} - 4Q_{66}\right)\text{sen}^2\theta\cos^2\theta + Q_{12}\left(\text{sen}^4\theta + \cos^4\theta\right) \qquad (15b)$$

$$\bar{Q}_{22} = Q_{11}\text{sen}^2\theta + 2\left(Q_{12} + 2Q_{66}\right)\text{sen}^2\theta\cos^2\theta + Q_{22}\cos^4\theta \qquad (15c)$$

$$\bar{Q}_{16} = \left(Q_{11} - Q_{12} - 2Q_{66}\right)\text{sen}\theta\cos^3\theta + \left(Q_{12} - Q_{22} + 2Q_{66}\right)\text{sen}^3\theta\cos\theta \qquad (15d)$$

$$\bar{Q}_{26} = \left(Q_{11} - Q_{12} - 2Q_{66}\right)\text{sen}^3\theta\cos\theta + \left(Q_{12} - Q_{22} + 2Q_{66}\right)\text{sen}\theta\cos^3\theta) \qquad (15e)$$

$$\bar{Q}_{66} = \left(Q_{11} + Q_{22} - 2Q_{12} - 2Q_{66}\right)\text{sen}^2\theta\cos^2\theta + Q_{66}\left(\text{sen}^4\theta + \cos^4\theta\right) \qquad (15f)$$

$$Q_{11} = \left[\frac{E_1\left(1-D\right)}{1-\nu_{12}\nu_{21}}\right] \qquad (16a)$$

$$Q_{12} = \left[\frac{\nu_{12}E_2\left(1-D\right)}{1-\nu_{12}\nu_{21}}\right] \qquad (16b)$$

$$Q_{22} = \left[\frac{E_2\left(1-D\right)}{1-\nu_{12}\nu_{21}}\right] \qquad (16c)$$

$$Q_{66} = G_{12}\left(1-D\right) \qquad (16d)$$

where:
E_1 is the longitudinal elastic modulus in direction x;
E_2 is the longitudinal elastic modulus in direction y;
$\upsilon_{12} = \upsilon_{21}$ is the major Poisson´s ratio of layer associates to directions x and y;
G_{12} is the shear modulus associates to directions x and y;
D represents the damage of material.
In this formulation, the loads and moments can be expressed in matrix form as (Figure 2):

$$\begin{Bmatrix}N_{xx}\\ N_{yy}\\ N_{xy}\end{Bmatrix} = \begin{bmatrix}A_{11} & A_{12} & A_{16}\\ A_{12} & A_{22} & A_{26}\\ A_{16} & A_{26} & A_{66}\end{bmatrix}\begin{bmatrix}\frac{\partial u_0}{\partial x}\\ \frac{\partial v_0}{\partial y}\\ \frac{\partial u_0}{\partial y} + \frac{\partial v_0}{\partial x}\end{bmatrix} + \begin{bmatrix}B_{11} & B_{12} & B_{16}\\ B_{12} & B_{22} & B_{26}\\ B_{16} & B_{26} & B_{66}\end{bmatrix}\begin{bmatrix}-\frac{\partial^2 w_0}{\partial x^2}\\ -\frac{\partial^2 w_0}{\partial y^2}\\ -2\frac{\partial^2 w_0}{\partial x \partial y}\end{bmatrix} \qquad (17a)$$

$$\begin{Bmatrix}M_{xx}\\ M_{yy}\\ M_{xy}\end{Bmatrix} = \begin{bmatrix}B_{11} & B_{12} & B_{16}\\ B_{12} & B_{22} & B_{26}\\ B_{16} & B_{26} & B_{66}\end{bmatrix}\begin{bmatrix}\frac{\partial u_0}{\partial x}\\ \frac{\partial v_0}{\partial y}\\ \frac{\partial u_0}{\partial y} + \frac{\partial v_0}{\partial x}\end{bmatrix} + \begin{bmatrix}D_{11} & D_{12} & D_{16}\\ D_{12} & D_{22} & D_{26}\\ D_{16} & D_{26} & D_{66}\end{bmatrix}\begin{bmatrix}-\frac{\partial^2 w_0}{\partial x^2}\\ -\frac{\partial^2 w_0}{\partial y^2}\\ -2\frac{\partial^2 w_0}{\partial x \partial y}\end{bmatrix} \qquad (17b)$$

where N_{xx}, N_{yy} and N_{xy} are in plane membrane forces per unit length (due to stretching of the plate mid surface), M_{xx} and M_{yy}

Figure 2 – Coordinate system and layer numbering used for a laminated plate

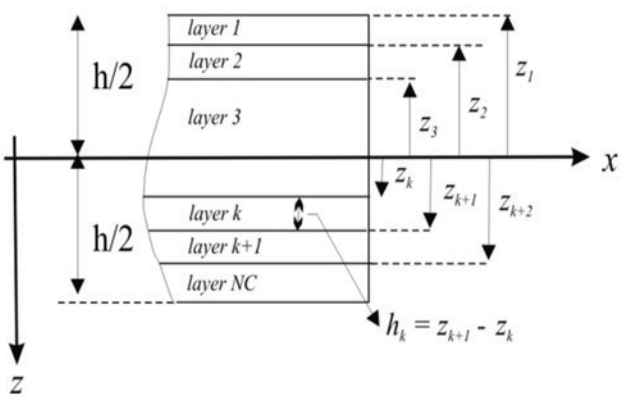

are bending moments per unit length about the y and x axes, respectively, and M_{xy} are twisting moment per unit length (similar to torsion in a beam).

These matrices are termed: A_{ij} = extensional stiffness matrix; D_{ij} = bending stiffness matrix; B_{ij} = extension-bending coupling matrix. A convenient form for the $[A]$, $[B]$ and $[D]$ matrices can be established by examining the position of the k^{th} lamina in Figure 2:

$$A_{ij} = \sum_{k=1}^{n} \bar{Q}_{ij}^{(k)} \left(z_{k+1} - z_k\right) dz \qquad (18a)$$

$$B_{ij} = \frac{1}{2} \sum_{k=1}^{n} \bar{Q}_{ij}^{(k)} \left((z_{k+1})^2 - z_k{}^2\right) dz \qquad (18b)$$

$$D_{ij} = \frac{1}{3} \sum_{k=1}^{n} \bar{Q}_{ij}^{(k)} \left(\left(z_{k+1}\right)^3 - z_k{}^3\right) dz \qquad (18c)$$

Can be observed in equation 17 that internal forces and moments are dependent of displacements, layer position and material properties. Therefore, the application of nonlinear models (damage model of concrete and plasticity of steel) affect directly the mechanical behavior of laminated plates.

The virtual work done by internal forces is expressed by:

$$\delta W_{int} = \int_{r_0} \left\{ N_{xx}\delta\left(\frac{\partial u_0}{\partial x}\right) + N_{yy}\delta\left(\frac{\partial v_0}{\partial y}\right) + N_{xy}\left[\delta\left(\frac{\partial u_0}{\partial y}\right) + \delta\left(\frac{\partial v_0}{\partial x}\right)\right] - M_{xx}\delta\left(\frac{\partial^2 w_0}{\partial x^2}\right) - M_{yy}\delta\left(\frac{\partial^2 w_0}{\partial y^2}\right) - 2M_{xy}\delta\left(\frac{\partial^2 w_0}{\partial x \partial y}\right) \right\} dxdy \qquad (19)$$

where r_0 is the area of the mid-surface of the plate.

The virtual work done by external forces can be expressed by Eq. (20) considering loads acting on the domain and on the boundary of the plate (Figure 3 shows positive directions of loads) and according assumption 7:

$$\delta W_{ext} = \int_{r_0} q_z(x,y)\delta w_0 dxdy + \int_0^b \left(\bar{F}_{xx}\delta u_0 + \bar{F}_{xy}\delta v_0 + \bar{F}_{xz}\delta w_0 - \bar{M}_{xx}\delta\left(\frac{\partial w_0}{\partial x}\right)\right)_{x=0}^{x=a} dy + \int_0^a \left(\bar{F}_{yx}\delta u_0 + \bar{F}_{yy}\delta v_0 + \bar{F}_{yz}\delta w_0 - \bar{M}_{yy}\delta\left(\frac{\partial w_0}{\partial y}\right)\right)_{y=0}^{y=b} dx \qquad (20)$$

which

is the transversal force per unit area acting on mid-surface of the plate; $\bar{F}_{xx}$, $\bar{F}_{xy}$ and $\bar{F}_{xz}$ are the forces per length unit along the edges $x = 0$ and $x = a$, second to the directions x, y e z, respectively; $\bar{M}_{xx}$ is the bending moment per unit length, applied along the edges $x = 0$ and $x = a$;

$\bar{F}_{yx}$, $\bar{F}_{yy}$ and $\bar{F}_{yz}$ are the forces per length unit along the edges $y = 0$ and $y = b$, according to the directions x, y e z, respectively; $\bar{M}_{yy}$ is the Bending moment per unit length applied along the edges $y = 0$ and $y = b$.

The moment of torsion was not considered in the external work since it is not usually applied in slabs, despite it appears the internal efforts.

Figure 3 – Forces and moment resultants on a plate element

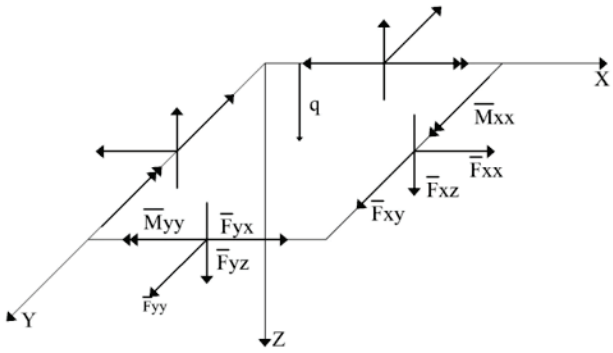

3. Numerical formulation

After expressing the work done by internal forces as a function of displacement, by replacing the expressions of internal efforts (17a) and (17b) in (19), the numerical treatment according to EFDM can be applied.

First, it is necessary to introduce in equations of the δW_{int} and δW_{ext} the representations used in finite differences for the derivatives of the displacements. It is assumed, for evaluation these virtual works, that the plate is divided into sections of integration (area elements) in which all magnitudes involved are supposed constant. After determination of δW_{int} e δW_{ext}, by the summation of the contributions of the various sections of integration, a system of algebraic equations of equilibrium is obtained by application of principle of virtual work. The resolution of this system permits to obtain the numerical solution based in unknowns nodal displacements u_0, v_0 e w_0. To determination of the system of algebraic equations it is considered the kinematic condition of the boundary and others variation of displacements, arbitrary and independent of each other.

In the numerical formulation developed in this work are used two types of representations for the derivatives of the displacements: centered representation and reduced representation. For this, consider the Figure 4, where $f(x)$ represents the function u_0, v_0 e w_0 and m is the point where the derivatives are evaluated (pivotal point). The nodal spacing is λ. First and second derivative of the function $f(x)$ evaluated at point m are $f'_m = \frac{1}{2\lambda}\left(f_{m+1} - f_{m-1}\right)$ and $f''_m = \frac{1}{\lambda^2}\left(f_{m+1} - 2f_m + f_{m-1}\right)$.

Figura 4 – Function f (x) used to represent the derivative of displacement

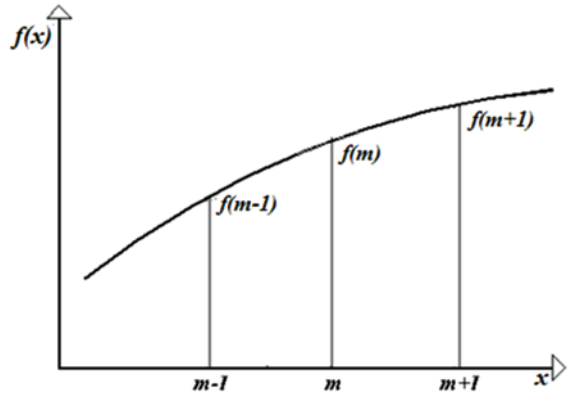

In areas located along the edges of the board, the use of representation centered at the first derivative of u_0 and v_0 can cause singularity in the coefficient matrix. Therefore, for those derivatives is assumed to reduced representation, as suggested by Graça [14]. This representation can be defined by $f'_m = \frac{1}{\lambda}\left(f_{m+1} - f_m\right)$.

For the numerical discretization of the domain $L_a \times L_b$ of plate, the method provides a generation of sections of integration obtained from subdivisions in the x and y directions: n_x and n_y, respectively. Thus, an generic section of integration presents the rectangular dimensions $\lambda_x = L_a / n_x$ and $\lambda_y = L_b / n_y$, with a total of $\left(n_x+3\right)\times\left(n_y+3\right)$ nodes and $\left(n_x+1\right)\times\left(n_y+1\right)$ area elements for integration, with nine different types of section, as shown in Figure 5. The area element type 1, 3, 7 and 9 are located in the corners of the plate and display area $\frac{\lambda_x \times \lambda_y}{4}$, while the element type 2, 4, 6 and 8, the area is $\frac{\lambda_x \times \lambda_y}{2}$. The remaining sections of integration

Figure 5 – Finite difference discretization of plate: nine sections of integration; virtual nodes and real nodes

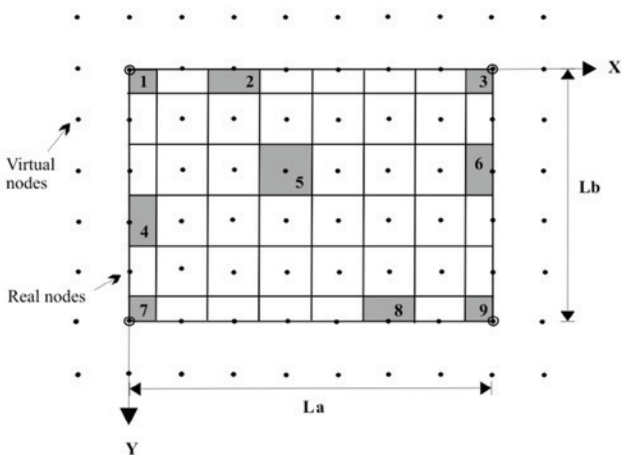

(type 5) have area $\lambda_x \times \lambda_y$, as illustrated in Figure 5.
The section of integration (see Figure 5) is composed of nine nodal points and for each of these points are associated with three degrees of freedom u_0, v_0 and w_0, which incorporates, for each area element a total of 27 displacements. Note that the second-order derivatives of the displacements of the nodes, associated with the edges of the board, require external nodes, called virtual nodes.
More information about the sequence of development of the numerical treatment, according to EFDM, can be found in [13-15].

4. Comparisons with experimental results

Two slabs solved in the literature was resolved by the aid of the newly developed computer program: a two-way slab supported by its four edges and submitted to distributed loading [27]; a two-way slab supported by its four corner and submitted to

Table 1 – Material properties

Slab supported by its four edges										
	E(GPa)	v_c	f_c (MPa)	A_c	B_c	f_t (MPa)	ε_{d0}	A_t	B_t	f_y (MPa)
Concrete	32,42	0,18	35,04	1,00	1600	3,60	1,11 x 10^{-4}	0,80	10000	–
steel	206,91	–	–	–	–	–	–	–	–	375,90

Slab supported by its four corners										
	E(GPa)	v_c	f_c (MPa)	A_c	B_c	f_t (MPa)	ε_{d0}	A_t	B_t	f_y (MPa)
Concrete	28,61	0,15	37,92	1,00	1650	3,80	1,33 x 10^{-4}	0,80	10000	–
steel	201,30	–	–	–	–	–	–	–	–	345,40

Figure 6 – Analytical stress-strain curves using Damage Model of Mazars

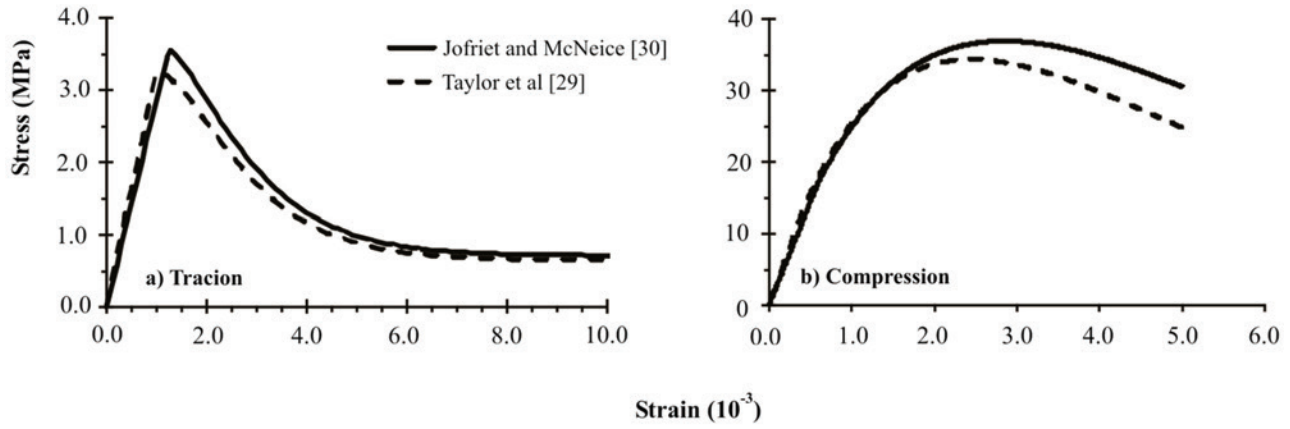

concentrated load [28]. The numerical discretization used the geometry and loading symmetry, analyzing thus, a quarter of plate. The numerical results were compared with experimental load-deflection curves of slabs and rupture load.

4.1 Computer simulation of stress–strain curves

Table 1 shows the experimental dates of used concrete (E_c, f_c, f_t e υ_c) and steel (E_s e f_y) and the parameter values associated with damage model. Based on dates, the theoretical stress-strain curves (Figure 6) were obtained using equations (10) and (11). Initially, the strain value $\varepsilon_{do} = \frac{f_t}{E}$ was determined. After this, appropriate constants A_t, B_t, A_c and B_c .are tested until to obtain a good agreement between experimental and theoretical values.

The obtained tensile parameter A_t shown similarity with values indicated by Lemaitre e Mazars [34] and Challamel [35]. How the experimental stress-strain curves were not obtained by authors, the compressive parameters A_c and B_c were changed until to obtain a same experimental compressive strength f_c and a peak strain between 2‰ and 3‰. Similar procedure was used by many researchers [18, 19, 23, 25, 34, 36].

Reinforcing steel was modeled as an uniaxial layer considered as an one-dimensional material in the reinforcement direction. The center of steel layer coincides with reinforcement center of experimental slabs and has an equivalent area. An elastoplastic model was used and three parameters are necessary as input data to define the steel model: the initial Young´s modulus E_s, the yield stress f_y and the ultimate strain ε_{su} (adopted as 10‰).

Figure 7 – Geometry, structure and material parameters of RC-slab according to (16)

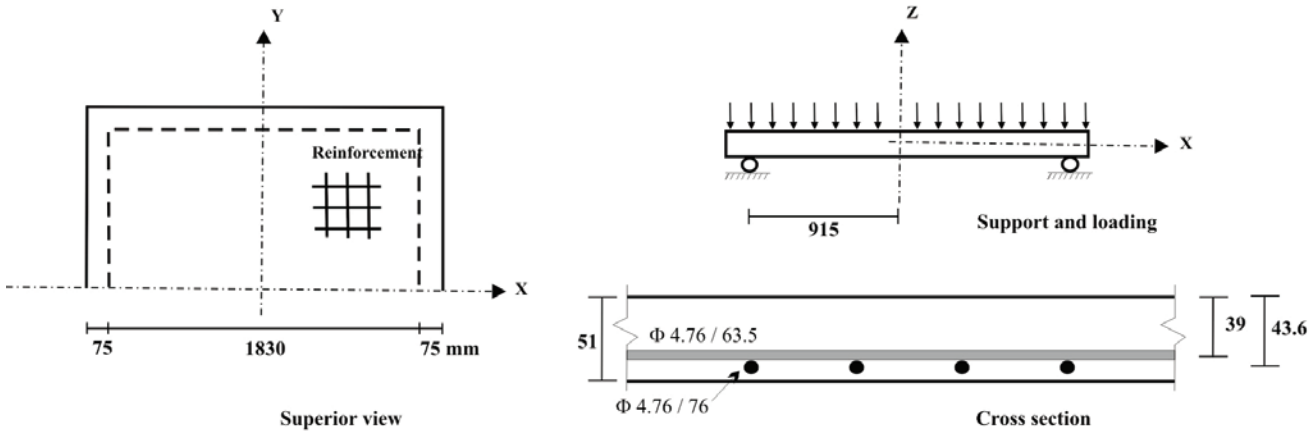

Figure 8 – Effect of damage of transversal elastic modulus on load-displacement behavior

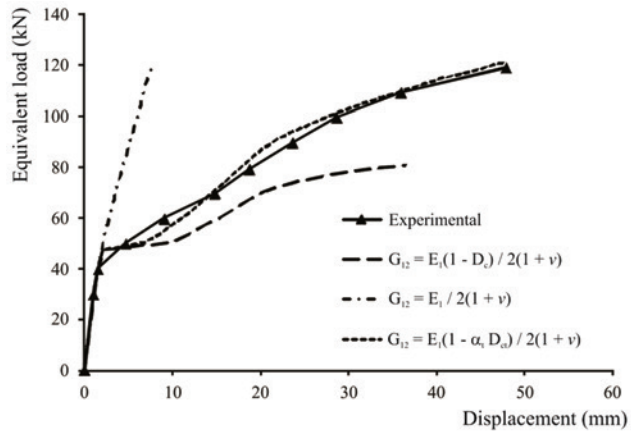

4.2 Two-way slab supported by its four edges

Figure 7 shows the geometry, structure and reinforcement characteristics of RC-slab experimented by Taylor et al [27]. The slab, supported by its four edges and subjected to a distributed load at the top, has a square shape with 915 mm side length and 51 mm thickness.

One very important feature of non-linear models applied to the analysis of structural reinforced concrete elements is the problem of mesh size. In this example, two numerical parameters were tested. The ideal discretization was obtained after several tests and resulted in a plate with 8 x 8 subdivisions. The cross section was divided into 10, 15, 22 and 36 concrete and steel layers superimposed.

Figure 9 – Influence of quantity of layers on numerical modeling at slab supported by its four edges

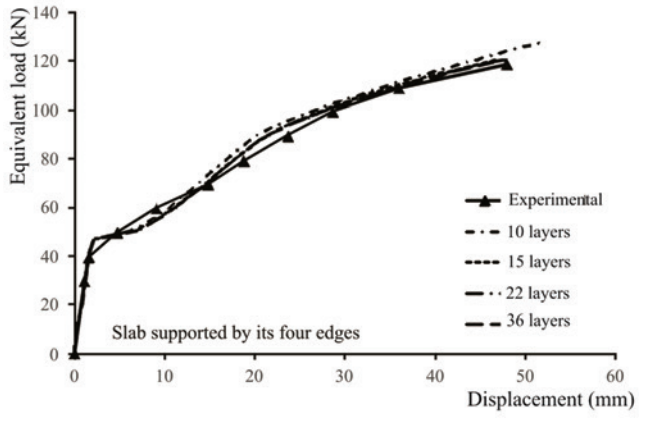

The load–deflection curve, calculated with 8 x 8 subdivisions and 15 layers is depicted in Fig. 8, together with the experimental results. Can be observed the presence of three numerical curves resultant of application, or not, of different damage parameter to shear modulus G_{12}:

1) $G_{12} = \frac{E_1}{2(1+\upsilon)}$, where $E_1 = E_c$ and $\upsilon = \upsilon_c$;

2) $G_{12} = \frac{E_1(1-D_c)}{2(1+\upsilon)}$, where $E_1 = E_c$, $\upsilon = \upsilon_c$ and $D_c = \alpha_t D_{ct} + \alpha_c D_{cc}$;

3) $G_{12} = \frac{E_1(1-\alpha_t D_{ct})}{2(1+\upsilon)}$, where $E_1 = E_c$ and $\upsilon = \upsilon_c$.

It was observed a great influence of variation of transversal modulus on load-deflection behaviour of slabs. The adoption of undamaged modulus (situation 1) results in the more stiffness solution where the loss of load after the concrete cracking cannot to be adequately modeled. However, the application of damage coefficient The results illustrated in Fig. 19 indicate in a numerical curve with lower stiffness, after cracking, than experimental curve. In fact, the main factor that affect the loss of transversal stiffness of concrete is the cracking of slab in region under traction. In situation 3 the isotropic damage of G_{12} is associated with the D_{ct} parameter and a best agreement between experimental and numerical results is observed. The fail of slab was characterized by yielding of steel of reinforcement ($\varepsilon_s > 10‰$).

In order to study the influence of layer, the example was analyzed by three other meshes, composed of 10, 22 and 36 layers for the cross section. The results illustrated in Fig. 12 indicate, for the presented example, that the increasing of the number of layers from 15 to 36 produced almost the same results for the load-displacement curve. So, it is important to point out that 15 layers for the cross section is really enough, even when the non-linearity effects are very significant.

The load–deflection relationship obtained by this model is again shown in Fig. 10 in addition to results presented by Jiang e Mirza

Figure 10 – Comparison between experimental, proposed model and FEM model

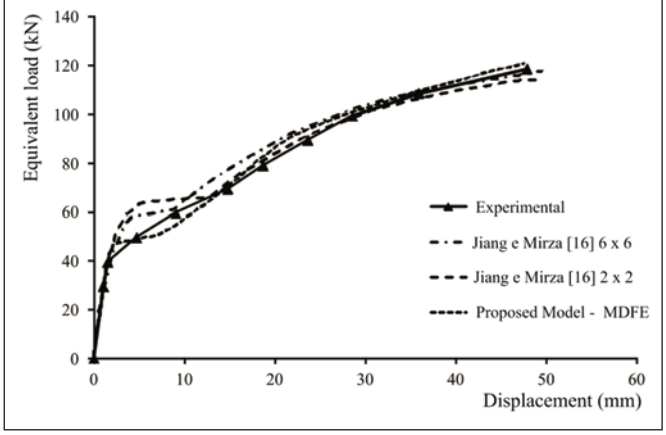

Figure 11 – Geometry and structure of slab supported by its four corners according to (37)

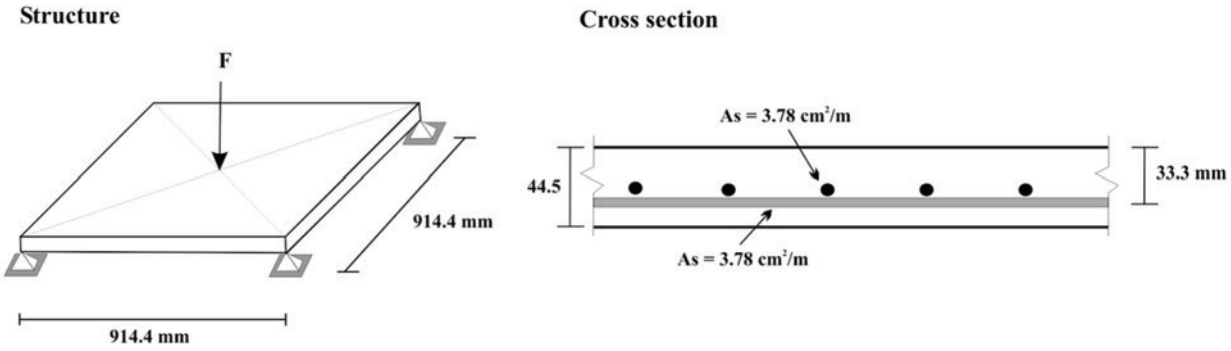

[16]. This last model is based in Finite Element Method, Plastic Model to concrete and Classic Theory of Plates. The obtained results are very close to the numerical ones, showing the good accuracy of the present model with a similar degree of freedom.

4.3 Two-way slab supported by its four corners

The second example examined (tested by McNeice [28]) consisted of square corner-supported slab subjected to a point load applied at the center. The two-way slab was 915x915 mm square and 44 mm thick, and reinforced with an orthogonal mesh giving a reinforcement ratio of 0.85%. Geometric properties, reinforcement and material parameters are shown in Fig. 11. Material parameters are shown in Table 1. The transversal modulus was damage according situation 3 indicated in the last item.

In representing this specimen, a 14 x 14 subdivision (15 x 15 area elements) was used to model one-quarter of the slab. This example also was analyzed by meshes composed of 10, 15, 22 and 36 layers for the cross section. The results illustrated in Fig. 12 indicate reasonably accurate predictions of load-deflection curve and they confirm the use of 15 layers as the better solution. The modification of stiffness, after cracking of concrete, is resultant of numerical application of damage to concrete. In ultimate load it is verified a large concrete strain ($\varepsilon_c > 5.7‰$) and a steel strain in elastic regime ($\varepsilon_s < 10‰$) that indicate a rupture of slab by crushing of concrete under compression.

The McNiece slab is one often used as a benchmark for calibrating nonlinear analyses. Comparison of present model with another numerical model are shown in Figure 13. Kratz e Polling [37] used elastoplastic damage model to represent the stress-strain behavior of concrete under tension and compression in a Finite Element Method (FEM) program. Crisfield [38] evaluated the combination of FEM, using square elements, with linear softening behavior of concrete under traction. The criterion of Von Mises was adopted as the failure criterion for the concrete under compression. Doulah e Kabir [39] used FEM (square element with 4 degrees of freedom) and Classic Theory of Plates of Mindlin. To concrete behavior was adopted the linear softening in traction and bi-lin-

Figure 12 – Influence of quantity of layers on numerical modelling at slab supported by its four corners

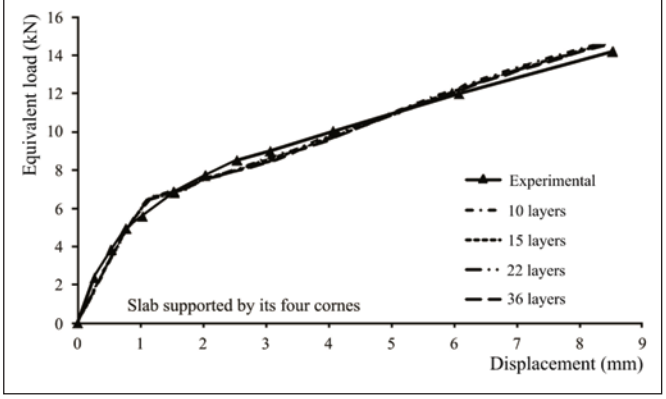

Figure 13 – Comparison between proposed model and FEM models to slab supported by its four corners

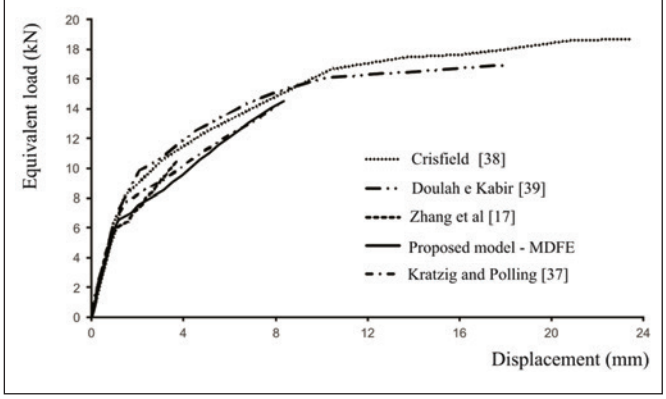

ear curve in compression. Zhang et al [17] used FEM (square element with 24 degrees of freedom) associated with Classic Theory of Plates of Mindlin and Reissner. Concrete was modeled as elastic linear under compression and to the tensile behavior under traction was used a new model that consider the cracking of concrete in orthogonal direction with main direction. It is observed a better agreement with Krazt and Polling model while another models shown a more stiffness solution after first crack and rupture load very different of the experimental results. Thus the damage model appears as a good alternative for modeling concrete behavior.

5. Conclusion

A new model was presented in this work to predict the flexural behavior of reinforced concrete slabs. Combining the Finite Difference Energy Method with Classical Theory of Laminates it was possible to perform a nonlinear analyses by application of Damage Model, proposed by Mazars, to represent the concrete behavior under tracion and compression.

The results indicate the necessity of the application of tensile damage parameter (D_{ct}) to reduces the transversal elastic modulus after cracking of concrete. In fact, how the evaluation of reinforced concrete slab is a bidimensional problem, the cracking affect the properties in all directions.

The comparison with experimental results demonstrate the efficiency of method to describe the load-deflection behavior and to determine the rupture load. Comparing with other numerical solutions, using FEM, it is observed a higher accuracy of proposed model, mainly considering the low discretization necessary.

6. Aknowledgements

The authors would like to thank the CNPq and FAPESB (PPP 010/2010) and CAPES for financial support.

7. References

[01] KURRER K-E., RAMM, E. The History of the Theory of Structures. From Arc Analysis to Computational Mechanics. John Wiley & Sons, 2008, 848pp.

[02] THOMÉE, V.. From finite differences to finite elements: A short history of numerical analysis of partial diferential equations. Journal of Computational and Applied Mathematics, vol. 128, 2001, p.1–54.

[03] HAGIYA, H., MORISHITA, M., ANDO, T.; TANAKA, H. MATUO, K. Damage evaluation of reinforced concrete slabs subjected to contact detonation loads with numerical simulation. Science and tecnhnology of energetic materials, vol. 64, n. 5, 2003, p.192-200.

[04] FERRETI, D. ;SAVOIA, M. Non-linear model for R/C tensile members strengthened by FRP-plates. Engineering Fracture Mechanics, vol. 70, 2003, p.1069–1083.

[05] HABIB, A.; MOHARRAMI,H. Nonlinear sensitivity analysis of reinforced concrete frames, Finite Elements in Analysis and Design, vol. 46, 2010, p. 571–584.

[06] VIRDI, K. S. Finite difference method for nonlinear analysis of structures, Journal of Constructional Steel Research, vol. 62, 2006, p. 1210–1218.

[07] JONES, J., C. WUA,, D.J. OEHLERS , A.S. WHITTAKER , W. SUN, S. MARKS, R. COPPOLA. Finite difference analysis of simply supported RC slabs for blast loadings. Engineering Structures, vol. 31, 2009, p.2825-2832.

[08] HOUBOLT, J.C. A Study of Several Aerothermoelastic Problems of Aircraft Structures in High-Speed Flight. Zurich, 1958, Doctoral Thesis - The Swiss Federal Institute of Technology.

[09] GRIFFIN, D. S.; VARGA, R.S. Numerical solution of plane elasticity problems. Journal of Society of Industrial Applied Mathematic, vol. 11, n. 4, 1963.

[10] BUSHNELL, D. Finite-difference energy models versus finite-element models- Two variational approaches in one computer program. Numerical and computer methods in structural mechanics.(A 74-17756 06-32) New York, Academic Press, Inc., 1973, p. 291-336

[11] PLETZ, E. Análise de estrutura laminares pelo método da energia discretizada. Rio de Janeiro, 1983, Tese (Mestrado) - Universidade Federal do Rio de Janeiro.

[12] NISHIKAVA, L. K. Análise numérica de placas com cantos reentrantes. Rio de Janeiro, 1991, Tese (Mestrado) - Universidade Federal do Rio de Janeiro.

[13] GRAÇA, M. S. B. A. Método das diferenças finitas energéticas na análise estática e dinâmica de placas delgadas e espessas, Rio de Janeiro, 2000, Tese (Doutorado) - Universidade Federal do Rio de Janeiro.

[14] LIMA, J. M. F. Estudo comparativo entre formulações geometricamente não lineares para a flexo-torção de hastes de paredes delgadas de seção aberta, Rio de Janeiro, 2004, Tese (Doutorado) - Universidade Federal do Rio de Janeiro.

[15] NEVES, J. B; LIMA, J. M. F.; LIMA, P. R. L. Método das Diferenças Finitas Energéticas para simulação do comportamento sob flexão do concreto reforçado com fibras curtas de aço. Revista Sul-americana de Engenharia Estrutural, vol.10, n.2, 2013, p.31-55.

[16] JIANG, J.; MIRZA, F. A. Nonlinear analysis of reinforced concrete slabs by a discret finite element approach. Computers & Structures, vol.65, n.4, 1997, p. 585-592.

[17] ZHANG, Y. X.; BRADFORD, M. A.; GILBERT, R. I. A layered shear-flexural plate/shell element using Timoshenko beam functions for nonlinear analysis of reinforced concrete plates. Finite elements in analyses and design, vol.43, 2007; p.888-900.

[18] MAZARS, J. A Description of micro and macroscale damage of concrete structures, Engineering Fracture Mechanics, vol.25, 1986; p.729-737.

[19] FERNANDES, G. R. Método dos elementos de contorno aplicado à análise não linear de placas, São Paulo, 1998, Dissertação (Mestrado) - Escola de Engenharia de São Carlos - Universidade de São Paulo.

[20] CRESCE, S. H. Análise não-linear de pavimento de concreto armado pelo método de elementos de contorno, São Paulo, 2003, Tese (Doutorado) - Universidade de São Paulo.

[21] BANDEIRA M. S. Análise não-linear de lajes de concreto armado pelo método dos elementos finitos, Goiás, 2006, Dissertação (Mestrado) - Universidade Federal de Goiás.

[22] WANG, T.; HSU, T. Nonlinear finite element analysis of concrete structures using a new constitutive models. Computer and structures, vol. 19, 2001, p.2781-2791.

[23] ASSAN, A.E., Nonlinear analysis of reinforced concrete cylindrical shells. Computer and structures, vol. 80, 2002, p.2177–2184.

[24] HAIDO, J. BAKAR, B.H.; ABDUL-RAZZAK, A.A.; JAYAPRAKASH, J. Dynamic response simulation for reinforced concrete slabs. Simulation Modelling Practice and Theory, vol. 18, 2010, p.696–711.

[25] SANCHES, F. J.; VENTURINI, W. S. Damage modeling of reinforced concrete beams. Advances in Engineering Software, vol.38, 2007, p.538-546.

[26] LIMA, J.M.F.; NAGAHAMA. K.J.; LIMA, P.R.L.; SANTOS, G. J. B dos. Um modelo para análise não linear física da flexão de vigas de concreto armado. Mecânica Computacional, vol. XXIX, 2010, p.9839-9853.

[27] TAYLOR, R.; MATHER, D. R. H.; HAYES, B. Effect of the arrangement of reinforcment on the behaviour of reinforced concrete slabs. Magazine Concrete Research, vol.18, 1966, p.85-94.

[28] MCNEICE, G. M., Elastic-Plastic Bending of Plates and Slabs by the Finite Element Method, Ph. D. Thesis, London University, 1967.

[29] NOH, H.C.. Nonlinear behavior and ultimate load bearing capacity of reinforced concrete natural draught cooling tower shell. Engineering Structures, vol. 28, 2006, p. 399–410.

[30] OLIVEIRA, R.S.; RAMALHO, M.A.; CORREA, M.R.S. A layered finite element for reinforced concrete beams with bond–slip effects. Cement & Concrete Composites, vol. 30, 2008, p. 245–252.

[31] GUAN, H.; COOPER, C.; LEE,, D-J. Ultimate strength analysis of normal and high strength concrete wall panels with varying opening configurations. Engineering Structures, vol. 32, 2010, p. 1341-1355.

[32] JONES, R. M. Mechanics of composite materials. Taylor & Francis Group, 1999.

[33] REDDY, J. N. Mechanics of Laminated Composite Plates and Shells: Theory and analysis. CRC, 2004.

[34] LEMAITRE, J.; MAZARS, J. Application de la théorie de l'endommagement au comportement non linéaire et à la rupture du béton de structure. De l'institut technique Du batiment et dês travaux publics, vol.401, 1982, p.114-137.

[35] CHALLAMEL, N. A variationally based nonlocal damage model to predict diffuse microcracking evolution. International Journal of Mechanical Sciences, vol.52, 2010, p.1783-1800.

[36] PITUBA, J. J. C. Avaliação de um modelo anisótropo de dano considerando a perda de resistência devido ao cisalhamento do concreto. Asociación Argentina de Mecánica Computacional, vol.29, 2010; p.5397-5410

[37] KRATZIG, W.B., AND POLLING, R. An elasto-plastic damage model for reinforced concrete with minimum number of material parameters, Computers and structures, vol.82, n.15-16, 2004, p.1201-1215.

[38] CRISFIELD, M. A. Accelerated solution techniques and concrete cracking. Her Majesty's Stationery Office, London, v. 33, pp. 585-607, 1981.

[39] DOULAH, N.; KABIR, A. Non linear Finite Element analysis of reinforced concrete rectangular and skiw slabs. Journal of Civil Engineering, Institutions of Engineers, Bangladesh, v. 29, 2001.

Volume 7, Number 6 (December 2014) p. 940-964 • ISSN 1983-4195

IBRACON

REVISTA IBRACON DE ESTRUTURAS E MATERIAIS

IBRACON STRUCTURES AND MATERIALS JOURNAL

Finite Difference Energy Method for nonlinear numerical analysis of reinforced concrete slab using simplified isotropic damage model

Análise não linear numérica via MDFE de lajes de concreto armado utilizando a mecânica do dano



M. V. A. LIMA [a]
mveniciosalmeida@gmail.com

J. M. F. LIMA [a]
lima.jmf@gmail.com

P. R. L. LIMA [a]
lima.prl@pq.cnpq.br

Abstract

This work presents a model to predict the flexural behavior of reinforced concrete slabs, combining the Mazars damage model for simulation of the loss of stiffness of the concrete during the cracking process and the Classical Theory of Laminates, to govern the bending of the structural element. A variational formulation based on the principle of virtual work was developed for the model, and then treated numerically according to the Finite Difference Energy Method, with the end result a program developed in Fortran. To validate the model thus proposed have been simulated with the program, some cases of slabs in flexure in the literature. The evaluation of the results obtained in this study demonstrated the capability of the model, in view of the good predictability of the behavior of slabs in flexure, sweeping the path of equilibrium to the rupture of the structural element. Besides the satisfactory prediction of the behavior observed as positive aspects of the model to its relative simplicity and reduced number of experimental parameters necessary for modeling.

Keywords: reinforced concrete slabs, damage mechanics, finite difference energy method.

Resumo

Neste trabalho é apresentado um modelo para previsão do comportamento à flexão de lajes de concreto armado, combinando o modelo de dano de Mazars, para simulação da perda de rigidez do concreto durante o processo de fissuração e a Teoria Clássica de Laminados, para reger a flexão do elemento estrutural. Uma formulação variacional com base no princípio dos trabalhos virtuais foi desenvolvida para o modelo, sendo em seguida tratada numericamente segundo o Método das Diferenças Finitas Energéticas (MDFE), tendo como resultado final um programa desenvolvido em Fortran. Para validar o modelo proposto, foram simulados com o programa dois casos de lajes sob flexão, encontrados na literatura. A avaliação dos resultados obtidos nas análises demonstrou a potencialidade do modelo, tendo em vista a boa capacidade de previsão do comportamento de lajes sob flexão, varrendo a trajetória de equilíbrio até a ruptura do elemento estrutural. Além da satisfatória previsão do comportamento observou-se, como aspectos positivos do modelo, a sua relativa simplicidade e o número reduzido de parâmetros experimentais necessários à modelagem.

Palavras-chave: laje de concrero armado, mecânica do dano, método das diferenças finitas energéticas.

[a] *Universidade Estadual de Feira de Santana, Programa de Pós-graduação em Engenharia Civil e Ambiental, Feira de Santana, Bahia, Brasil.*

Received: 25 Sep 2013 • Accepted: 11 Jul 2014 • Available Online: 01 Dec 2014

© 2014 IBRACON

1. Introdução

As estruturas de concreto são utilizadas em todo o mundo nas mais diferentes aplicações como pontes, edificações, estradas, etc. Por outro lado, devido à necessidade de redução do consumo de recursos naturais e do consumo de energia, na produção do cimento e aço, torna-se necessário que as estruturas usem todo o potencial destes materiais. Como as normas de dimensionamento permitem a adoção de modelos simplificados para o cálculo dos elementos de concreto armado, o que se verifica, muitas vezes, é a utilização de estruturas mais robustas, e mais caras, do que seria necessário para manter a segurança e uso esperados. Para minimizar esse problema é importante a utilização de métodos de análise mais avançados, que incorporem a não lineridade física do material e possam prever com maior precisão o comportamento estrutural de elementos de concreto em estágios avançados de fissuração e deformação.

Desde 1904 o Método das Diferenças Finitas (MDF) tem sido utilizado na solução de equações diferenciais para análise estrutural de vigas contínuas e placas [1]. Como método computacional o MDF, junto com o Método dos Elementos Finitos (MEF), surgiu na literatura técnica na década de 50. Muitas idéias e técnicas são comuns aos dois métodos, mas devido ao uso mais sistemático da abordagem variacional e maior flexibilidade geométrica o MEF tornou-se o mais utilizado ao longo do anos [2]. No entanto, estudos posteriores tem demonstrado a capacidade do MDF na análise de estruturas de concreto armado como lajes [3], elementos tracionados [4], pórticos [5] e colunas [6]. Devido a versatilidade do MDF a análise destas estruturas tem sido desenvolvida com a incorporação de não lineridade física e/ou geométrica para avaliação de fissuração, carga de ruptura, escorregamento aço-concreto, deflexão, flambagem e mesmo “spalling” do concreto. Os resultados desses estudos indicam que: i) a comparação com o resultado experimental confirma a validade do método; ii) o procedimento de análise em diferenças finitas é ao mesmo tempo rápido e preciso, e, dessa forma, adequado para utilização em escritórios de projeto estrutural, visto que combina a velocidade de análise com a precisão do MEF [7].

Uma evolução do MDF é o Método das Diferenças Finitas Energéticas (MDFE) que possui algumas vantagens sobre a abordagem tradicional, a exemplo da utilização de derivadas de menor ordem e, portanto, de maior precisão. Isto é decorrente do fato de que as representações em diferenças finitas das derivadas dos deslocamentos, serem inseridas diretamente nas equações do princípio variacional. Outra vantagem é o fato de somente condições de contorno cinemáticas serem requisitadas, por ser o MDFE baseado em equações de energia, fato este que o faz ter uma estrutura similar ao MEF, sendo a discretização concebida em termos de trechos de integração e graus de liberdade nodais.Todavia, cabe ressaltar que há redução do número de graus de liberdade por nó, comparativamente a um tratamento via MEF. Um último aspecto é o fato da matriz de coeficientes dos deslocamentos resultar simétrica para uma grande variedade de problemas, o que implica em considerável economia do esforço computacional. Portanto, o potencial do MDFE para análise mecânica de estruturas complexas fica evidente. De fato, aplicações estruturais do MDFE foram apresentadas por Houbolt [8], Griffin e Varga [9] e Bushnell [10]. No Brasil o MDFE tem sido utilizado desde a década de 1980 para análise de vigas, placas e cascas isotrópicas [11-14]. e mais recentemente tem sido utilizado para análise de vigas de concreto armado e concreto com fibras [15]. Para tal, foi utilizada a mecânica do dano para predição do comportamento tensão-deformação do concreto sob tração e compressão o que resultou em uma boa aproximação do resultado numérico com os resultados experimentais de vigas de concreto. Isso credencia o modelo para análise de estruturas mais complexas como lajes de concreto armado. Quanto à aplicação de modelos não lineares para o estudo de lajes de concreto armado, embora se constate um volume menos expressivo de trabalhos publicados em comparação à literatura voltada às vigas de concreto armado, podem ser destacadas importantes contribuições para a previsão teórica do comportamento à flexão de lajes. A consideração da não linearidade tem sido feita através de modelos elastoplásticos combinado com o MEF [16-17] ou pelo modelo de dano de Mazars [18] através do método dos elementos de contorno [19] sozinho ou combinado com o MEF [20]. Modelos baseados na Mecânica da Fratura foram utilizados por Bandeira [21], que analisou lajes de concreto armado utilizando o programa Diana, este baseado no MEF. A análise desse conjunto de resultados revela que a utilização de modelos não lineares para modelagem do comportamento tensão-deformação do concreto é fundamental para se conseguir prever de forma satisfatória o comportamento estrutural de lajes de concreto armado sob flexão.

O objetivo principal deste trabalho é verificar a aplicação do MDFE na análise não linear de lajes de concreto armado usando o modelo de dano de Mazars [18]. Outros modelos não lineares, baseados em resultados experimentais, têm sido utilizados para descrever o comportamento do concreto sob tensão [22-24], mas o modelo de Mazars foi escolhido por seu bom desempenho na análise de vigas de concreto armado [25-26] e pelo fato deste requerer poucos parâmetros experimentais, e todos de obtenção relativamente simples. Para validação do modelo proposto foram analisadas duas lajes de concreto armado avaliadas experimentalmente por Taylor et al. [27] e McNeice [28].

2. Desenvolvimento da formulação analítica

2.1 Modelo de dano

O modelo de dano de Mazars [18] é um modelo relativamente simples quando comparado a outros. Nesse modelo a variável de dano é medida em função do alongamento do material e possui as seguintes hipóteses básicas:

a) O processo de dano do concreto ocorre no estado elástico, não apresentando deformações plásticas;
b) O concreto é considerado isotrópico mesmo após o início da danificação;
c) A evolução do dano ocorre quando o limite de deformação elástica de alongamento é ultrapassado.

As tensões em uma dada direção principal $i\,(i=1,2\,\text{e}\,3)$ podem ser representadas em função de suas parcelas positiva e negativa da seguinte forma:

$$\sigma_i^+ = \sigma_i \text{ se } \sigma_i > 0 \text{ e } \sigma_i^+ = 0 \text{ se } \sigma_i \le 0 \qquad (1a)$$

$$\sigma_i^- = \sigma_i \text{ se } \sigma_i < 0 \text{ e } \sigma_i^- = 0 \text{ se } \sigma_i \geq 0 \quad (1b)$$

Dessa forma as deformações por tração e por compressão podem ser escritas em função das tensões, através da lei de Hooke, como a seguir:

$$\varepsilon_{ti} = \frac{1+\upsilon}{E}\sigma_i^+ - \frac{\upsilon}{E}\sum_{j=1}^{3}\sigma_j^+ \quad (2a)$$

$$\varepsilon_{ci} = \frac{1+\upsilon}{E}\sigma_i^- - \frac{\upsilon}{E}\sum_{j=1}^{3}\sigma_j^- \quad (2b)$$

onde υ é o coeficiente de Poisson do concreto.
A deformação principal na direção i pode então ser expressa por:

$$\varepsilon_i = \varepsilon_{ti} + \varepsilon_{ci} \quad (3)$$

As deformações associadas aos alongamentos desenvolvidos em cada direção principal i são dadas por:

$$\varepsilon_i^+ = \frac{1}{2}\left(\varepsilon_i + |\varepsilon_i|\right) \quad (4)$$

Nota-se assim, que só são contabilizadas as deformações que geram alongamento em (4). Portanto, de acordo com as deformações apresentadas na equação (3), a deformação equivalente $\bar{\varepsilon}$ pode ser assim definida:

$$\bar{\varepsilon} = \sqrt{\left(\varepsilon_1^+\right)^2 + \left(\varepsilon_2^+\right)^2 + \left(\varepsilon_3^+\right)^2} \quad (5)$$

Para compatibilizar o modelo de dano com a Teoria Clássica de Laminados, será adotada a medição das deformações em pontos da superfície média de cada camada que constitui a placa.
Segundo o modelo de Mazars [18], o processo de danificação do material só ocorre para valores de deformações superiores a ε_{do}, ou seja o limite de tração do material, a partir do qual tem inicio a fissuração do concreto. Portanto, a condição para permanência do concreto no regime linear fica assim expressa:

$$\bar{\varepsilon} - \varepsilon_{do} \leq 0 \quad (6)$$

Devido ao comportamento assimétrico do concreto em relação à tração e compressão, existe a necessidade de determinação de duas variáveis distintas para o dano, uma para compressão D_{cc}, e outra para tração D_{ct}. Para o caso multiaxial, o dano do concreto D_c deve ser obtido através de uma combinação linear dessas duas variáveis, ficando o dano assim representado:

$$D_c = \alpha_t D_{ct} + \alpha_c D_{cc} \quad (7)$$

onde:

$$\alpha_t = \frac{\sum_{i=1}^{3}\varepsilon_{ti}^+}{\varepsilon_v^+} \quad (8a)$$

$$\alpha_c = \frac{\sum_{i=1}^{3}\varepsilon_{ci}^+}{\varepsilon_v^+} \quad (8b)$$

com

$$\varepsilon_{ti}^+ = \frac{1}{2}\left(\varepsilon_{ti} + |\varepsilon_{ti}|\right) \quad (9a)$$

$$\varepsilon_{ci}^+ = \frac{1}{2}\left(\varepsilon_{ci} + |\varepsilon_{ci}|\right) \quad (9b)$$

$$\varepsilon_v^+ = \sum_{i=1}^{3}\left(\varepsilon_{ti}^+ + \varepsilon_{ci}^+\right) \quad (9c)$$

cabendo observar que: $0 \leq \alpha_t \leq 1; 0 \leq \alpha_c \leq 1; e\, \alpha_t + \alpha_c = 1$.
As equações definidas por Mazars [18] para a evolução do dano por tração D_{ct} e compressão D_{cc} são apresentadas a seguir:

$$D_{ct} = 1 - \frac{\varepsilon_{do}\left(1 - A_t\right)}{\bar{\varepsilon}} - \frac{A_t}{exp\left[B_t\left(\bar{\varepsilon} - \varepsilon_{do}\right)\right]} \quad (10a)$$

$$D_{cc} = 1 - \frac{\varepsilon_{do}\left(1 - A_c\right)}{\bar{\varepsilon}} - \frac{A_c}{exp\left[B_c\left(\bar{\varepsilon} - \varepsilon_{do}\right)\right]} \quad (10b)$$

onde as constantes A_t, B_t, A_c e B_c são parâmetros do material

(concreto) determinados a partir das correspondentes curvas experimentais tensão-deformação (σ-ε), à tração e à compressão uniaxial, respectivamente. Para tanto, são geradas duas curvas teóricas (σ-ε), ajustadas às experimentais (uma para tração e outra para compressão), utilizando a equação baseada no modelo de dano, ou seja:

$$\sigma = E_c\left(1 - D_c\right)\varepsilon \qquad (11)$$

sendo E_c o módulo de elasticidade longitudinal do concreto.

2.2 Modelo de flexão

Na formulação analítica foi utilizada a Teoria Clássica dos Laminados. Na abordagem discreta o concreto e o aço são modelados separadamente e a construção do modelo torna-se mais difícil e demorada uma vez que um grande número de graus de liberdade é necessário [17]. Na abordagem por camadas o elemento estrutural é formulado como um compósito laminado que consiste de camadas finas, de concreto ou de aço, totalmente aderidas entre si. As tensões de tração e de compressão são monitoradas progressivamente, em cada camada, para verificar a fissuração ou esmagamento do concreto e o escoamento ou ruptura do aço. Modelos em MEF por camadas têm sido amplamente utilizados para análise de estruturas de concreto armado [17, 24, 29-31] e têm se mostrado eficiente.

Para análise do laminado as seguintes hipóteses são consideradas [32-33]:

1) O laminado consiste de lâminas perfeitamente coladas entre si, isto é, sem deslizamento ou descolamento. Isto significa que os deslocamentos são descritos por funções contínuas;

Figura 1 – Geometria de deformação da placa no plano xz

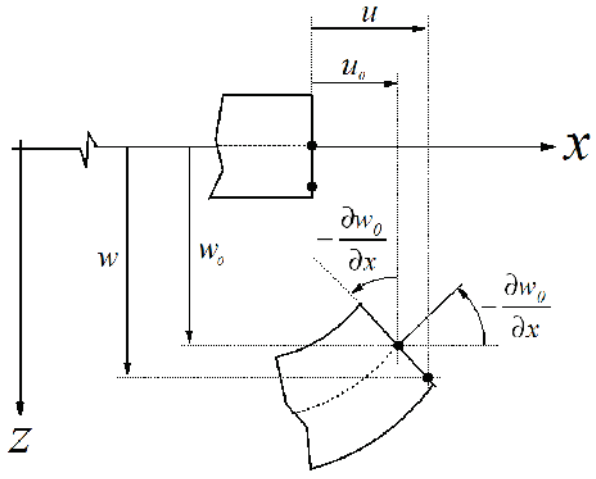

2) A placa é considerada delgada, ou seja, a espessura é relativamente pequena em relação às outras duas dimensões (superfície);
3) Linhas inicialmente retas e perpendiculares à superfície que define a geometria da estrutura (superfície média da placa) permanecem retas e perpendiculares a essa superfície, quando o laminado for solicitado;
4) As linhas normais à superfície de referência são consideradas inextensíveis, isto é, têm comprimentos constantes;
5) Supõe-se que o carregamento na placa acarreta rotações e deformações pequenas perante a unidade, enquadrando o problema no âmbito geometricamente linear;
6) As lâminas são formadas por materiais ortotrópicos de comportamento linear elástico (observa-se que o comportamento deixa de ser linear, por conta das considerações feitas para as relações tensão-deformação do concreto e do aço);
7) Admite-se que todas as cargas são aplicadas na superfície média da placa.

As hipóteses 2 a 5, usadas na teoria de Kirchhoff para placas delgadas, juntamente com a hipótese 1, permitem deduzir as relações mostradas a seguir, entre as componentes de deslocamento u, v e w de um ponto qualquer da placa, e as componentes u_0, v_0 e w_0 de um ponto correspondente situado sobre a superfície média (Figura 1):

$$u\left(x,y,z\right) = u_0\left(x,y\right) - z\frac{\partial w_0}{\partial x} \qquad (12a)$$

$$v\left(x,y,z\right) = v_0\left(x,y\right) - z\frac{\partial w_0}{\partial y} \qquad (12b)$$

$$w\left(x,y,z\right) = w_0\left(x,y\right) \qquad (12c)$$

onde as derivadas $\frac{\partial w_0}{\partial x}$ e $\frac{\partial w_0}{\partial y}$ são, respectivamente, as declividades da superfície média nas direções x e y.

Com base na hipótese 5 têm-se as seguintes relações deformação-deslocamentos:

$$\varepsilon_x = \frac{\partial u_0}{\partial x} - z\frac{\partial^2 w_0}{\partial x^2} \qquad (13a)$$

$$\varepsilon_y = \frac{\partial v_0}{\partial y} - z\frac{\partial^2 w_0}{\partial y^2} \qquad (13b)$$

$$\gamma_{xy} = \frac{\partial u_0}{\partial y} + \frac{\partial v_0}{\partial x} - 2z\frac{\partial^2 w_0}{\partial x \partial y} \quad (13c)$$

$$\varepsilon_z = 0 \quad (13d)$$

$$\gamma_{xz} = 0 \quad (13e)$$

$$\gamma_{yz} = 0 \quad (13f)$$

Considerando que as lâminas estão em um estado plano de tensões, tem-se para uma lâmina k as seguintes relações entre tensões e deformações atuantes, já incorporando a não linearidade física dos materiais, através do dano contínuo de Mazars (Concreto) e do modelo elastoplástico perfeito (aço):

$$\begin{bmatrix} \sigma_x \\ \sigma_y \\ \tau_{xy} \end{bmatrix} = \begin{bmatrix} \bar{Q}_{11} & \bar{Q}_{12} & \bar{Q}_{16} \\ \bar{Q}_{12} & \bar{Q}_{22} & \bar{Q}_{26} \\ \bar{Q}_{16} & \bar{Q}_{26} & \bar{Q}_{66} \end{bmatrix} \begin{bmatrix} \varepsilon_x \\ \varepsilon_y \\ \gamma_{xy} \end{bmatrix} \quad (14)$$

com as propriedades mecânicas das lâminas (ortotrópicas), como mostra a hipótese 6, calculadas por:

$$\bar{Q}_{11} = Q_{11}\cos^4\theta + 2\left(Q_{12} + 2Q_{66}\right)\text{sen}^2\theta\cos^2\theta + Q_{22}\text{sen}^2\theta \quad (15a)$$

$$\bar{Q}_{12} = \left(Q_{11} + Q_{22} - 4Q_{66}\right)\text{sen}^2\theta\cos^2\theta + Q_{12}\left(\text{sen}^4\theta + \cos^4\theta\right) \quad (15b)$$

$$\bar{Q}_{22} = Q_{11}\text{sen}^2\theta + 2\left(Q_{12} + 2Q_{66}\right)\text{sen}^2\theta\cos^2\theta + Q_{22}\cos^4\theta \quad (15c)$$

$$\bar{Q}_{16} = \left(Q_{11} - Q_{12} - 2Q_{66}\right)\text{sen}\theta\cos^3\theta + \left(Q_{12} - Q_{22} + 2Q_{66}\right)\text{sen}^3\theta\cos\theta \quad (15d)$$

$$\bar{Q}_{26} = \left(Q_{11} - Q_{12} - 2Q_{66}\right)\text{sen}^3\theta\cos\theta + \left(Q_{12} - Q_{22} + 2Q_{66}\right)\text{sen}\theta\cos^3\theta) \quad (15e)$$

$$\bar{Q}_{66} = \left(Q_{11} + Q_{22} - 2Q_{12} - 2Q_{66}\right)\text{sen}^2\theta\cos^2\theta + Q_{66}\left(\text{sen}^4\theta + \cos^4\theta\right) \quad (15f)$$

com representando o ângulo de orientação das fibras de reforço na camada k, e

$$Q_{11} = \left[\frac{E_1(1-D)}{1-\nu_{12}\nu_{21}}\right] \quad (16a)$$

$$Q_{12} = \left[\frac{\nu_{12}E_2(1-D)}{1-\nu_{12}\nu_{21}}\right] \quad (16b)$$

$$Q_{22} = \left[\frac{E_2(1-D)}{1-\nu_{12}\nu_{21}}\right] \quad (16c)$$

Figura 2 – Camadas de um laminado

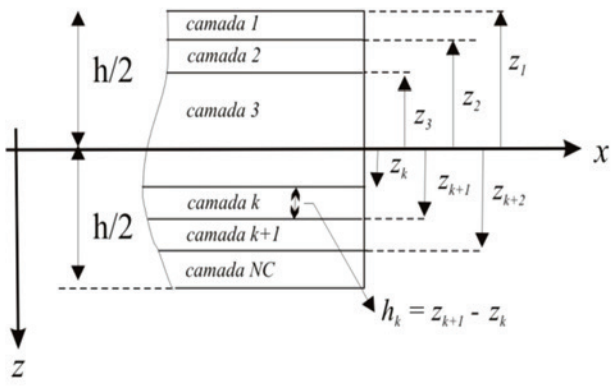

$$Q_{66} = G_{12}\left(1 - D\right) \tag{16d}$$

onde:
E_1 é o módulo de elasticidade longitudinal da camada na direção x;
E_2 é o módulo de elasticidade longitudinal da camada na direção y;
υ_{12} e υ_{21} são os coeficientes de Poisson da camada, associados as direções x e y;
G_{12} é o módulo de elasticidade transversal da camada, associado às direções x e y;
D representa o dano no material constituinte da camada estudada (ou, em outras palavras a relação entre a perda de rigidez do material e sua rigidez inicial).
Na presente formulação são definidos os seguintes esforços solicitantes por unidade de comprimento, avaliados na espessura h da placa laminada (Figura 2):

$$\begin{Bmatrix} N_{xx} \\ N_{yy} \\ N_{xy} \end{Bmatrix} = \begin{bmatrix} A_{11} & A_{12} & A_{16} \\ A_{12} & A_{22} & A_{26} \\ A_{16} & A_{26} & A_{66} \end{bmatrix} \begin{bmatrix} \frac{\partial u_0}{\partial x} \\ \frac{\partial v_0}{\partial y} \\ \frac{\partial u_0}{\partial y} + \frac{\partial v_0}{\partial x} \end{bmatrix} + \begin{bmatrix} B_{11} & B_{12} & B_{16} \\ B_{12} & B_{22} & B_{26} \\ B_{16} & B_{26} & B_{66} \end{bmatrix} \begin{bmatrix} -\frac{\partial^2 w_0}{\partial x^2} \\ -\frac{\partial^2 w_0}{\partial y^2} \\ -2\frac{\partial^2 w_0}{\partial x \partial y} \end{bmatrix} \tag{17a}$$

$$\begin{Bmatrix} M_{xx} \\ M_{yy} \\ M_{xy} \end{Bmatrix} = \begin{bmatrix} B_{11} & B_{12} & B_{16} \\ B_{12} & B_{22} & B_{26} \\ B_{16} & B_{26} & B_{66} \end{bmatrix} \begin{bmatrix} \frac{\partial u_0}{\partial x} \\ \frac{\partial v_0}{\partial y} \\ \frac{\partial u_0}{\partial y} + \frac{\partial v_0}{\partial x} \end{bmatrix} + \begin{bmatrix} D_{11} & D_{12} & D_{16} \\ D_{12} & D_{22} & D_{26} \\ D_{16} & D_{26} & D_{66} \end{bmatrix} \begin{bmatrix} -\frac{\partial^2 w_0}{\partial x^2} \\ -\frac{\partial^2 w_0}{\partial y^2} \\ -2\frac{\partial^2 w_0}{\partial x \partial y} \end{bmatrix} \tag{17b}$$

onde N_{xx}, N_{yy} e N_{xy} são os esforços de membrana, M_{xx} e M_{yy} os esforços flexionais e M_{xy} o esforço torsional, todos por unidade de comprimento.
A matriz contendo os coeficientes A_{ij} é denominada matriz de rigidez extensional, a que contém os elementos D_{ij} é a matriz de rigidez flexional e a composta pelos elementos B_{ij} é a matriz de rigidez de acoplamento flexo-extensional. Esses coeficientes são definidos em termos da matriz de rigidez de cada lâmina, conforme a seguir:

$$A_{ij} = \sum_{k=1}^{n} \bar{Q}_{ij}^{(k)} \left(z_{k+1} - z_k\right) dz \tag{18a}$$

$$B_{ij} = \frac{1}{2} \sum_{k=1}^{n} \bar{Q}_{ij}^{(k)} \left((z_{k+1})^2 - z_k{}^2\right) dz \tag{18b}$$

$$D_{ij} = \frac{1}{3} \sum_{k=1}^{n} \bar{Q}_{ij}^{(k)} \left(\left(z_{k+1}\right)^3 - z_k{}^3\right) dz \tag{18c}$$

Como se vê os esforços internos (17) são definidos para todos os pontos do plano médio da placa, dependendo tanto dos deslocamentos do plano médio, quanto das propriedades mecânicas dos materiais da placa. Portanto, ao incorporar o modelo de dano para o concreto e o regime elastoplástico perfeito para o aço as propriedades mecânicas são afetadas à medida que a não linearidade física é atingida, modificando também as inúmeras rigidezes A_{ij}, B_{ij} e D_{ij} da estrutura.

Figura 3 – Carregamento da placa

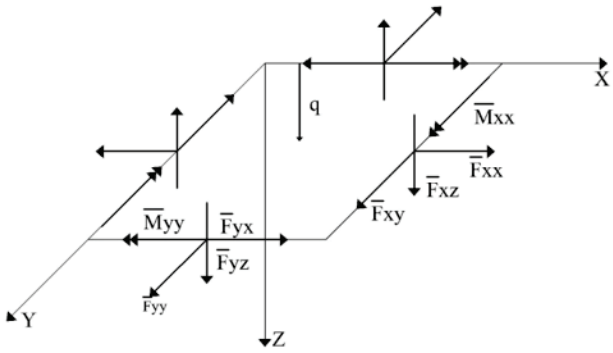

O trabalho virtual realizado pelas forças internas é assim expresso:

$$\delta W_{int} = \int_{r_0} \left\{ N_{xx}\delta\left(\frac{\partial u_0}{\partial x}\right) + N_{yy}\delta\left(\frac{\partial v_0}{\partial y}\right) + N_{xy}\left[\delta\left(\frac{\partial u_0}{\partial y}\right) + \delta\left(\frac{\partial v_0}{\partial x}\right)\right] - M_{xx}\delta\left(\frac{\partial^2 w_0}{\partial x^2}\right) - M_{yy}\delta\left(\frac{\partial^2 w_0}{\partial y^2}\right) - 2M_{xy}\delta\left(\frac{\partial^2 w_0}{\partial x \partial y}\right) \right\} dxdy \tag{19}$$

onde r_0 representa a área da superfície média da placa. Considerando-se a Figura 3, associada a hipótese 7, onde as cargas atuantes no domínio e no contorno da placa são mostradas com seus sentidos positivos, pode-se escrever para o trabalho virtual realizado pelas forças externas a seguinte expressão:

$$\begin{aligned} \delta W_{ext} &= \int_{r_0} q_z(x,y)\delta w_0 dxdy + \\ &\int_0^b \left(\bar{F}_{xx}\delta u_0 + \bar{F}_{xy}\delta v_0 + \bar{F}_{xz}\delta w_0 - \bar{M}_{xx}\delta\left(\frac{\partial w_0}{\partial x}\right)\right)_{x=0}^{x=a} dy + \\ &+ \int_0^a \left(\bar{F}_{yx}\delta u_0 + \bar{F}_{yy}\delta v_0 + \bar{F}_{yz}\delta w_0 - \bar{M}_{yy}\delta\left(\frac{\partial w_0}{\partial y}\right)\right)_{y=0}^{y=b} dx \end{aligned} \tag{20}$$

onde:
$q_z(x,y)$ é a força transversal à superfície média da placa, por unidade de área, aplicada no domínio;
$\bar{F}_{xx}$, $\bar{F}_{xy}$ e $\bar{F}_{xz}$ são as forças por unidade de comprimento ao longo dos bordos $x = 0$ e $x = a$, segundo as direções x, y e z, respectivamente;

Figura 4 – Função f (x) utilizada nas representações em diferenças finitas para as derivadas dos deslocamentos

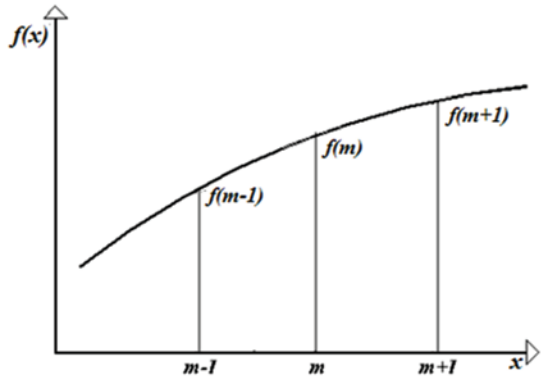

Figura 5 – Discretização da placa: trechos de integração, nós reais e nós virtuais

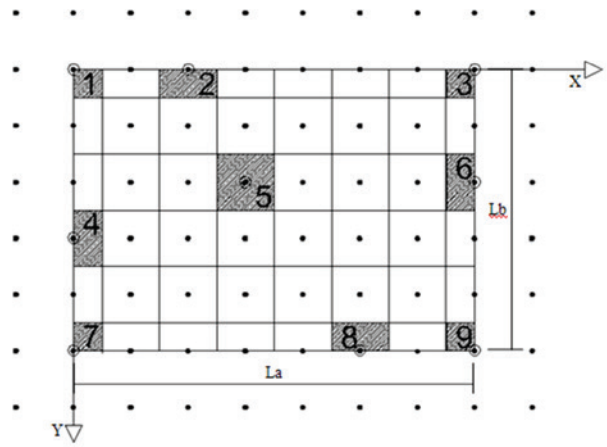

$\bar{M}_{xx}$ é o Momento de flexão por unidade de comprimento, aplicado ao longo dos bordos $x = 0$ e $x = a$;
$\bar{F}_{yx}$, $\bar{F}_{yy}$ e $\bar{F}_{yz}$ são as forças por unidade de comprimento ao longo dos bordos $y = 0$ e $y = b$, segundo as direções x, y e z, respectivamente;
$\bar{M}_{yy}$ - Momento de flexão por unidade de comprimento, aplicado ao longo dos bordos $y = 0$ e $y = b$.
Embora o momento de torsão tenha sido considerado no âmbito dos esforços internos, não foi associado um carregamento correspondente, no cômputo do trabalho externo, por não ser usualmente aplicado em lajes.

3. Formulação computacional

Após expressar o trabalho realizado pelas forças internas em função dos deslocamentos, mediante a substituição das expressões dos esforços internos (17a) e (17b) em (19), o tratamento numérico segundo o MDFE pode ser aplicado. Este consiste em introduzir nas expressões das parcelas que compõem o princípio dos trabalhos virtuais (PTV), δW_{int} e δW_{ext}, as representações em diferenças finitas utilizadas para as derivadas dos deslocamentos supondo, para fins de avaliação desses trabalhos virtuais, a barra subdividida em trechos de integração, ao longo dos quais todas as grandezas envolvidas são supostas constantes. Uma vez computados δW_{int} e δW_{ext}, mediante o somatório das contribuições dos diversos trechos de integração, e considerando-se as condições cinemáticas de vinculação da placa, e as demais variações dos deslocamentos arbitrárias e independentes entre si, surge, pela aplicação do PTV, um sistema de equações algébricas de equilíbrio que, uma vez resolvido, permite obter a solução em termos dos deslocamentos nodais u_0, v_0 e w_0 incógnitos.
Na formulação numérica do problema aqui estudado são utilizados dois tipos de representações para as derivadas dos deslocamentos: a representação centrada e a representação reduzida. Para tanto, considere o esquema da Figura 4, onde $f(x)$

Tabela 1 – Propriedades dos materiais utilizados na modelagem

Laje simplesmente apoiada										
	E(GPa)	ν_c	f_c (MPa)	A_c	B_c	f_t (MPa)	ε_{d0}	A_t	B_t	f_y (MPa)
Concreto	32,42	0,18	35,04	1,00	1600	3,60	1,11 x 10^{-4}	0,80	10000	–
Aço	206,91	–	–	–	–	–	–	–	–	375,90

Laje apoiada nos cantos										
	E(GPa)	ν_c	f_c (MPa)	A_c	B_c	f_t (MPa)	ε_{d0}	A_t	B_t	f_y (MPa)
Concreto	28,61	0,15	37,92	1,00	1650	3,80	1,33 x 10^{-4}	0,80	10000	–
Aço	201,30	–	–	–	–	–	–	–	–	345,40

Figura 6 – Diagramas tensão-deformação obtidos a partir do modelo de dano de Mazars para os concretos empregados nas lajes estudadas

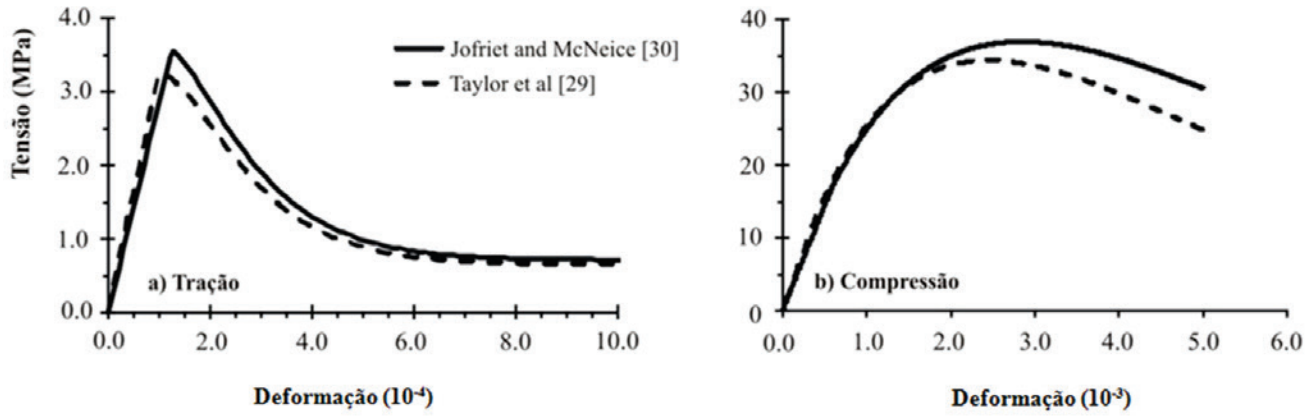

representa as funções u_0, v_0 e w_0 e m é o ponto no qual são avaliadas as derivadas (ponto pivotal). Sendo λ o espaçamento nodal, as derivadas centradas de primeira e segunda ordem de $f(x)$, avaliadas no ponto m, são: $f'_m = \frac{1}{2\lambda}(f_{m+1} - f_{m-1})$ e $f''_m = \frac{1}{\lambda^2}(f_{m+1} - 2f_m + f_{m-1})$.

Em trechos localizados junto aos bordos da placa, o uso da representação centrada para as derivadas primeiras dos deslocamentos u_0 e v_0 podem causar singularidade na matriz dos coeficientes, impossibilitando a resolução do problema. Por esse motivo, para essas derivadas na região dos bordos da placa será adotada a representação reduzida, conforme sugerido por Graça [14]. Esta representação pode ser definida por: $f'_m = \frac{1}{\lambda}(f_{m+1} - f_m)$.

Para a discretização do domínio $L_a \times L_b$ da placa, o MDFE prevê a geração de trechos de integração obtidos a partir de subdivisões nas direções x e y, quais sejam n_x e n_y respectivamente. Desse modo um trecho de integração genérico apresenta a forma retangular de dimensões $\lambda_x = L_a / n_x$ e $\lambda_y = L_b / n_y$, com um total de $(n_x + 3) \times (n_y + 3)$ nós e $(n_x + 1) \times (n_y + 1)$ trechos de integração distribuídos em nove tipos diferentes de trechos, conforme mostrado na Figura 5. Os trechos 1, 3, 7 e 9 localizam-se nos cantos da placa e apresentam área $\frac{\lambda_x \times \lambda_y}{4}$, enquanto os trechos 2, 4, 6 e 8, de área $\frac{\lambda_x \times \lambda_y}{2}$, situam-se ao longo dos bordos da placa. Os demais trechos de integração da placa pertencem ao trecho tipo 5, de área $\lambda_x \times \lambda_y$, como ilustrado na Figura 5.

Figura 7 – Características geométricas da laje e do respectivo reforço FONTE: Adaptado de Jiang e Mirza (16)

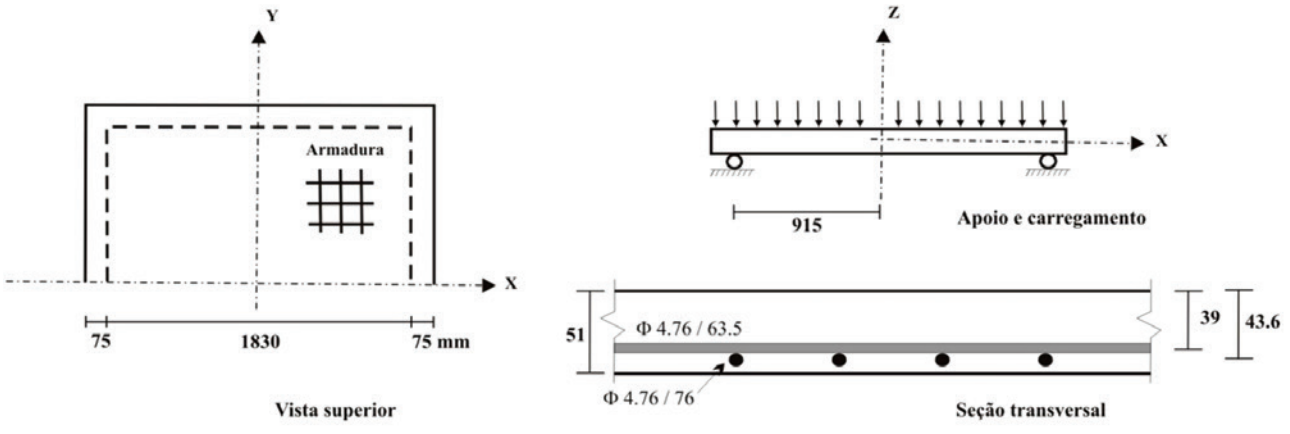

Figura 8 – Efeito do tipo de redução do módulo de elasticidade transversal do concreto no comportamento da laje

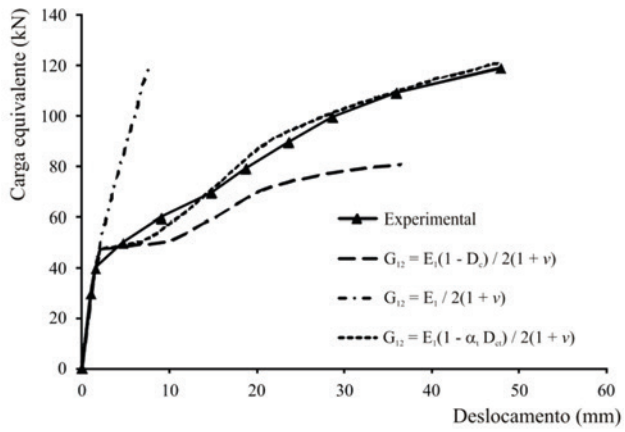

Cabe observar que cada trecho de integração é composto por nove pontos nodais (Figura 5) e para cada um desses pontos são associados três graus de liberdade u_0, v_0 e w_0, o que incorpora, para cada trecho, um total de 27 deslocamentos. Notar que as derivadas de segunda ordem dos deslocamentos dos nós associados aos bordos da placa necessitam de nós externos à mesma, denominados de nós virtuais. Cabe destacar ainda que os nós da estrutura podem compor mais de um trecho de integração.

Maiores explicações sobre a seqüência do desenvolvimento do tratamento numérico, segundo o MDFE, podem ser encontradas em [13-15].

Figura 9 – Influência da quantidade de camadas na modelagem da laje simplesmente apoiada

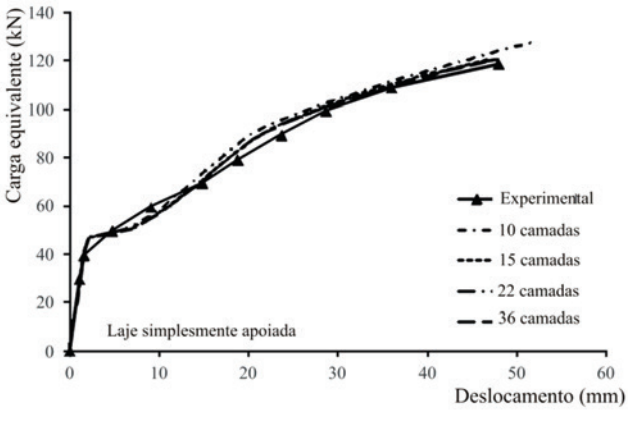

4. Validação do modelo

A validação do modelo numérico apresentado foi realizada através da determinação da curva carga-deslocamento de duas lajes de concreto armado ensaiadas experimentalmente por Taylor, Mather e Hayes [27] e McNeice [28]. Ambos os problemas apresentam dupla simetria, o que permitiu a modelagem de um quarto da placa, possibilitando uma melhor discretização do elemento estrutural com menor esforço computacional. A simulação será baseada no diagrama carga-flecha, e na previsão do colapso da estrutura.

A Tabela 1 apresenta os dados experimentais dos concretos (E_c, f_c, f_t e υ_c) e dos aços (E_s e f_y) utilizados nas duas lajes estudadas. Para o concreto da laje apoiada nos cantos [28] foi admitido que $f_t = 0.1 f_c$. A partir dos valores apresentados para o concreto de ambas as lajes, foram obtidos diagramas tensão-deformação teóricos (Figura 6), utilizando as equações de dano, equações (10) e (11), com a escolha de valores adequados para os parâmetros A_t, B_t, e B_c. Para tanto, inicialmente determina-se o parâmetro de deformação ε_{do} a partir da tensão máxima de tração do concreto (f_t), pela aplicação direta da forma uniaxial da Lei de Hooke, assumindo a igualdade entre o módulo de elasticidade à tração e o módulo de elasticidade à compressão, indicado na Tabela 1. Em seguida, passa-se a geração das curvas teóricas tensão-deformação buscando-se ajustá-las às curvas experimentais correspondentes (tração uniaxial e compressão uniaxial), pela manipulação das constantes A_t, B_t, e B_c. No caso da tração, as constantes A_t e B_t são determinadas de modo a gerar um diagrama tensão-deformação associado ao comportamento frágil do concreto, sendo f_t a tensão máxima observada (onde ocorre ε_{do}). Cabe mencionar nesse ponto que os valores adotados para A_t foram similares aos encontrados por Lemaitre e Mazars [34] e Challamel [35], na modelagem de vigas de concreto armado. No tocante à compressão, os parâmetros A_c e B_c são determinados de forma a se obter a tensão máxima de compressão do material (f_c) associada a uma deformação (de pico) entre 2‰ e 3‰. Ressalta-se que o procedimento acima, para determinação dos parâmetros do Modelo de Mazars, foi similar ao adotado por

Figura 10 – Carga x deslocamento transversal do ponto central da placa

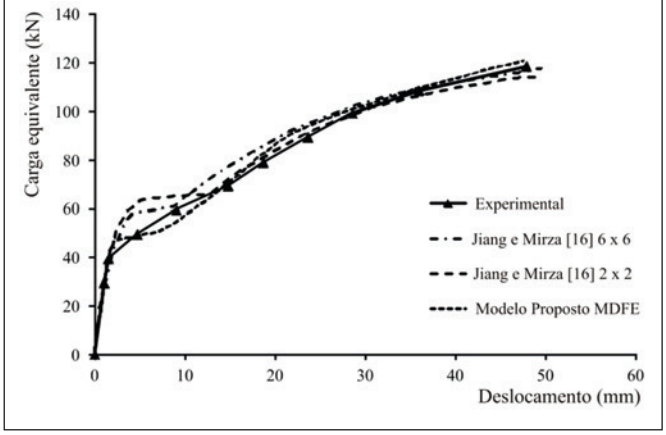

Figura 11 – Características geométricas da laje estudada. FONTE: Adaptado de Krätzig e Pöling (37)

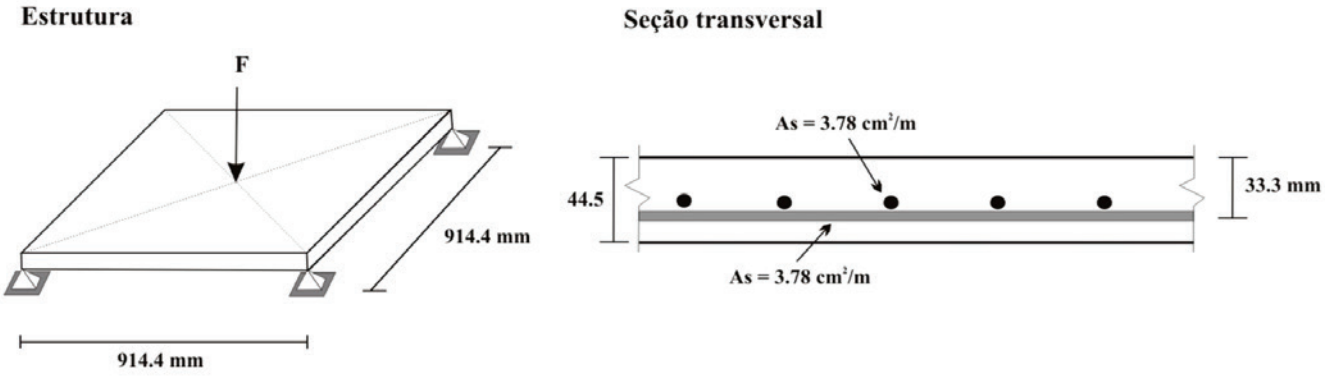

diversos autores [18, 19, 23, 25, 34, 36] que utilizaram esse modelo de dano para modelagem numérica de concreto.

Cabe registrar que para os dois concretos assim modelados não foram apresentadas as curvas experimentais correspondentes na Figura 6, por não terem sido determinadas pelos autores dos respectivos experimentos. Todavia, isto não se mostrou uma dificuldade já que foi levado em consideração apenas o conhecimento já estabelecido para a forma do diagrama tensão--deformação dos concretos convencionais, conforme descrito na metodologia acima. Este aspecto pode ser destacado como uma vantagem de se empregar o modelo de dano aqui utilizado na modelagem de lajes.

O reforço (armaduras de aço) foi modelado como uma camada uniaxial (com módulo de elasticidade longitudinal apenas na direção do reforço), sendo o centro da camada coincidente com o centro geométrico da armadura, e a espessura da camada definida de forma que a área da seção transversal da camada resulte igual à área do reforço. A partir da tensão de escoamento do reforço (f_y) é estabelecido o patamar de escoamento do diagrama tensão-deformação elasto-plástico correspondente, sendo a deformação última assumida igual a 10‰ (tração e compressão).

4.1 *Laje simplesmente apoiada com carregamento uniforme*

Inicialmente foi simulado numericamente o comportamento de uma laje simplesmente apoiada sob carga distribuída uniforme, conforme mostrado na Figura 7, ensaiada experimentalmente por Taylor, Mather e Hayes [27] e analisada teoricamente por Jiang e Mirza [16]. Além das características geométricas da laje a figura mostra que a laje possui armaduras com diâmetro de 4,76 mm nas duas direções, mas com espaçamentos distintos. As propriedades dos materiais utilizados na laje estão listadas na Tabela 1, bem como os parâmetros de dano encontrados para o respectivo concreto.

Depois de uma série de testes foi definida para a modelagem da placa uma discretização em 8×8 subdivisões (ou seja 9×9 trechos de integração). Para este exemplo além do confronto com o

Figura 12 – Influência da quantidade de camadas na modelagem da laje apoiada nos cantos

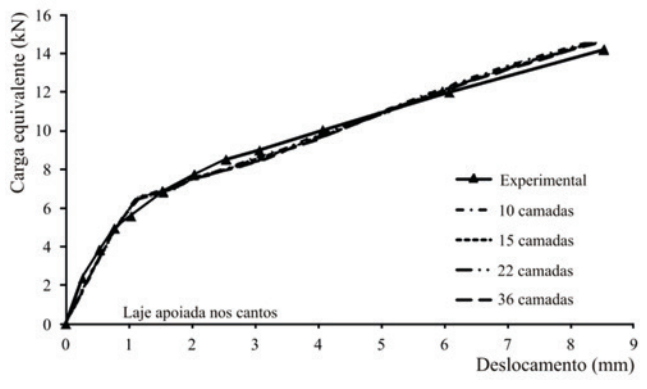

Figura 13 – Comparação do modelo proposto com Método dos Elementos Finitos

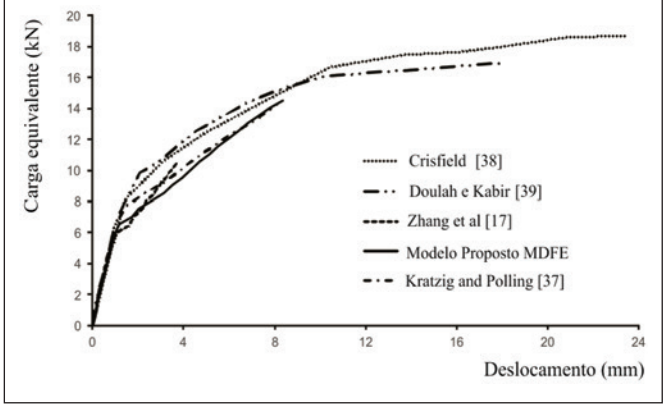

resultado experimental também foi realizado um estudo da influência das diferentes formas de avaliação da redução do módulo de elasticidade transversal do concreto durante o processo de fissuração. Foram então testadas três situações:

1) A consideração da redução do módulo de elasticidade transversal em função do dano do concreto, ou seja:

$$G_{12} = \frac{E_1\left(1-D_c\right)}{2\left(1+\upsilon\right)}$$, com $E_1 = E_c$, $\upsilon = \upsilon_c$ e $D_c = \alpha_t D_{ct} + \alpha_c D_{cc}$;

2) A consideração de que o módulo de elasticidade transversal mantém-se constante, mesmo após o início do processo de fissuração, e proporcional ao módulo de elasticidade longitudinal inicial:

$$G_{12} = \frac{E_1}{2\left(1+\upsilon\right)}$$, onde $E_1 = E_c$ e $\upsilon = \upsilon_c$;

3) A consideração da redução do módulo de elasticidade transversal em função do dano por tração, ou seja,

$$G_{12} = \frac{E_1\left(1-\alpha_t D_{ct}\right)}{2\left(1+\upsilon\right)}$$, sendo $E_1 = E_c$ e $\upsilon = \upsilon_c$.

Os resultados numéricos para o diagrama carga-deslocamento no centro da laje são apresentados na Figura 8, em comparação com o resultado experimental, devendo ser observado que a carga registrada no gráfico é a carga resultante sobre a placa (força concentrada).

Observa-se que o módulo de elasticidade transversal do concreto exerce uma influência bastante significativa. Percebe-se que a situação 02 proporciona uma resposta demasiadamente rígida na modelagem, tornando-a uma opção inviável para o modelo. Por outro lado, a situação 01 representa bem o início da fissuração, porém fornece respostas pouco rígidas após esse ponto, e com a previsão de uma carga de ruptura menor que a verificada experimentalmente. A situação 03 consegue representar de forma satisfatória o início da fissuração, mantendo proximidade com a curva experimental e boa precisão na previsão da carga de ruptura.

Cabe ressaltar que, apesar da utilização de uma abordagem isotrópica para prever a variação do módulo de elasticidade transversal do concreto (portanto mais simplificada que a adotada por outros autores a exemplo de Pituba [36], que utiliza um dano anisotrópico), verifica-se uma boa aproximação dos resultados numéricos com os resultados experimentais.

Partindo para a avaliação do resultado obtido para a situação 03, nota-se uma perda de rigidez no início da danificação, seguida de uma recuperação com posterior estabilização em relação ao resultado experimental. A simulação prosseguiu até o programa abortar, o que caracteriza a ausência de uma nova configuração de equilíbrio, ou seja colapso estrutural. Uma investigação mais detalhada da ruptura revelou que, de acordo com os resultados apresentados pelo programa, o escoamento da armadura teve início há uma carga (resultante) de 83,72 kN, e o colapso da estrutura ocorreu pela ruptura da armadura (deformação superior a 10‰), com uma deformação do concreto da camada mais comprimida com valor de aproximadamente 0,002, o que caracteriza uma ruptura do tipo pouco armada para a laje. Portanto, pode-se concluir que os resultados obtidos para o presente caso foram satisfatórios, tanto do ponto de vista carga-deslocamento quanto da previsão do colapso.

A análise da influência do número de camadas na modelagem da laje também foi estudada e está apresentada na Figura 9: a espessura da laje foi simulada com 10, 15, 22 e 36 camadas. Pode ser observado que a partir de 15 camadas não ocorreram alterações significativas nos resultados, sendo essa, portanto, a quantidade de camadas adotada para a modelagem deste tipo de laje.

Por fim, é apresentado na Figura 10, um comparativo do modelo proposto com os resultados apresentados por Jiang e Mirza [16], utilizando modelagem em Elementos Finitos com 4 (2 x 2) e 36 (6 x 6) elementos finitos. No modelo de [16] foi desenvolvido um modelo combinando o MEF, através de um elemento finito quadrilátero, com 20 graus de liberdade por elemento, a Teoria Clássica de Flexão de Placas e um modelo de plasticidade para o comportamento mecânico do concreto. O comparativo entre os resultados novamente evidencia a eficiência do modelo baseado no MDFE, tendo em vista que o modelo baseado no MEF e o baseado em MDFE apresentam convergência para um número próximo de graus de liberdade (245 e 243 graus de liberdade respectivamente).

4.2 Laje apoiada nos cantos com carga aplicada no centro

Neste exemplo foi simulado o comportamento carga-deslocamento no centro de uma laje ensaiada experimentalmente por McNeice [28], com as características mostradas na Figura 11 e na Tabela 1, onde estão também listados os parâmetros de dano utilizados na simulação. Para reger a variação do módulo de elasticidade transversal do concreto, foi aplicada a situação 3 apresentada no item anterior.

Mediante um estudo de convergência da solução, foi adotada uma discretização da laje em 14 x 14 subdivisões (15 x 15 trechos de integração). E quanto à discretização da espessura da laje esta foi modelada como um laminado de 10, 15, 22 e 36 camadas. Os resultados para o comparativo estão apresentados na Figura 12, onde se pode observar que, da mesma forma que no exemplo anterior, a partir de 15 camadas não houve alteração significativa nos resultados.

Na Figura 13 é apresentado o resultado numérico do modelo proposto em comparação com o resultado experimental e com resultados obtidos por Kratz e Polling [37]. Observa-se novamente uma perda de rigidez após a danificação, com posterior recuperação e ruptura coincidente com o observado experimentalmente. A este respeito, informa-se que na última condição de equilíbrio o aço encontrava-se em estágio de escoamento, com deformação da ordem de 0,0063, e o concreto comprimido com deformação máxima de 0,0057. Portanto, o colapso da estrutura aconteceu pelo esmagamento do concreto e escoamento do reforço, caracterizando uma ruptura de laje super armada.

Avaliando a trajetória de equilíbrio dos modelos numéricos já implementados para modelagem da laje de Mcneice [28], verifica-se na Figura 13 que o modelo proposto apresenta um comportamento mais aproximado do que outros modelos numéricos já testados. Crisfield [38] que desenvolveu o seu modelo a partir do MEF, utilizando elementos finitos retangulares, o critério de ruptura de Vom Misses para modelar o concreto a compressão, e um modelo de amolecimento linear para seu comportamento à tração. Na Figura 14 também é apresentado o resultado encontrado por Doulah e Kabir [39] que combinaram a Teoria de Flexão de Placas de Mindlin, com um modelo de comportamento à tração para o concreto similar ao apresentado por Crisfield [38] e comportamento bi-linear à compressão, utilizando elementos finitos quadriláteros com oito nós por elemento e 4 graus de liberdade por nó. Zhang et al [17] também utilizaram o MEF em sua

modelagem, com elementos quadriláteros com 24 graus de liberdade por elemento, associados a Teoria de Flexão de Placas de Mindlin e Reissner. Para o concreto à compressão esses autores utilizaram o modelo de comportamento elástico perfeito, e para o concreto sob tração foi aplicado um modelo que leva em consideração o aparecimento de fissuras perpendiculares as direções principais após se atingir a tensão máxima de resistência à tração.

5. Conclusões

No presente artigo, visando prever de forma satisfatória a trajetória de equilíbrio de lajes sob flexão até a sua ruptura, foi apresentado um modelo de flexão de placas de concreto armado combinando a Teoria Clássica de Laminados, o modelo de dano isotrópico de Mazars, para modelar o concreto, e o comportamento elastoplástico perfeito, para descrever o aço das armaduras. Para validação do modelo foram utilizandos os resultados experimentais de duas lajes de concreto armado sob flexão.

Os resultados obtidos apontaram que a redução do módulo de elasticidade transversal está associada ao dano ocasionado por tração (D_{CT}). Um segundo estudo, ligado a convergência da solução, indicou que 15 camadas são suficientes para garantir uma boa discretização da seção transversal das lajes. Finalmente, foi observado nas simulações numéricas utilizado o Método das Diferenças Finitas Energéticas que houve uma boa aproximação da trajetória de equilíbrio numérica com a experimental. Comparando-se com resultados numéricos do Método dos Elementos Finitos, realizados por outros autores, verifica-se que o MDFE apresentou melhor aproximação que os demais. Ressalta-se que os resultados foram obtidos a partir de uma discretização com poucas subdivisões da placa e poucas camadas o que destaca a eficiência computacional da associação entre o MDFE e o modelo téorico.

6. Agradecimentos

À SECTI/FAPESB e CNPq (PPP 010/2010) pelo apoio financeiro à pesquisa e à CAPES pela bolsa de estudos (Mestrado) destinada ao primeiro autor deste trabalho.

7. Referências bibliográficas

[01] KURRER K-E., RAMM, E. The History of the Theory of Structures. From Arc Analysis to Computational Mechanics. John Wiley & Sons, 2008, 848pp.

[02] THOMÉE, V.. From finite differences to finite elements: A short history of numerical analysis of partial diferential equations. Journal of Computational and Applied Mathematics, vol. 128, 2001, p.1–54.

[03] HAGIYA, H., MORISHITA, M., ANDO, T.; TANAKA, H. MATUO, K. Damage evaluation of reinforced concrete slabs subjected to contact detonation loads with numerical simulation. Science and tecnhnology of energetic materials, vol. 64, n. 5, 2003, p.192-200.

[04] FERRETI, D. ;SAVOIA, M. Non-linear model for R/C tensile members strengthened by FRP-plates. Engineering Fracture Mechanics, vol. 70, 2003, p.1069–1083.

[05] HABIB, A.; MOHARRAMI,H. Nonlinear sensitivity analysis of reinforced concrete frames, Finite Elements in Analysis and Design, vol. 46, 2010, p. 571–584.

[06] VIRDI, K. S. Finite difference method for nonlinear analysis of structures, Journal of Constructional Steel Research, vol. 62, 2006, p. 1210–1218.

[07] JONES, J., C. WUA,, D.J. OEHLERS , A.S. WHITTAKER , W. SUN, S. MARKS, R. COPPOLA. Finite difference analysis of simply supported RC slabs for blast loadings. Engineering Structures, vol. 31, 2009, p.2825-2832.

[08] HOUBOLT, J.C. A Study of Several Aerothermoelastic Problems of Aircraft Structures in High-Speed Flight. Zurich, 1958, Doctoral Thesis - The Swiss Federal Institute of Technology.

[09] GRIFFIN, D. S.; VARGA, R.S. Numerical solution of plane elasticity problems. Journal of Society of Industrial Applied Mathematic, vol. 11, n. 4, 1963.

[10] BUSHNELL, D. Finite-difference energy models versus finite-element models- Two variational approaches in one computer program. Numerical and computer methods in structural mechanics.(A 74-17756 06-32) New York, Academic Press, Inc., 1973, p. 291-336

[11] PLETZ, E. Análise de estrutura laminares pelo método da energia discretizada. Rio de Janeiro, 1983, Tese (Mestrado) - Universidade Federal do Rio de Janeiro.

[12] NISHIKAVA, L. K. Análise numérica de placas com cantos reentrantes. Rio de Janeiro, 1991, Tese (Mestrado) - Universidade Federal do Rio de Janeiro.

[13] GRAÇA, M. S. B. A. Método das diferenças finitas energéticas na análise estática e dinâmica de placas delgadas e espessas, Rio de Janeiro, 2000, Tese (Doutorado) - Universidade Federal do Rio de Janeiro.

[14] LIMA, J. M. F. Estudo comparativo entre formulações geometricamente não lineares para a flexo-torção de hastes de paredes delgadas de seção aberta, Rio de Janeiro, 2004, Tese (Doutorado) - Universidade Federal do Rio de Janeiro.

[15] NEVES, J. B; LIMA, J. M. F.; LIMA, P. R. L. Método das Diferenças Finitas Energéticas para simulação do comportamento sob flexão do concreto reforçado com fibras curtas de aço. Revista Sul-americana de Engenharia Estrutural, vol.10, n.2, 2013, p.31-55.

[16] JIANG, J.; MIRZA, F. A. Nonlinear analysis of reinforced concrete slabs by a discret finite element approach. Computers & Structures, vol.65, n.4, 1997, p. 585-592.

[17] ZHANG, Y. X.; BRADFORD, M. A.; GILBERT, R. I. A layered shear-flexural plate/shell element using Timoshenko beam functions for nonlinear analysis of reinforced concrete plates. Finite elements in analyses and design, vol.43, 2007; p.888-900.

[18] MAZARS, J. A Description of micro and macroscale damage of concrete structures, Engineering Fracture Mechanics, vol.25, 1986; p.729-737.

[19] FERNANDES, G. R. Método dos elementos de contorno aplicado à análise não linear de placas, São Paulo, 1998, Dissertação (Mestrado) - Escola de Engenharia de São Carlos - Universidade de São Paulo.

[20] CRESCE, S. H. Análise não-linear de pavimento de concreto armado pelo método de elementos de contorno, São Paulo, 2003, Tese (Doutorado) - Universidade de São Paulo.

[21] BANDEIRA M. S. Análise não-linear de lajes de concreto armado pelo método dos elementos finitos, Goiás, 2006, Dissertação (Mestrado) - Universidade Federal de Goiás.

[22] WANG, T.; HSU, T. Nonlinear finite element analysis of concrete structures using a new constitutive models. Computer and structures, vol. 19, 2001, p.2781-2791.
[23] ASSAN, A.E., Nonlinear analysis of reinforced concrete cylindrical shells. Computer and structures, vol. 80, 2002, p.2177–2184.
[24] HAIDO, J. BAKAR, B.H.; ABDUL-RAZZAK, A.A.; JAYAPRAKASH, J. Dynamic response simulation for reinforced concrete slabs. Simulation Modelling Practice and Theory, vol. 18, 2010, p.696–711.
[25] SANCHES, F. J.; VENTURINI, W. S. Damage modeling of reinforced concrete beams. Advances in Engineering Software, vol.38, 2007, p.538-546.
[26] LIMA, J.M.F.; NAGAHAMA. K.J.; LIMA, P.R.L.; SANTOS, G. J. B dos. Um modelo para análise não linear física da flexão de vigas de concreto armado. Mecânica Computacional, vol. XXIX, 2010, p.9839-9853.
[27] TAYLOR, R.; MATHER, D. R. H.; HAYES, B. Effect of the arrangement of reinforcment on the behaviour of reinforced concrete slabs. Magazine Concrete Research, vol.18, 1966, p.85-94.
[28] MCNEICE, G. M., Elastic-Plastic Bending of Plates and Slabs by the Finite Element Method, Ph. D. Thesis, London University, 1967.
[29] NOH, H.C.. Nonlinear behavior and ultimate load bearing capacity of reinforced concrete natural draught cooling tower shell. Engineering Structures, vol. 28, 2006, p. 399–410.
[30] OLIVEIRA, R.S.; RAMALHO, M.A.; CORREA, M.R.S. A layered finite element for reinforced concrete beams with bond–slip effects. Cement & Concrete Composites, vol. 30, 2008, p. 245–252.
[31] GUAN, H.; COOPER, C.; LEE,, D-J. Ultimate strength analysis of normal and high strength concrete wall panels with varying opening configurations. Engineering Structures, vol. 32, 2010, p. 1341-1355.
[32] JONES, R. M. Mechanics of composite materials. Taylor & Francis Group, 1999.
[33] REDDY, J. N. Mechanics of Laminated Composite Plates and Shells: Theory and analysis. CRC, 2004.
[34] LEMAITRE, J.; MAZARS, J. Application de la théorie de l'endommagement au comportement non linéaire et à la rupture du béton de structure. De l'institut technique Du batiment et dês travaux publics, vol.401, 1982, p.114-137.
[35] CHALLAMEL, N. A variationally based nonlocal damage model to predict diffuse microcracking evolution. International Journal of Mechanical Sciences, vol.52, 2010, p.1783-1800.
[36] PITUBA, J. J. C. Avaliação de um modelo anisótropo de dano considerando a perda de resistência devido ao cisalhamento do concreto. Asociación Argentina de Mecánica Computacional, vol.29, 2010; p.5397-5410
[37] KRATZIG, W.B., AND POLLING, R. An elasto-plastic damage model for reinforced concrete with minimum number of material parameters, Computers and structures, vol.82, n.15-16, 2004, p.1201-1215.
[38] CRISFIELD, M. A. Accelerated solution techniques and concrete cracking. Her Majesty's Stationery Office, London, v. 33, pp. 585-607, 1981.
[39] DOULAH, N.; KABIR, A. Non linear Finite Element analysis of reinforced concrete rectangular and skiw slabs. Journal of Civil Engineering, Institutions of Engineers, Bangladesh, v. 29, 2001.

Volume 7, Number 6 (December 2014) p. 965-975 • ISSN 1983-4195

REVISTA IBRACON DE ESTRUTURAS E MATERIAIS

IBRACON STRUCTURES AND MATERIALS JOURNAL

Development of high performance fiber reinforced cement composites (HPFRCC) for application as a transition layer of reinforced beams

Desenvolvimento de compósitos cimentícios de elevado desempenho armados com fibras para aplicação como substrato de transição de vigas de concreto




V. J. FERRARI [a]
vladimirjf@hotmail.com

A. P. ARQUEZ [b]
anaeng@hotmail.com

J. B. DE HANAI [c]
jbhanai@sc.usp.br

R. A. DE SOUZA [a]
rsouza@uem.br

Abstract

This study presents the development and behavior analysis of high performance fiber reinforced cement composites (HPFRCC). The described materials were specifically developed for application as a transition layer: a repair layer that constitutes the stressed chord of reinforced concrete beams strengthened in flexure with carbon fiber reinforced polymers (CFRP). Nineteen different composites were produced by the hybridization process, varying the conventional short steel fiber and steel microfiber (manufactured exclusively for this research) contents to modify the microstructure of the material, thus enhancing the stress transfer process from the cement matrix to the fibers. To analyze the response to flexural loading, the composites underwent three point bending tests in notched prism specimens. The response of the material was obtained considering strength and tenacity parameters (flexural and fracture). There was evidence of high performance by the composites with a pseudo-hardening behavior.

Keywords: higher performance fiber reinforced cement composite (HPFRCC), reinforced concrete beams, transition layer, steel microfiber.

Resumo

Este estudo apresenta o desenvolvimento e a análise do comportamento de compósitos cimentícios de elevado desempenho armado com fibras. O material descrito foi especificamente desenvolvido para aplicação como um substrato de transição: uma camada de transição que forma o banzo tracionado de vigas de concreto armado reforçadas à flexão com polímeros reforçados com fibras de carbono (PRFC). Dezenove diferentes compósitos foram produzidos pelo processo de hibridização, variando o volume de fibras curtas convencionais de aço e microfibras de aço (produzidas especificamente para este estudo) para modificar a microestrutura do material numa tentativa de melhorar o processo de transferência das tensões da matriz para as fibras. Para analisar a resposta do material à flexão, os compósitos foram submetidos a ensaios de flexão em três pontos em corpos de prova prismáticos com entalhe central. A resposta do material foi obtida considerando-se parâmetros de resistência e de tenacidade (flexional e ao fraturamento). Ficou evidenciado o elevado desempenho dos compósitos com um comportamento de pseudo-encruamento.

Palavras-chave: compósitos cimentícios de elevado desempenho armados com fibras; vigas de concreto armado; substrato de transição, microfibras de aço

[a] *State University of Maringa, Department of Civil Engineering, Maringa, Brazil;*
[b] *Structural Engineer, Sao Paulo, Brazil;*
[c] *University of Sao Paulo, School of Engineering of São Carlos, Sao Carlos, Brazil.*

Received: 07 Aug 2014 • Accepted: 21 Oct 2014 • Available Online: 01 Dec 2014

© 2014 IBRACON

1. Introduction

It is well known that concrete is a relatively brittle material. Randomly distributed short fibers may improve toughness of cementitious matrices by preventing or controlling the initiation, propagation or coalescence of cracks (Bentur and Mindess [1]). In this way, concrete properties may be improved in a certain level (but not in all levels) if one type of fiber is chosen as reinforcement (Yao et al. [2]). If two types of fibers are used the influence in concrete properties will be even higher.

It has been shown by using the concept of hybridization with two different types of fibers incorporated in a common cement matrix, that the hybrid composite can offer more attractive properties. It occurs because the presence of one type of fiber enables a more efficient utilization of the potential properties of the other type of fiber (Mobasher and Li [3]).

According to Ferreira et al. [4], the modifications resulting from the addition of steel fibers to concrete, at relatively low rates (a maximum of 2%), are restricted only to the post-peak stage of the loading history. Under such conditions (at low rates), the steel fibers are not sufficient to inhibit the matrix cracking process which precedes the maximum load (subcritical growth of cracks).

In order to improve the cement-based composite behavior during the pre-peak stage, the effect of incorporating steel microfibers with the conventional steel fibers was studied. In this way, a modification of the microstructure of the composite occurs, improving the process of stress transference from the matrix to the fibers.

These materials were specifically developed for an application as a transition layer (Figure [1]) and nineteen different composites were prepared in two stages (Stage I and Stage II). In the Stage I, the composites were developed for application as a transition layer of reinforced concrete beams strengthened by bonding CFRP sheets. In the Stage II, the composites were developed for application in transition layers of strengthened beams by the insertion of CFRP laminates in notches executed in this layer (near-surface mounted technique).

In engineering practice (Figure [1]), the tensile bottom chord of reinforced concrete beams to be strengthened are frequently found

Figure 1 – Aspect of a tensile bottom chord of beam damaged by concreting deficiency and by reinforcement corrosion

Figure 2 – Transition layer of a reinforced concrete beam strengthened with CFRP

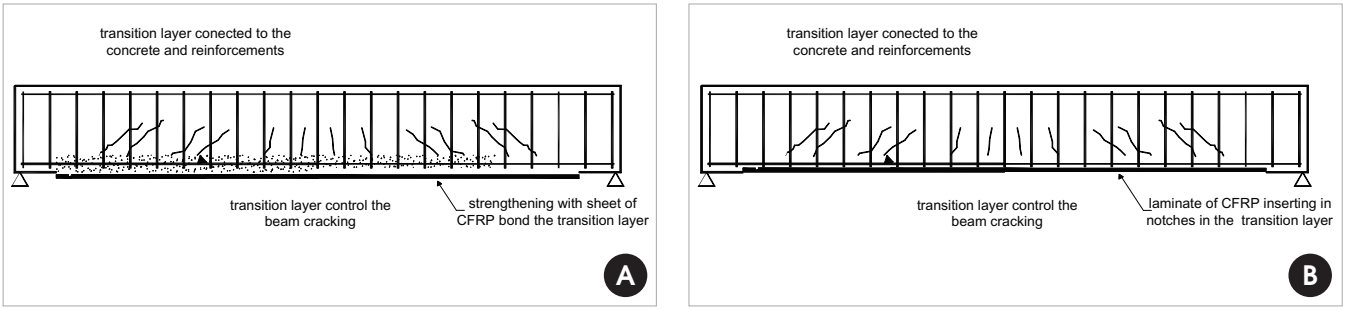

Externally bonded reinforcement with sheet of CFRP bond the transition layer (Ferrari (5))

Near-surface mounted with laminate of CFRP inserting in notches in the transition layer (Arquez (7))

Figure 3 – Dimensions of the specimens and general test configuration

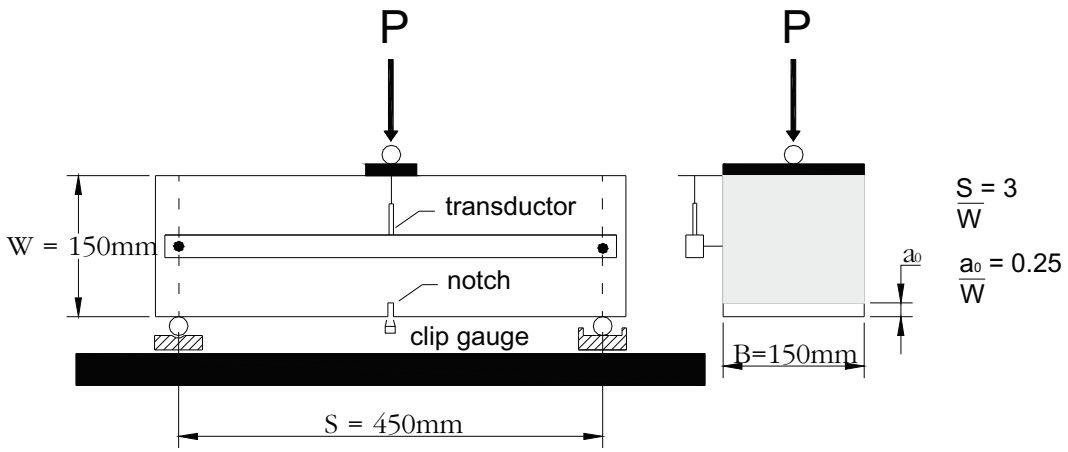

to be damaged by mechanical actions, corrosion effects or cracking. In such cases, the strengthening process must be preceded by the recovery of the bottom chords.

For this purpose, Ferrari [5] proposed the development of a high performance Portland cement-based composite with steel fibers and microfibers, destined to construct a transition layer as indicated in Figure [2a]. The mains idea was to remove part of the tensile bottom chord of the beams and reconstitute them using cement composite. The concept of transition layer is to create news bottom chords composed of a cement-based material with more appropriate characteristics for bonding the polymer reinforcement.

Thus, in this study, new results were added to the results already presented in Ferrari [5]. These new results were obtained through the development and analysis of new composites using the near-surface mounted technique, i.e., by inserting carbon fiber laminates in notches prepared in the transition zone (Figure 2b).

2. High performance fiber reinforced cement composites (HPFRCC)

2.1 Test setup

In order to evaluate the tensile strength of the developed cement-based composites, three point bending tests of prismatic specimens (150 mm x 150 mm x 500 mm) with central notch as recommended by Rilem [6] has been carried out. The tests were conducted in the Laboratory of Structures of the School of Engineering of São Carlos. Figure [3] shows the general configuration of the test, conducted by controlling the crack mouth opening displacement (CMOD), using a clip gauge. A servo hydraulic Instron apparatus was employed with a load cell of 100 kN capacity.

2.2 Composites analyzed

In the Stage I, thirteen composites were analyzed as shown in Table [1]. The composites were constituted by different volumes and types of steel fiber and also different types of cement matrix (mortar and microconcrete). The obtained composites were divided into groups formed by three prisms molded with the same characteristics. In the Stage II, an additional group of six composites (all of them made of microconcrete) was analyzed.

The steel fiber specified by "A" has the commercial name *FS8-Wirand* (provided by the company *Maccaferri – América Latina*); it is 25 mm long (with hooks at its extremities) and has a diameter of 0,75 mm diameter, which results in a shape factor equal to 33. Fiber "C" was designed by Ferrari (2012) and produced by the same company specifically for this research, once this fiber is not available commercially. It is 13 mm long (with hooks at its extremities) and has a diameter of 0.75 mm, which results in a shape factor equal to 17. Because of these special characteristics, these fibers are called as steel microfibers (Fig. 4).

In the Stage II, composites containing 1,5% type A fiber were analyzed. A repetition using the composites CMP1A1C and CPM1A2C (produced at the Stage I) was performed, but the composite CPM1A1.5C was also included. The selection of a fiber rate of 1,5% was motivated by the fact that in the Stage I this fiber rate was kept in 1%.

Figure 4 – Steel microfibers (left) and common steel fibers (right)

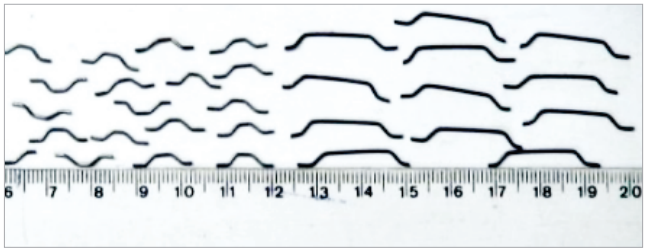

2.3 Composites composition and preparation

The composition of the constituting materials (Table [2]) was designed to fulfill certain practical criteria, such as:

- the use of Portland cement of high initial strength in order to obtain high strength at the first ages;
- compressive strength of 50 MPa;
- addition of superplasticizer additive to contribute to the workability of the cement paste;
- observations of the dimensional compatibility of the maximum aggregate size, which should not be greater than 1/3 of the fiber length.

The composites were produced using an electric mortar mixer with a capacity of 50 liters and an electric concrete mixer with a capacity of 300 liters. Six cylindrical specimens (100 mm x 200 mm) were molded for each composite to determine the compressive strength, the tensile strength by diametral compression and the elasticity modulus. These specimens were kept at the same curing conditions of the prism specimens (humid chamber). Fig. 5 shows the details of the material mixtures.

In the present research, the development of composites with cement matrix constituted by mortar and microconcrete was conducted. Taking into account the fluidity of this materials when compared to concrete, they may be applied with great facility in reduced regions as the substrate of beams to be strengthened (tensile bottom chords of beams to strengthened).

It is important to note that the composites for Stages I and II were not molded at the same time. Hence, for the preparation of the composites from Stage II, the trace of the cement-based matrix from Stage I was used as initial reference, with small adjustments made according to the dosage methodology and considering the characteristics of the aggregates involved in the mixture. From Table [2], the cement consumption is observed, and the w/c ratio of the composites produced in each of the two stages are practically the same.

Table 1 – Composites analyzed

Matrix	Stage	Group	Composites	Fiber volume	Fiber type	Material	Age (days)
Mortar (A)	I	1	CPA	0%	–	mortar	29
		2	CPA1A	1%	A	mortar	29
		3	CPA1.5A	1.5%	A	mortar	29
		4	CPA2A	2%	A	mortar	29
		5	CPA1.5A0.5C	1.5%+0,5%	A+C	mortar	28
		6	CPA1.5A1.5C	1.5%+1.5%	A+C	mortar	28
		7	CPA1.5A2.5C	1,5%+2.5%	A+C	mortar	28
		8	CPA1.5A3.5C	1.5%+3.5%	A+C	mortar	28

Matrix	Stage	Group	Composites	Fiber volume	Fiber type	Material	Age (days)
Microconcrete (M)	I	9	CPM	0%	–	microconcrete	28
		10	CPM1A	1%	A	microconcrete	28
		11	CPM1A1C	1%+1%	A+C	microconcrete	28
		12	CPM1A2C	1%+2%	A+C	microconcrete	28
		13	CPM1A2.5C	1%+2.5%	A+C	microconcrete	28

Matrix	Stage	Group	Composites	Fiber volume	Fiber type	Material	Age (days)
Microconcrete (M)	II	1	CPM1A1C	1%+1%	A+C	microconcrete	50
		2	CPM1A1.5C	1%+1.5%	A+C	microconcrete	50
		3	CPM1A2C	1%+2%	A+C	microconcrete	50
		4	CPM1.5A1C	1,5%+1%	A+C	microconcrete	50
		5	CPM1.5A1.5C	1.5%+1.5%	A+C	microconcrete	50
		6	CPM1.5A2C	1.5%+2%	A+C	microconcrete	50

Nomenclature of composites

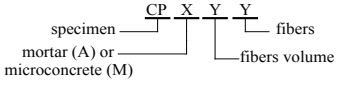

Table 2 – Composition of composite materials

Material	Mix proportion – Stage I		Mix proportion – Stage II
	Mortar	Microconcrete	Microconcrete
CP-V ARI PLUS Cement	1.0	1.0	1.00
Sand	3.0	2.13	2.30
Gravel 0	–	1.83	1.70
a/c	0.5	0.48	0.48
Cement consumption (kg/m³)	512	446	443
Steel fiber content	variable	Variable	variable
Glenium 51	0.4%*	0.5%*	0.5%*

* The superplasticizer additive was dosed relative to the weight of the cement:
Cement density: 3.15 kg/dm³; Sand density: 2.65 kg/dm³; Gravel density: 2.87 kg/dm³; Additive density: 1.09 kg/dm³.

3. Results and discussions

3.1 Compression tests of the cylindrical specimens

The values for the mechanical properties of the composites, namely the average compressive strength (f_{cm}), the average tensile strength by diametral compression ($f_{ctm,sp}$), and the elasticity modulus (E_{cs}), are presented in Table [3] and were obtained on the same date of the flexural tests.

In general, the addition of steel fibers decreases the compressive strength of the composites for both the mortar and the microconcrete. In addition, increasing the fiber volume influenced significantly the reduction in the compressive strength. Regarding the indirect tensile strength values, a strong dispersion of the results was observed. However, for the mortar composites, an increasing in the tensile strength may be observed when increasing the volumes of type A fiber (composites 2 to 4) and microfiber (composites 5 to 8).

For the microconcrete composites produced at the Stage I, the tensile strength decreased with the increasing of the fiber volume. The exception was for the composite CPM1A2C, which presented a high value for this strength. Additionally, for the composites produced in Stage II, the highest strength value is obtained for this same composite, i.e, the composite CPM1A2C .

Figure 5 – Detail of the appearance of the material mixture

3.2 Loads and strengths

The flexural tenacity of the composites was determined following Rilem recommendations [6]. The criteria for tenacity evaluation is based on the energy absorption capacity, understood as the area under the force (F) *versus* displacement (d) curve. The contribution of these fibers to the composite tenacity is evaluated subtracting the portion of tenacity attributable to the response of the cement-based matrix.

Figure [6] illustrates a typical response of the behavior of the fiber composites under flexure, along with the expressions used for the calculation of the equivalent flexural tensile strength ($f_{eq,2}$ and $f_{eq,3}$), and the residual strengths in flexure (f_{R1} and f_{R4}). The meaning of the parameters presented in this figure are as follows:

F_L: maximum *offset* force in the interval of δ = 0.05 mm. Calculated using a straight line parallel to the initial tangent, passing by the point that characterizes the displacement δ;

δ_L: value of vertical displacement corresponding to F_L;

$f_{fct,L}$: stress corresponding to F_L, given by:

$$f_{fct,L} = \frac{3.F_L.L}{2.b.h_{sp}^2} \quad (1) \qquad (1)$$

L: specimen clearance;

b: specimen width;

h_{sp}: distance from the top of the notch top to the top face of the specimen;

D^b_{BZ}, $D^f_{BZ,2}$, and $D^f_{BZ,3}$: energy absorption capacity of the matrix and the fibers, respectively. Calculated by the area under the F-δ curve until specific displacements, as shown in Figure 6;

$F_{R,1}$ and $F_{R,4}$: forces corresponding to the displacements δ_{R1} = 0.46 mm and δ_{R4} = 3.0 mm. These values are used to calculate the residual flexural tensile strengths.

The tenacity parcels $D^f_{BZ,2}$ and $D^f_{BZ,3}$ are transformed into equivalent flexural tensile strength for the two different displacement levels d_2 and d_3, respectively, as indicated by Figure 6. The material load capacity relative to the pre-defined maximum displacement value is evaluated using the concept of residual flexural strength ($F_{R,1}$ and $F_{R,4}$).

Table [4] presents the strength and load values calculated based on Rilem recommendations [6]. The value of the maximum load of composite is also presented (F_M).

Table 3 – Average results of composite characterization under compression

Matrix	Stage	Groups	Composites	f_{cm} (MPa)	$f_{ctm,sp}$ (MPa)	E_{cs} (GPa)
Mortar (A)	I	1	CPA	52.5	3.1	23.8
		2	CPA1A	43.8	3.7	22.7
		3	CPA1.5A	42.2	3.7	23.1
		4	CPA2A	45.7	4.9	24.0
		5	CPA1.5A0.5C	49.2	4.4	28.2
		6	CPA1.5A1.5C	47.2	4.9	32.3
		7	CPA1.5A2.5C	43.6	4.8	31.0
		8	CPA1.5A3.5C	42.8	4.9	29.1
Matrix	**Stage**	**Groups**	**Composites**	**f_{cm} (MPa)**	**$f_{ctm,sp}$ (MPa)**	**E_{cs} (GPa)**
Microconcrete (M)	I	9	CPM	62.3	3.8	35.2
		10	CPM1A	42.0	3.0	30.6
		11	CPM1A1C	40.6	3.7	26.3
		12	CPM1A2C	42.8	5.1	30.0
		13	CPM1A2.5C	20.8	2.8	19.9
Matrix	**Stage**	**Groups**	**Composites**	**f_{cm} (MPa)**	**$f_{ctm,sp}$ (MPa)**	**E_{cs} (GPa)**
Microconcrete (M)	II	1	CPM1A1C	33.2	2.5	32.3
		2	CPM1A1.5C	30.6	2.2	31.0
		3	CPM1A2C	33.4	3.2	32.4
		4	CPM1.5A1C	28.3	2.6	29.8
		5	CPM1.5A1.5C	30.5	2.9	31.0
		6	CPM1.5A2C	29.2	2.4	30.2

For each composite, three specimens were subjected to axial compression test and three to the diametral compression tensile test.

E_{cs} – secant deformation modulus corresponding to the inclination of the secant line in the stress-strain diagram, passing by the points corresponding to the 0.5 MPa stress and 30% of the compressive strength.

The value of the parameter $f_{fct,L}$ represents the portion of the composite strength due to the cement-based matrix. The addition of steel fibers visibly contributed to the increasing of this strength (Figure [7]). It can also be stated that the addition of microfibers to the steel fibers improved even more the composite strength for the mortar composites. Once the values of

Figure 6 – Rilem criteria for the evaluation of the behavior of fibrous material

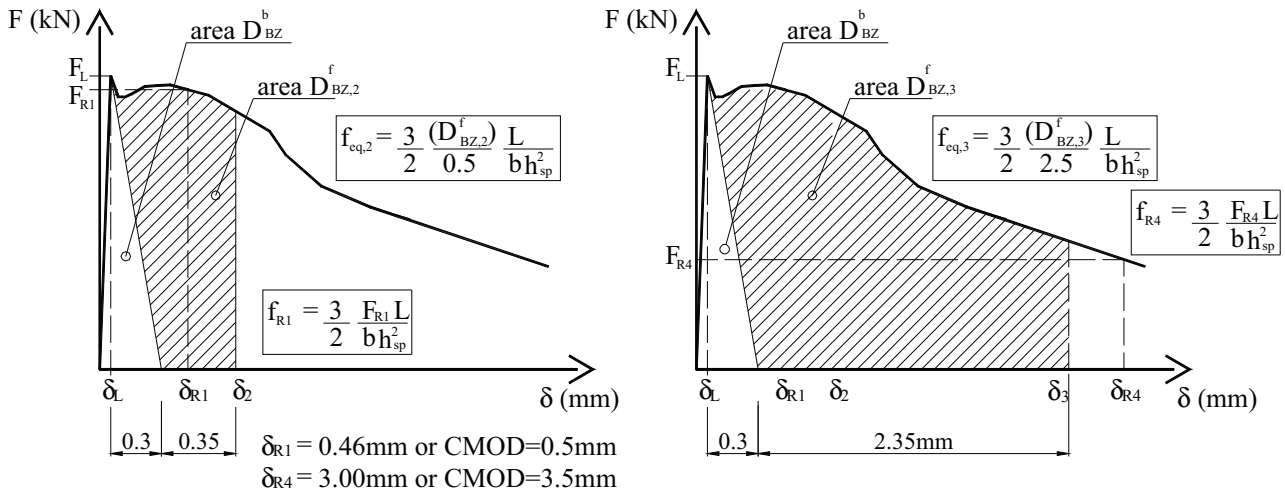

Table 4 – Load and strength according to RILEM

Matrix	Stage	Composites	Loads (kN)				Loads (kN)				
			F_L	F_M	$F_{R,1}$	$F_{R,4}$	$f_{fct,L}$	$f_{eq,2}$	$f_{eq,3}$	$f_{R,1}$	$f_{R,4}$
Mortar (M)	I	CPA	8.0	8.0	1.3	–	2.3	–	–	0.4	–
		CPA1A	13.4	13.4	12.5	5.2	3.9	3.3	2.6	3.6	1.5
		CPA1.5A	13.1	16.1	16.0	6.1	3.7	4.6	3.2	4.5	1.7
		CPA2A	14.5	17.6	17.4	7.6	4.6	5.5	4.2	5.5	2.4
		CPA1.5A0.5C	16.4	17.8	17.2	9.3	4.6	4.9	4.0	4.8	2.6
		CPA1.5A1.5C	16.0	21.0	20.9	9.4	4.8	6.5	4.8	6.3	2.8
		CPA1.5A2.5C	22.1	23.7	23.5	12.8	6.1	6.5	5.0	6.5	3.6
		CPA1.5A3.5C	20.0	21.4	20.8	6.1	5.5	5.7	3.8	5.7	1.7
Microconcrete (M)	I	CPM	14.1	14.2	1.3	–	4.0	–	–	0.4	–
		CPM1A	12.0	12.1	7.5	3.7	3.3	2.0	1.6	2.1	1.0
		CPM1A1C	17.6	18.5	16.9	7.5	5.2	5.1	3.7	5.0	2.2
		CPM1A2C	19.4	21.9	19.7	8.0	5.5	5.7	4.1	5.7	2.3
		CPM1A2.5C	10.0	10.0	6.3	2.3	2.9	1.5	1.1	1.9	0.7
Microconcrete (M)	II	CPM1A1C	12.2	14.3	11.4	1.0	3.6	3.5	2.4	3.4	0.3
		CPM1A1.5C	12.0	15.2	12.1	2.7	3.5	3.8	2.5	3.6	0.8
		CPM1A2C	14.4	18.9	15.9	1.8	4.1	4.9	3.0	4.5	0.5
		CPM1.5A1C	12.8	18.5	16.0	2.4	3.7	5.0	2.4	4.6	0.7
		CPM1.5A1.5C	15.2	19.8	17.5	1.3	4.3	5.3	3.6	5.0	0.4
		CPM1.5A2C	11.0	15.6	13.4	3.2	3.2	4.4	2.9	4.0	1.0

equivalent flexural strength ($f_{eq,2}$ and $f_{eq,3}$) represent the behavior of the composites based on the contribution of the fibers, Figure [7] also suggests an increasing in the flexural strength due to the increasing of fiber A volume, especially when steel microfibers are added.

Figure 7 – Mortar composites: comparison between strength values

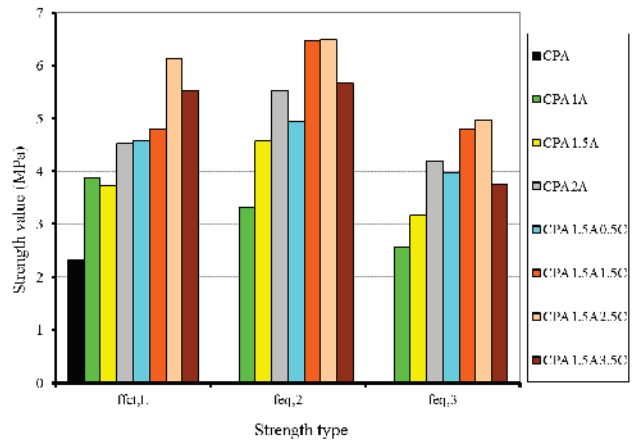

The strength values for the microconcrete composites are compared in Figure [8]. It is important to note the drop in the strength $f_{fct,L}$ of the composite CPM1A in comparison to the composite CPM, which demonstrates that the isolated presence of steel fiber A did not improve the strength of the cement-based matrix. By incorporating steel microfiber (C) with fiber (A), the contribution of fibers to the flexural strength is significantly increased for the composites CPM1A1C and CPM1A2C.

Regarding the flexural strength values, the increase of such strengths by the addition of steel microfiber to fiber A is notable. In the majority of composites, the equivalent strength $f_{eq,2}$ surpasses the value of the strength $f_{fct,L}$. This result indicates significant strength gains even after the cracking. Particular attention is drawn to the behavior of the composites CPM1A2C and CPM1.5A1.5C-II, with the latter produced in the Stage II. It should be mentioned that composite CPM1.5A1.5C-II was produced intending to complement the amount of fibers investigated in the Stage I.

Regarding the values of equivalent flexural strength ($f_{eq,3}$), which represents the graph area until the vertical displacement (d_3), the higher tenacity of the previously cited composites can be highlighted, as well as the high tenacity of composite CPM1A1C.

Figure 8 – Microconcrete composites: comparison between the strength results

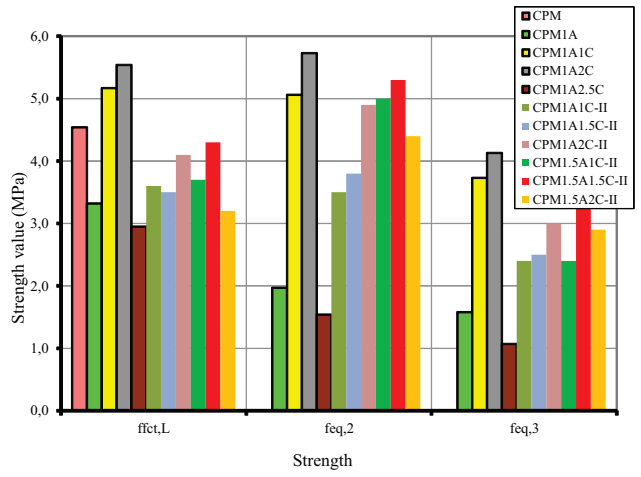

3.3 P-CMOD curves

The P-CMOD curves of mortar composites are presented in Figure [9]. The presence of steel fibers and steel microfibers in the cement-based mortar matrix increased the energy absorption capacity and the strength levels before and after the matrix cracking. Increasing the type A fiber volume delivered some improvement in the composites ductility. With the addition of 0,5% of steel microfibers, however, it was possible to elevate the energy absorption capacity of the composite CPA1.5A to the same level as CPA2A. This elevation is advantageous taking into account that the workability of the composite is not modified by the microfiber. By another hand, the workability of the composite is significantly influenced by the increasing of the type A fiber.

The maximum values of force (F_M), obtained for composites CPA1.5A0.5C and CPA2A, are practically the same, i.e., 17,78 kN and 17,59 kN, respectively. The same behavior may be also observed for the flexural strength ($f_{fct,L}$), with values of 4,58 MPa and 4,56 MPa, respectively. The same statement may be established to the residual strength ($f_{R,1}$ e $f_{R,4}$) for this two mentioned composites.

To visualize the effect of the steel microfibers in the initial Stage of the composite performance, Figure [10] shows the same curves displayed by Figure [9], but now emphasizing the initial composite loading interval (CMOD up to 0.15 mm). In the composites with fiber A isolated, the branch after the matrix cracking is well defined with constant strength and variable CMOD. However, in the presence of microfibers, the stress transfer is gradual and occurs with increasing strength of the composites. The stress transfer process with cracking of the matrix is facilitated by the presence of microfibers. The dispersion of microfibers in the matrix increases the possibility of interception of cracks, sewing the cracks and increasing the composite strength.

All P-CMOD curves of microconcrete composites are shown in Figure [11]. The presence of fibers and microfibers particularly improved the energy absorption capacity of these composites. The strength capacity was decreased with the isolated presence of fiber A (composite CPM1A). However, with the incorporation of 1% of type A steel fibers and 2% of microfibers, higher strength and energy absorption levels were reached. The same phenomenon was not verified for the incorporation of 2.5% microfibers.

The maximum force reached by the composite CPM1A2C was 37% and 61% above the forces obtained for the composites CPM and CPM1A, respectively. By another hand, the equivalent flexural strength ($f_{eq,2}$) of the composite CPM1A2C was 110% and 13% above the strength obtained for the composites CPM1A and CPM1A1C, respectively.

Figure 9 – P-CMOD curves of the mortar composites

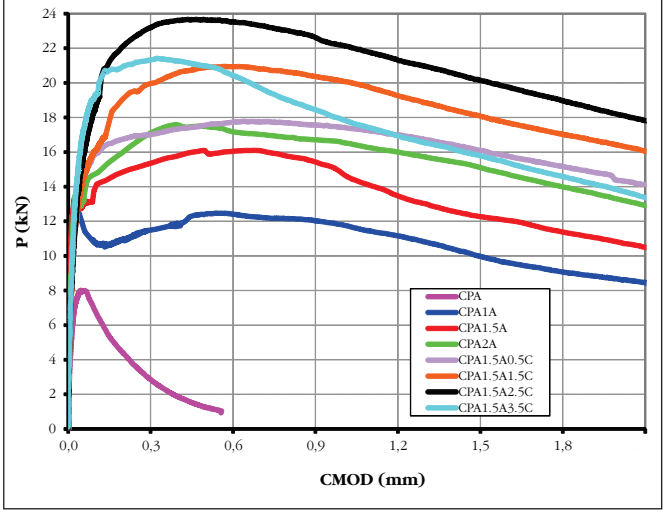

Figure 10 – Initial P-CMOD behavior of the mortar composites

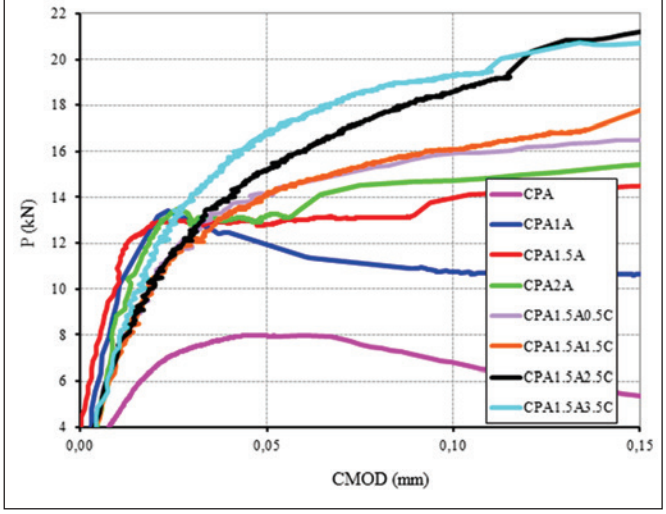

Figure 11 – P-CMOD curves of the microconcrete composites

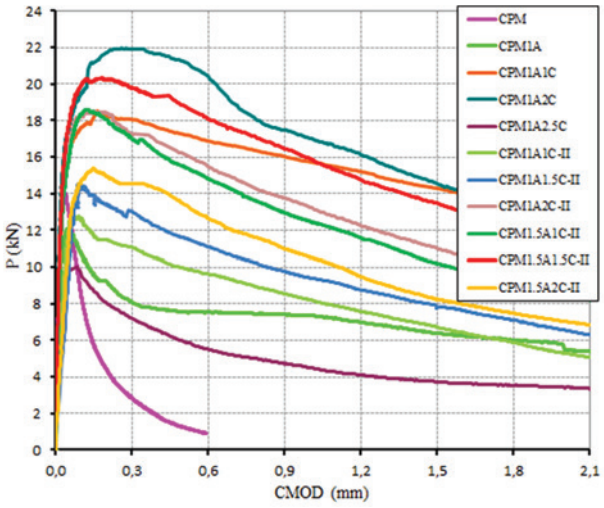

Figure [12] visualizes the effect of microfibers on the stress transfer process in the microconcrete matrix. Note that, as the matrix cracks, the matrix-fiber stress transfer process occurs with the elevation of strength levels in the composites CPM1A1C and CPM1A2C due to the presence of microfibers.

With the matrix cracking, based on the presence of microfibers, it was observed that the matrix-fiber stress transfer process occurred with increasing strength levels for the composites CPM1A1C, CPM1A2C, CPM1A2C-II, CPM1.5A1C-II and CPM1.5A1.5C-II. Furthermore, an improvement on the behavior of these materials was observed when microfiber volume increases from 1% to 2%, and from 1% to 1,5% for the composites produced in Stages I and II, respectively.

Figure 12 – Initial P-CMOD behavior of microconcrete composites

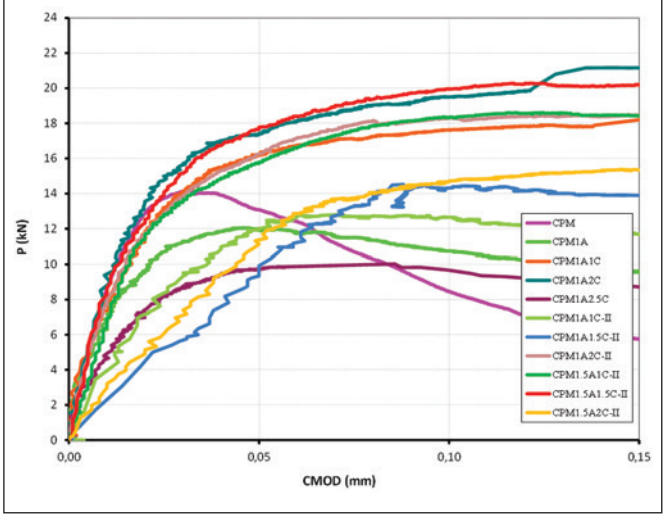

3.4 Fracture strength curves

Figure [13] presents the fracture strength curves of each cement-based mortar composites. Figures [14] and [15] present the fracture strength curves of microconcrete composites produced in Stages I and II, respectively. In these figures, "K_R" indicates the fracture strength of the composite, and parameter "a" is the depth of the crack (a) standardized by the height (W) of the prism specimen, i.e., a = a/W.

For the prism specimens (see Figure [3]) the values of K_R were obtained from the P-CMOD values using equation [2], which is only valid for fracture Mode I. In this equation, the parameters are as described in Figure [3], where function f(a) depends on the geometry and is determined using the procedures described by Ferreira [4].

$$K_R = \frac{1.5PS\sqrt{\pi a}}{BW^2} f(\alpha) \qquad (2)$$

From the analysis of the strength curves, it is possible to extract information about the performance of the composites in terms of strength to crack propagation. The final branches of the strength curves of the composites are rising, representing the post-peak phase of the loading history, where the gain of strength to crack propagation given by the steel fibers and microfibers is high.

From Figure [13], regarding the matrix without fibers (CPA), the expected low strength capacity to crack propagation is observed, evidenced by the small extension of the initial vertical branch. This fact suggests the subcritical spread of cracks even at low loading levels, eventually caused by the absence of coarse aggregates in the mixture. Nevertheless, the presence of fibers and microfibers in the matrix slowed this phenomenon.

Even for small propagations of cracks (a = 0,2), the fracture strength of the composites with fibers were higher (between 33% to 18% depending on the volume of fibers) than the composites without fibers (CPA). The higher and the lower strengths to the

Figure 13 – Strength curves for the mortar composites

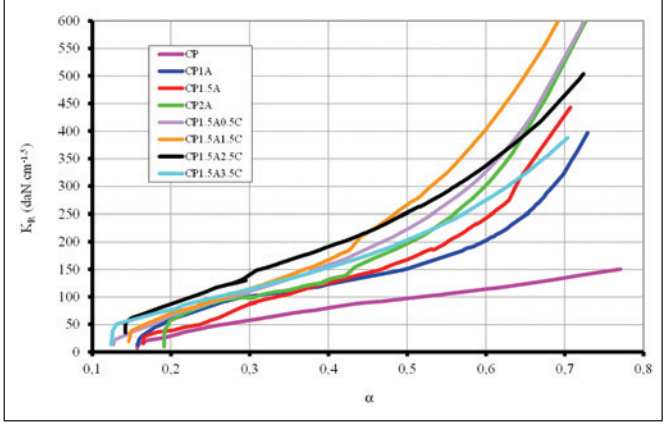

Figure 14 – Strength curves for microconcrete composites – Stage I

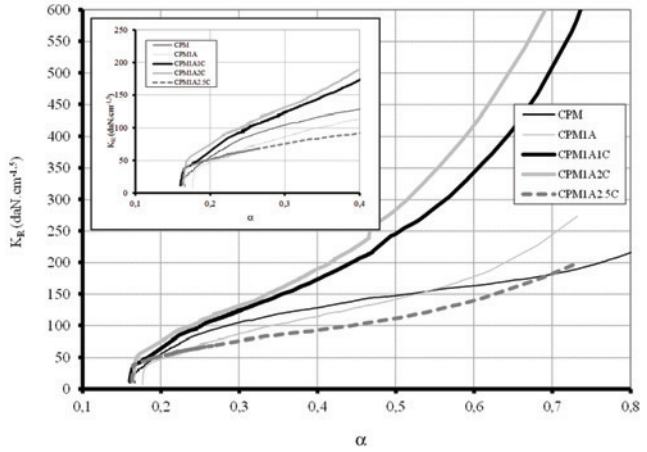

Figure 15 – Strength curves for microconcrete composites – Stage II

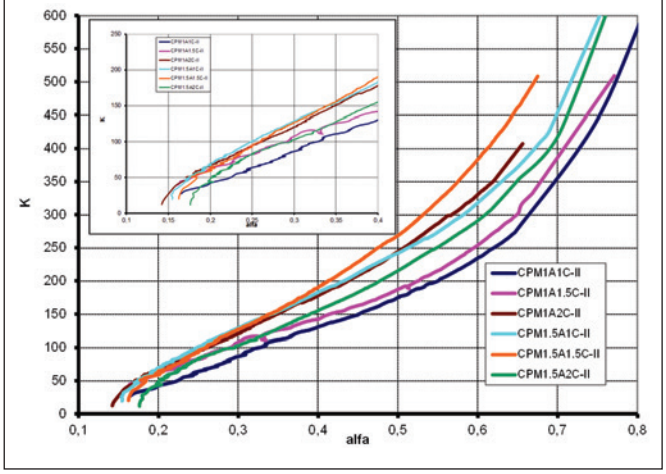

propagation of cracks were obtained for composites CPA1.5A2.5C and CPA1.5A, respectively. From Figure [13], is possible to observe that the higher gains of strength were obtained adding the type C microfibers to the type A fibers.

The fracture strength gain was well evidenced, especially in the post-peak branch. Among the mortar composites, the greatest fracture strength gain were observed for the composites CPA1.5A1.5C and CPA1.5A2.5C.

From Figure [14], it can be observed that for small crack propagation, the fracture strength of the composites CPM1A and CPM1A2.5C are lower than that one for composites without fibers. However, for more advanced stages of crack propagation, a > 0.6, the fracture strength of these composites surpass the fracture strength of the matrix without fibers. For the latter, the curve configuration (small declivity compared to the others) indicates low strenght of the material to the crack propagation.

For a = 0.2, the fracture strengths of composites CPM1A1C and CPM1A2C were, respectively, 18% and 36% higher than the matrix without fibers. Compared to composite CPM1A, the increases were even more significant, 44% and 66%, respectively, demonstrating the beneficial effects of the microfibers on the fracture strength.

From Figure [15], it is evident that the fracture strength performance of the composites containing 1% of fibers improved gradually with increasing steel microfiber content. The same behavior is observed only for composites CPM1.5A1C-II and CPM1.5A1.5C-II containing 1.5% of steel fibers. Additionally, the performance of composite CPM1.5A2C-II was inferior to the others of its series.

4. Conclusions

From the conducted research, the following observations may be established:

- The hybridization process is an interesting alternative for application in the recovery of tensile bottom chord of beams, once the addition of microfibers to the steel fibers increased the tensile stress in flexure and increased the flexural tenacity of the cement-based mortar and microconcrete composites;
- With the cracking of the cement-based matrix, the stress transfer was facilitated by the steel microfibers, which being dispersed in the matrix in higher amounts, conditioned the crack propagation to the increase of the loading level;
- Considering the pseudo-hardening characteristic and its specific application, composite CPM1A2C presented the greatest qualities among the products of the Stage I, designed for application to the reconstruction of the tensile bottom chords of reinforced concrete beams strengthened in flexure with CFRP sheets;
- Among the composites produced in the Stage II, the behavior of CPM1.5A1.5C-II was noteworthy, as the hybridization process provided considerable increases in the maximum load as well as in the flexural and fracture strengths.

5. Acknowledgements

We thank FAPESP, CAPES and CNPq for financial support. We also thank Maccaferri-Latin America for the production, under contract, of the steel microfibers.

6. References

[01] Bentur, A., Mindess, S. (1995). Fiber Reinforced Cementitious Composites, Elsevier, London, 1990.

[02] Yao, W., Li, J., Wu, K. (2003). Mechanical properties of hybrid fiber-reinforced concrete at low fiber volume fraction. Cement and Concrete Research, 33, 27-30.

[03] Mobasher, B., Li, C.Y. (1996). Mechanical properties of hybrid cement-based composites. ACI Mater. J. 93 (3), 284-292.

[04] Ferreira, L.E.T.; Bittencourt, T.N.; Souza, J.L.A.O.; Gettu, R. (2012). R-Curve behavior in notched beam tests of rocks. Engineering Fracture Mechanics, N. 32, 27-40.

05] Ferrari, V. J.; Hanai, J.B. (2012). "Flexural strengthening of reinforced concrete beams with carbon fibers reinforced polymer (CFRP) sheet bonded to a transition layer of high performance cement-based composite". Ibracon Structures and Materials Journal, v. 5, n. 5, 596-626.

[06] Rilem TC 162-TDF (2002). “Test and design methods for steel fibre reinforced concrete. Bending test” Materials and Structures, v. 35, 579-582.

[07] Arquez, A. P. Aplicação de laminado de polímero reforçado com fibras de carbono (PRFC) inserido em substrato de microconcreto com fibras de aço para reforço à flexão de vigas de concreto armado. Dissertação – Escola de Engenharia de São Carlos da Universidade de São Paulo, 2010.

IBRACON

REVISTA IBRACON DE ESTRUTURAS E MATERIAIS

IBRACON STRUCTURES AND MATERIALS JOURNAL

Volume 7, Number 6
December 2014
ISSN: 1983-4195

Contents